Theory and Application of the Density-Matrix Renormalization Group

Im Fachbereich Physik

der

Freien Universität Berlin

eingereichte

Dissertation

vorgelegt von

Ming-Chiang Chung

aus Taipeh, Taiwan

Berlin 2002

Erster Gutachter: Prof. Dr. I. Peschel
                       Institut für Theoretische Physik
                       Freie Universität Berlin
                       Arnimallee 14, 14195 Berlin

Zweiter Gutachter: Prof. Dr. K. D. Schotte
                       Institut für Theoretische Physik
                       Freie Universität Berlin
                       Arnimallee 14, 14195 Berlin

Tag der Disputation: 29.05.2002

Zusammenfassung

Die Dichtematrix–Renormierungsgruppe (DMRG), die 1992 von White entwickelt wurde, ist eine numerische Methode, sehr genaue Näherungen für Grundzustand und tiefliegende Anregungszustände eindimensionaler Quantensysteme zu finden. Wegen des exponentiellen Wachstums der Anzahl der Zustände mit der Systemgröße, gerät man in Schwierigkeiten bei der numerischen Berechnung endlicher Systeme. Zwar kann man für kleine Systeme den Hamiltonoperator noch exakt diagonalisieren, aber wenn man größere Systeme berechnen will, müssen andere Methoden wie das Monte–Carlo–Verfahren benutzt werden. Wegen statistischer Fehler ist jedoch die Genauigkeit der Quanten–Monte–Carlo Methode beschränkt. Dagegen ist die DMRG nicht auf kleine Systeme eingeschränkt, und ihre Genauigkeit kann für eindimensionale Systeme extrem hoch sein. Ein günstiges Beispiel ist die Grundzustandsenergie für eine Spin–1–Kette: für ein System mit hundert Spins kann eine Genauigkeit von 10^{-10} erreicht werden. Mit der DMRG lassen sich nicht nur Energien, sondern auch Korrelationsfunktionen bestimmen, die nur sehr schwierig mit anderen Methoden berechenbar wären. Man kann die DMRG–Methode erweitern und auf Transfermatrizen, die zu zweidimensionalen klassischen Systemen gehören, und auf eindimensionale Quantensysteme bei endlicher Temperatur anwenden. Wegen aller dieser Möglichkeiten ist die DMRG auf die verschiedensten eindimensionalen Systeme und Probleme angewandt worden.

Die DMRG verfolgt die Hauptidee von Wilsons Renormierungsgruppen-Verfahren, wie sie für das Verunreinigungsproblem enwickelt worden war. Sie ist konzipiert, um die im Eindimensionalen auftretenden Probleme zu überwinden, wenn Wilsons RG–Prozedur auch im Ortsraum angewendet werden soll. Die Idee der Ortsraum-RG ist, daß man das System Schritt für Schritt vergrößert und mit einer festen Zahl von wichtigen Zuständen statt allen Zuständen auszukommen versucht. In Wilsons RG benutzt man Eigenzustände niedrigster Energien. Trotz des Erfolgs für Kondos und Andersons Verunreinigungsprobleme gab das Verfahren schlechte Ergebnisse für wechselwirkende eindimensionale Systeme. White erkannte, daß die Fehler aus der Auswahl von Eigenzustände des Hamiltonoperators kommen, die Knoten haben, die nicht im vergrößerten System erscheinen. Er schlug vor, daß man die Umgebung berücksichtigen muß, um diesen Fehler zu vermeiden, und bei der Auswahl die Eigenwerte der reduzier-

ten Dichtematrizen zu benutzen. Für ein besseres Verständnis wird der DMRG-Algorithmus in Kaptel 2 vorgestellt.

Der Erfolg der DMRG bei eindimensionalen Systemen hängt von den Eigenschaften der Dichtematrizen ab. Bei der DMRG-Prozedur konstruiert man zuerst ein System der Größe L, aus dem man die reduzierte Dichtematrix für eine Blockgröße $L/2$ bekommt. Als optimale Basis wählt man dann nur Eigenfunktionen mit den größten Eigenwerten der reduzierten Dichtematrix aus. Diese Basis wird verwendet, um ein weiteres größeres System aufzubauen. Deswegen hängt die Genauigkeit der DMRG–Berechnungen von den Dichtematrix-Spektren ab. Wenn das Spektrum schnell abfällt, wird das DMRG–Verfahren sehr gut funktionieren, weil die Eigenfunktionen mit kleinen Eigenwerten, die man fortläßt, das Resultat nicht sehr viel beeinflussen können.

Die Eigenschaft der Dichtematrix–Spektren sind von zentraler Bedeutung für die numerische Berechnungen. Ein Hauptziel meiner Arbeit ist, eine Theorie für die DMRG durch die Betrachtung der Dichtematrix–Spektren zu entwickeln. Denn mit Hilfe dieser Spektren kann man das Verhalten dieser Methode und den Grund verstehen, weswegen es in einem Fall besser als in einem anderen funktioniert. Am überzeugendsten sind diese Betrachtungen bei exakt lösbaren Modelle und ihren Spektren der reduzierten Dichtematrix.

In Kapitel 3 habe ich den Grundzustand von gekoppelten Oszillatoren in der Ortsraumdarstellung untersucht. Die reduzierte Dichtematrix ist ein Exponential von nichtwechselwirkenden Oszillatoren, so daß die Dichtematrizen für einen Gitterplatz oder für die Hälfte des Systems direkt berechnet werden können. Der Einfluß der verschiedenen Randbedingungen auf die reduzierten Dichtematrix wird auch untersucht. Der thermodynamische Grenzfall wird durch Eckentransfer–Matrizen erreicht wie im Falle der integrablen Spin-Ketten und die erhaltenen Spektren sind sehr ähnlich. Die gequetschten Oszillatorzustände, die durch die Dichtematrix für einen Platz erzeugt werden, wurden in numerischen Berechnungen benutzt und gaben sehr gute Übereinstimmung mit den analytischen Resultaten.

In den Kapiteln 4 and 5 habe ich kohärente Zustände benutzt, um die lösbaren bosonischen und fermionischen Systeme zu behandeln. Der Ausgangspunkt der Berechnungen ist eine einfache exponentielle Darstellung des Grundzustands. Es ergibt sich eine allgemeine Form der reduzierten Dichtematrizen – eine exponentielle Boltzmannartige Form. Beide Fälle sind sehr ähnlich. Trotz der verschieden Statistiken haben die bosonischen und fermionischen Systeme die selben Gleichungen für die Einteilcheneigenwerte der Dichtematrizen.

Auf diese Weise werden die reduzierten Dichtematrizen für die folgenden Spinmodelle in einer Dimension gewonnen: die tranversale Isingkette, die XX-Spinkette und die XY-Spinkette in einem äußeren Feld. Für die

transversale Isingkette werden die Dichtematrizen sowohl für den geordneten und den ungeordneten Bereich konstruiert als auch für den kritischen Punkt. Ich habe auch die Dichtematrizen für den ersten Anregungszustand untersucht. Die Dichtematrix-Spektren sind sehr ähnlich wie beim Grundzustand. Die Methode kann auch auf die Transfermatrix des zweidimensionalen Isingmodell angewandt werden. Die Spektren dafür sind sehr ähnlich zu denen für das transversale Isingmodell. Dies ist sehr plausibel, da die Transfermatrix in engem Zusammenhang mit dem Hamiltonoperator der transversalen Isingkette steht. Die Dichtematrix–Spektren für die XX–Spinkette zeigen die Eigenschaften für ein kritisches Modell. Für die XY–Kette wird die Unordnungslinie, wo der Grundzustand zweifach entartet ist, durch das Dichtematrix-Spektrum betrachtet. Wenn man sich der Linie nähert, fällt das ganze Spektrum zusammen.

Das wichtigste Ergebnis bezieht sich auf die Dichtematrizen für zweidimensionale Systeme. In den Kapiteln 3 und 5 habe ich zweidimensionale gekoppelte Oszillatoren und Tight-Binding-Modelle untersucht. Die resultierenden Spektren haben beide die gleiche Eigenschaft: sie fallen sehr langsam ab. Das Gleiche gilt auch für die Abschneidefehler. Für die Oszillatoren wird die Abhängigkeit der Dichtematrix-Spektren von der Breite des Systems besprochen. Anhand der Spektren sieht man die zunehmenden Schwierigkeiten bei der Berechnung des Eigenwertes für den Grundzustand, wenn das System immer zweidimensionaler wird. Diese Beobachtung stimmt mit aktuellen DMRG-Berechnungen für zweidimensionale Systeme überein. Zum Beispiel wurden bei einer vor kurzem von White und Scalapino publizierten Untersuchung des $t–J$–Modells auf einem 12×12 Gitter 4000 Zustände verwendet. Im Falle des zweidimensionalen Tight–Binding–Modells wird die Abhängigkeit der Dichtematrix–Spektren von verschiedenen Arten der Zerlegungen des Gitters studiert. Es zeigt sich, daß der langsame Abfall im Zusammenhang mit der Existenz von langen Grenzen zwischen den zwei Teilen der Systeme steht.

Außer der Grundbetrachtung der DMRG–Methode habe ich in Kapitel 6 diese Methodik auch für ein Problem der statistischen Physik verwendet, nämlich für die Isingebene mit linieförmigen Defekten. In diesem Fall benutzt man die Tranfermatrix und deren Eigenfunktionen statt eines Hamiltonoperators. Um die lokale spontane Magnetisierung genau zu berechnen, braucht man zunehmend größere Systeme, wenn man sich dem kritischen Punkt annähert. Wegen der günstigen Eigenschaft des Dichtematrix–Spektrums ist das in diesem Fall mit einer mäßigen Anzahl von Zuständen möglich. Auf diese Weise wurde der nicht–universelle magnetische Exponent β_l als Funktion der lokalen Kopplungen für mehrere Arten von Defekten bestimmt.

Contents

Chapter 1

Introduction

The Density Matrix Renormalization Group (DMRG) [1, 2, 3], developed by S. R. White in 1992, provides a numerical method for finding accurate approximations to the ground state and low-lying excited states of one-dimensional quantum systems. In treating such systems, the most important limitation for numerical calculations in finite systems is that the number of states grows exponentially with the system size. For small systems, one can still diagonalize the Hamiltonian exactly, while for reaching larger systems, other methods must be introduced such as Monte Carlo methods [4, 5, 6]. The disadvantage of the Monte-Carlo is that the accuracy is limited because of the statistical error. By contrast, DMRG is not limited to small sizes and is remarkable in the accuracy that can be reached for one-dimensional systems. A good example is the ground-state energy of the spin-one Heisenberg chain: for a system of hundreds of sites a precision of 10^{-10} can be achieved [1, 2]. Using DMRG, one can calculate not only energies of the ground state and low-lying excited states but also correlation functions, which are difficult to obtain from other methods. One can also extend the method to transfer matrices for two-dimensional classical systems [7], and to one-dimensional quantum systems at finite temperature [9, 8, 10]. Because of these features of the DMRG, it has been applied to various one-dimensional systems and problems, for example, spin chains, disordered models, fermionic and bosonic systems, impurities, phonons, the calculation of dynamical properties, etc [3].

DMRG follows the main idea of Wilson's RG treatment of impurity problems [11] and was originally developed to overcome the problems that arose in one dimension when real-space RG procedures were applied to interacting systems. The basic idea of real-space RG procedures is that one enlarges a system step by step from a small one by using a constant number of important states instead of all states, so that the computational effort required for each step stays the same. Now the question arises, which states one has to choose to represent the most important information for

a system. In Wilson's RG procedure one uses the m eigenstates of lowest energy. In spite of its success for Kondo and Anderson impurity problems, this procedure gave poor results when it was applied to several interacting quantum systems [12, 13, 14, 15]. White perceived that the main source of error comes from the selection of eigenstates via the Hamiltonian, because these eigenstates will have nodes at the boundaries, which would not be present in the enlarged system. He suggested that one should take the environment into account and use the eigenstates of the reduced density matrix as basis states.

The success of the DMRG in treating one-dimensional quantum systems is closely related to the properties of the density matrices. This can be seen as follows. In DMRG, one first constructs a system of size L, from which one obtains the reduced density matrix for a block of size $L/2$. Now only the eigenfunctions of the largest eigenvalues w_n of the reduced density matrix are selected as the optimal basis. Using this basis, one builds a system of size $L + 2$. (I will discuss the details in chapter 2.) Therefore the accuracy of the DMRG calculation depends on the reduced density-matrix spectra. If the eigenvalue spectrum drops rapidly, the DMRG will essentially work well, because most eigenfunctions with small eigenvalue will not influence the result much. For the quantum chains this is indeed the case. The numerical calculations show a roughly exponential decrease of the eigenvalues [2, 16].

Since the character of the density matrix spectra is the important ingredient for the numerical calculations, the question arises whether such spectra can be obtained explicitly for some solvable models. For non-critical systems this is possible by using the relation between the density matrices of quantum chains and the corner transfer matrices (CTMs) [17] of the associated two-dimensional classical problems. In this way, the spectra for the transverse Ising chain [18] and the XXZ Heisenberg chain [18] could be determined in the thermodynamic limit and compared with DMRG calculations. In these cases, the density matrices have simple analytic expressions and the spectra are strictly exponential functions apart from degeneracies. This does not hold for the chiral three-state Potts chain [19], or for nonintegrable models [20, 21], but qualitatively the spectra are similar. The CTM approach is limited to large noncritical systems and cannot be used for finite or critical systems. Therefore an alternative approach is necessary by which one can treat solvable systems of arbitrary size.

First I will consider bosons. Compared with the case of spins and fermions, relatively few DMRG studies have dealt with bosons [22]-[32]. The Hilbert space for bosons on one site has already infinite dimension, which differs from the case of fermion or spin systems. Therefore, any numerical treatment has to start with a truncation. As pointed out by White *et al.* [25], one can do this analogously to the DMRG procedure

by selecting optimal states through the density matrix for a single site. It is interesting to find this quantity in a solvable case due to the infinite number of eigenstates in a full treatment. The same holds, of course, for the more complicated density matrix of a half-chain which is used in the DMRG algorithm.

There are some advantages in studying coupled harmonic oscillators as an example for bosons. The model is integrable and solvable in any number of dimensions, and the ground state can be written down easily as a Gaussian form of the coordinates. Therefore the reduced density matrix for any partition of the system can be found, as will be seen, by integrating out some of the coordinates. Consequently, arbitrary reduced density matrices for coupled oscillators have the general form $\exp(-\mathcal{H})$. The operator $\mathcal{H}$ describes a collection of noninteracting oscillators with single-particle eigenvalues ε_l. One can obtain ε_l from the eigenvalues of an $M \times M$ matrix, where M is the number of oscillators in the chosen subsystem. In general, the ε_l have to be calculated numerically.

Since the density-matrix spectra for the oscillators can be obtained explicitly, one can study the physical content related directly to the spectra and numerics. The optimal basis for one site, obtained numerically in the case of an electron-phonon system by Jeckelmann and White [25], can be analyzed analytically for oscillators. In addition, one can even use these analytically obtained bases in the numerics. In particular, one can find the density matrices for a half system because in the DMRG algorithm they are used.

As for the transverse Ising chain, the thermodynamic limit of the reduced density matrices for coupled oscillators can be obtained from a corner transfer matrix (CTM). The related classical model in this case is the Gaussian model in two dimensions. Those results can also be compared with the single-particle eigenvalues extracted from the $M \times M$ matrices and they show very good agreement.

Other interesting features for oscillators will be discussed in this context. One of them is the problem of boundary conditions. Although periodic and open boundary conditions are both utilized in the DMRG calculation, one normally works with open boundary conditions. This is due to the fact that the reduced density-matrix spectra for open boundaries drop much more rapidly than for periodic boundary conditions and thereby give a faster convergence. With the explicit single-particle eigenvalues of the density matrices for the oscillators, one can obtain the density-matrix spectra for the OBC and PBC analytically. One interesting feature is that one can understand the physics from the single-particle eigenvalues very well. For example, the almost two-fold degeneracies in the single-particles eigenvalues for periodic boundary conditions represent the two interfaces between the subsystem and environment. This leads to the logarithmically two-fold slower drop of the density-matrix spectra compared to those for

11

the open boundaries. This is the reason why periodic boundary conditions are less advantageous than open boundaries. In addition, one can investigate different kinds of couplings for the oscillators, especially long-range interactions. Specifically next-nearest-neighbor couplings and exponential couplings will be studied. Again, the single-particle eigenvalues give an impression on the physics for such systems.

However, the oscillators are only one example of a solvable bosonic system. In general, such a model is described by a Hamiltonian which can be written as a quadratic form of creation and annihilation operators. Then the question arises if one can also treat such a problem. This is indeed possible with a different approach which uses coherent states. As will be seen, the ground state for such bosonic systems can be written as an exponential function of creation operators acting on the vacuum. As a result, the reduced density matrices can be obtained by using the coherent states to integrate out the other variables. The single-particle eigenvalues ε_l can again be obtained from the eigenvalues of an $M \times M$ matrix. For the oscillators this matrix differs from the previous one, but the resulting ε_l are the same as before.

The advantage of this method is that one can generalize it to the analogous fermionic systems. Using the coherent states for fermions connected via Grassmann variables and fermionic creation operators, arbitrary reduced density matrices can be calculated exactly and also have the general form $\exp(-\mathcal{H})$ as for bosons. In contrast to the bosonic case, the operator $\mathcal{H}$ describes now a collective of noninteracting *fermions* with single-particle eigenvalues ε_l. The ε_l, which determine the properties of the spectrum, also follow from the eigenvalue of an $M \times M$ matrix. Using this method, the reduced density matrices for the transverse Ising chain, which can be viewed as a fermionic model, can be found for all sizes and parameters. The gradual change of the reduced density matrices as one approaches the critical point can be analyzed via the single-particle eigenvalues. Also the properties of the spectra at the critical point can be studied. Another one-dimensional fermion problem, namely the spin one-half XY chain in a field, is interesting because it has a disorder point where the ground state simplifies and the spectrum collapses. This is seen directly in the single-particle spectra.

So far, the DMRG method has been applied to some two-dimensional systems [33, 34], but the results are not convincing, because only small sizes can be reached (for $t - J$ model 12×12 lattice has been reached [33]). The situation has been discussed in some detail for free fermions [35] and for the transverse Ising model [36]. It is found that, if one couples one-dimensional chains to form ladders, the number m of states one needs to maintain a certain accuracy grows exponentially with the width of the system. This was derived either from the limit of noninteracting chains, or from numerical calculations. The spectra themselves, however, have not

been discussed so far, although they are the essential of the problem. In one dimension one can obtain very accurate results because the density-matrix spectra usually drop rapidly. In two dimensions, on the other hand, they decrease very slowly. To see this, one can apply our methods to some solvable two-dimensional models. This is possible because the dimensionality of the system plays no essential role in the treatment. The coupled oscillators and the tight-binding model are good examples for bosonic and fermionic systems. These systems can serve as test cases to see if one can put the DMRG into practice for the two-dimensional systems. It will be shown that the spectra for these examples drop slowly, and one needs many more states to obtain a good accuracy.

On can also apply the DMRG to problems from statistical physics, for example two-dimensional classical systems. In this case one has to work with transfer matrices and their eigenfunctions instead of a Hamiltonian. Because transfer matrices here are one-dimensional operators, one can use the DMRG to calculate them [7]. We will do this for the planar Ising model with line-like defects. This system is unusual because its magnetic exponent β_l is non-universal. Bariev has obtained β_l for the Ising plane with chain and ladder defects analytically [37] because such systems are integrable and solvable free fermion problems. For the nonintegrable case, for example the Ising plane with one or two additional lines of spins, one can use transfer-matrix DMRG to obtain the spontaneous magnetizations. From that, the non-universal magnetic exponent β_l can be determined as a function of the local couplings of the defect. In our calculation, it could be determined with an accuracy of 10^{-4}. This demonstrates that DMRG is a good method to calculate the critical properties.

I begin, in chapter 2, by discussing the DMRG algorithms. The infinite-system algorithm and finite-system algorithm will be introduced. In chapter 3, coupled oscillators in one and two dimensions will be discussed in detail. At the beginning I will show how one can obtain the reduced density matrices using the coordinate representation. The resulting spectra will be presented in a number of figures. The spectra in the thermodynamic limit and for various boundaries will also be considered. At the end of this chapter I will discuss the difficulties of the DMRG if the systems become more two-dimensional. As a bridge between bosonic and fermionic systems, I will consider the coherent-state treatment for solvable bosons in chapter 4. In chapter 5 the solvable fermionic systems in one and two dimension will be the subject. I will first consider transverse Ising chains. The spectra for XX spin chains and XY spin chains in a transversal field will be shown in section 5.2. In section 5.3 I will introduce the density matrices for the two-dimensional tight-binding model. As an application, in chapter 6, the Ising plane with line-like defects will be treated using the transfer-matrix DMRG. The transfer-matrix DMRG will be introduced briefly and the physical quantities calculated from the

method will be shown. Chapter 7, finally, contains a summary of the main results. Some technical details can be found in the appendices.

Chapter 2

Density-Matrix Renormalization Group

In this chapter, I will briefly introduce the DMRG algorithms. More details can be found in the reference [3].

2.1 Density Matrices

The main difficulty in finding accurate expressions for the ground states and the low-lying exited states results from the fact that the number of the states grows exponentially with sizes. To diagonalize a system of L spinless fermions, one needs 2^L states. Such calculations can be accomplished for small L, nevertheless, the calculation will rapidly exceed the capacity of the computer. The situation is even worse for bosonic systems, due to the fact that the Hilbert space on a site is infinite. In order to overcome the difficulty, the renormalization-group algorithm in the coordinate space to solve the Kondo problem was proposed by Wilson [Wilson]. In this treatment an isolated block with size l is chosen that the Hamiltonian can be diagonalized exactly. Using the m low-energy eigenstates obtained for a system of size l, one adds a site to that and builds a block of size $l + 1$. In this way one can enlarge a system. Typically, the number of states m is kept constant, so the time and memory required for each diagonalization is held the same. One does not have to face the problem of the exponentially increasing number of states.

Except for the Kondo and Anderson impurity problems, which include an intrinsic separation of energy scales, Wilson's RG procedure worked poorly when applied to other systems such as the one-dimensional Heisenberg or Hubbard models [12, 13]. The main source of error come from the boundaries. In Wilson's treatment one chooses eigenstates of the Hamiltonian of size l as representative states of a superblock. Since this Hamiltonian has no connection to the added site, its eigenstates may have unwanted features (like nodes) at the end of the block and this cannot be
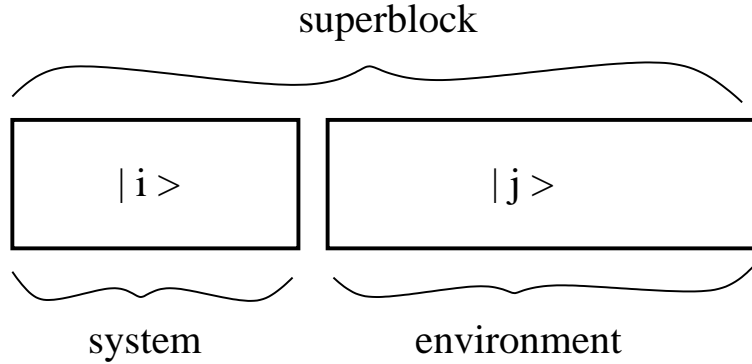
superblock

system environment

Figure 2.1: A superblock divided into a system block and an environment block

improved by increasing the number of kept states. Therefore an another RG procedure, where in the selected eigenfunctions the boundaries are considered, is needed.

White proposed a new algorithm - density-matrix renormalization group (DMRG) to solve such chain problems. Different from the Wilson's treatment, a system is only divided into two parts and the eigenfunctions of the reduced density matrices are used instead of those of the Hamiltonian. In this procedure the boundary effect is automatically included and therefore it gives good accuracies in the calculations.

To see the method clearly, I will introduce the principle of DMRG. The question is as follows: How can one find the best kept states used to enlarge the system? To construct these states, the entire system labelled the superblock is divided into a system block and an environment block (see Fig. 2.1). Let $\mid i \rangle$ label the states of the system block, and $\mid j \rangle$ label the states of the environment block. If ψ is a state of the superblock,

$$\mid \psi \rangle = \sum_{ij} \psi_{ij} \mid i \rangle \mid j \rangle. \tag{2.1}$$

The density matrix is then

$$\rho = \mid \psi \rangle \langle \psi \mid . \tag{2.2}$$

The reduced density matrix for the system is defined as

$$\rho_1 = \text{Tr}_j \rho = \sum_j \psi_{ij}^* \psi_{i'j} \mid i \rangle \langle i' \mid . \tag{2.3}$$

If ρ is chosen to be normalized, ρ_1 is automatically normalized. The matrix elements of reduced density matrix thus have the form

$$[\rho_1]_{ii'} = \sum_j \psi_{ij}^* \psi_{i'j}. \tag{2.4}$$

16

The reduced density matrix has all the information needed from the wave-function ψ to calculate any properties restricted to the system block. For example, if operator A acts only on the system block, its expectation value is given by

$$\langle A \rangle = \text{Tr}\rho_1 A = \sum_{ii'} A_{ii'}[\rho_1]_{i'i}. \tag{2.5}$$

Now one is searching for the best representative eigenstates for ρ_1, that can be reached by diagonalizing ρ_1. Let ρ_1 have eigenstates $\mid u^\alpha \rangle$ and eigenvalues $w_\alpha \geq 0$ with the descending arrangement. The normalization of ρ_1 means $\sum_\alpha w_\alpha = 1$. Hence for any system block operator A,

$$\langle A \rangle = \sum_\alpha w_\alpha \langle u^\alpha \mid A \mid u^\alpha \rangle. \tag{2.6}$$

Choosing only the m eigenstates with the largest eigenvalues w_α, the expectation value of A becomes

$$\langle A \rangle_t = \sum_{\alpha=1}^m w_\alpha \langle u^\alpha \mid A \mid u^\alpha \rangle. \tag{2.7}$$

Thus the error of the expectation value is given as

$$\delta \langle A \rangle = \langle A \rangle - \langle A \rangle_t = \sum_{\alpha > m} w_\alpha \langle u^\alpha \mid A \mid u^\alpha \rangle. \tag{2.8}$$

By defining the largest value of $|\langle u^\alpha \mid A | u^\alpha \rangle \mid$ to be $\mathcal{A}_l$, then $\delta \langle A \rangle$ corresponds to the relation

$$|\delta \langle A \rangle| \leq \mathcal{A}_l (1 - \sum_{\alpha=1}^m w_\alpha). \tag{2.9}$$

Therefore the error depends on the quantity

$$P = 1 - \sum_{\alpha=1}^m w_\alpha \tag{2.10}$$

defined as the truncation error. Throwing away states with small eigenvalues w_α, we make little errors in $\langle A \rangle$ as long as P is small. Thus those states $\{\mid u^\alpha \rangle, \alpha \leq m\}$ give the best representative ones for the system block.

2.2 DMRG Algorithms

In the last section, I described how to use reduced density matrices to construct the kept states. In this section, I will consider how to enlarge systems by adding degrees of freedom to the system.
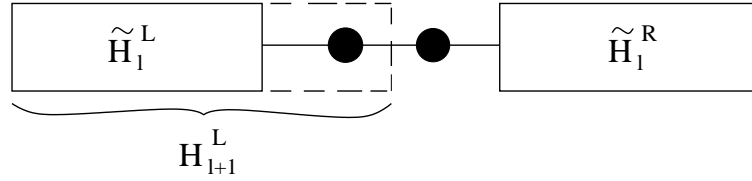
Figure 2.2: The superblock configuration for the infinite-system algorithm

One usually starts the DMRG algorithm with $L = 4$, then increases the its size (to $L+2, L+4, \ldots$) until the desired length is reached. There are two algorithms to enlarge the systems: the infinite-system algorithm and finite-system one, depending on how the environment block is chosen. I will discuss these algorithm in details below.

Using DMRG, one can find the properties for ground states and for the first few excited states. The superblock state or states used to form the reduced density matrix for the system block are called target states. If only ground state properties are desired, one uses the ground state as a target, otherwise more states are used. For simplicity, I will assume that only the ground state is targeted in the following.

2.2.1   The Infinite-System Algorithm

The straightforward way to extend the Wilson procedure is the infinite system algorithm. By tracing out the environment block or the system block and using m states for the superblock of size l, one forms the Hamiltonian $\tilde{H}_l^L$ for the system block in the reduced basis and the one $\tilde{H}_l^R$ for the environment block. These two Hamiltonians are used to form the superblock of size $l + 2$. This superblock configuration is shown in Fig. 2.2, where the solid dots represent single sites. Note that in the homogeneous and hermitian systems the $\tilde{H}_l^R$ is a reflection of the $\tilde{H}_l^L$, which can be formed by relabeling the sites in the system block so that they are reflected onto the right part of the lattice.

The infinite-system algorithm then proceeds as follows:

1. Form a small superblock of size L which is small enough to be exactly diagonalized. For the beginning, $L = 4$ is preferable.

2. Diagonalize the superblock Hamiltonian H_L^{super} numerically, giving the ground state $\mid \Phi_0 \rangle$.

3. Form the reduced density matrix ρ_1 using (2.3).

4. Diagonalize ρ_1 to obtain the m eigenvectors with the largest eigenvalues.

5. Construct H_{l+1}^L and other operators in the new system block.

6. Transform the H^L_{l+1} and the operators to the reduced density matrix eigenbasis using

$$\tilde{H}^L_{l+1} = \tilde{O}^\dagger_L H^L_{l+1} \tilde{O}_L$$
$$\tilde{A}^L_{l+1} = \tilde{O}^\dagger_L A^L_{l+1} \tilde{O}_L \tag{2.11}$$

   etc., where $\tilde{O}_L$ only contains the m highest eigenvectors of ρ_1, and A_{l+1} is an operator in the system block with size $l+1$.

7. Repeat steps 3-6 for the environment block to form $\tilde{H}^R_{l+1}$ and related operators for the environment block.

8. Form a superblock of size $L+2$ with $\tilde{H}^L_{l+1}$, $\tilde{H}^R_{l+1}$ and two single sites.

9. Repeat starting with step 2, substituting H^{super}_{L+2} for H^{super}_L.

The measurement in the reduced eigenbasis should be mentioned here. Measurements are made using the superblock wavefunction $\mid \psi \rangle$ to evaluate expectation values. To measure an on-site operator A_l on the l-th site, for example, the expectation value of A_l is given as

$$\langle \psi \mid A_l \mid \psi \rangle = \sum_{i,i',j} \psi^*_{ij} [A_l]_{ii'} \psi_{i'j}. \tag{2.12}$$

For a correlation function such as $\langle \psi \mid A_l A_m \mid \psi \rangle$, the evaluation depends on whether l and m are on the same block or not. If they are on the different blocks, the correlation value can be expressed as

$$\langle \psi \mid A_l A_m \mid \psi \rangle = \sum_{i,i',j,j'} \psi^*_{ij} [A_l]_{ii'} [A_m]_{jj'} \psi_{i'j'}. \tag{2.13}$$

If l and m are not on the same block, one should not only have kept track of $[A_l]_{ii'}$ and $[A_m]_{i'i''}$ as in (2.13), but needs to have kept track of $[A_l A_m]_{ii'}$ throughout the calculation, and one has

$$\langle \psi \mid A_l A_m \mid \psi \rangle = \sum_{i,i',j'} \psi^*_{ij} [A_l A_m]_{ii'} \psi_{i'j'}. \tag{2.14}$$

The reason is that if one would like to evaluate the correlation value of two operators from the two independent measurements of them, it is needed to separate them with a complete basis. Since an incomplete reduced eigenbasis has been chosen in the algorithm, the Eqn. (2.14) is needed to obtain the correlation function.

In the infinite-system algorithm, one makes an approximation that the reduced density matrix for the system block of size L offers a good basis for the construction of the superblock with the size $L+2$. This assumption is true for the homogeneous systems with the size much larger than the correlation length, but for some other systems one needs a sweeping process to improve the accuracy, this is so-called the finite-system algorithm.
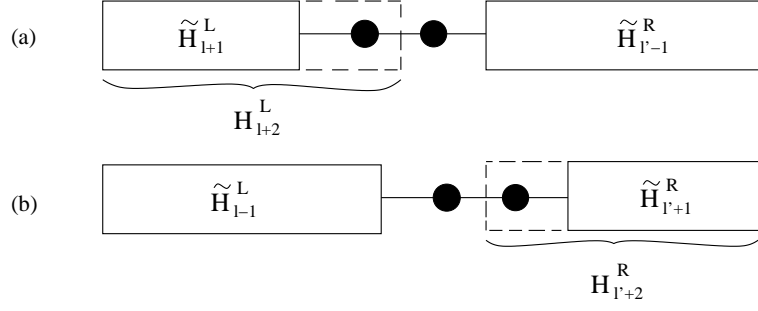
Figure 2.3: The superblock configuration for the finite-system algorithm, (a)a left to right sweeping process (b) a right to left sweeping process.

2.2.2   The Finite-System Algorithm

To improve the accuracy for the systems with finite sizes, the finite system algorithm is used. The difference between the infinite-system and finite-system algorithm is how to choose the environment block to form a superblock. In the finite-system algorithm, it is chosen so that the size of the superblock is maintained fixed at each step. Having run the infinite-system algorithm until the superblock reaches size L and having stored all the $\tilde{H}_l^L$ and $\tilde{H}_{l'}^R$ for $l, l' = 1, \ldots, L/2 - 2$ as well as the all the additional operators needed to connect the block at each steps, one can continue to build up the system block, but keep $L = l + l' + 2$ fixed by using the appropriate previously stored $\tilde{H}_{l'}^R$. The finite-system algorithm then is described below (see also Fig. 2.3):

1. Carry out the infinite-system algorithm until the superblock reaches size L, storing $\tilde{H}_l^L$, $\tilde{H}_{l'}^R$ and the operators needed to connect the blocks at each step.

2. Carry out step 3-6 of the infinite-system algorithm to obtain $\tilde{H}_{l+1}^L$. Store it.

3. Using $\tilde{H}_{l+1}^L$, two single sites and $\tilde{H}_{l'-1}^R$ ($l' = l$), form a superblock of size L. Store $\tilde{H}_{l+2}^L$ and needed operators.

4. Repeat steps 2-3 until $l = L - 3$ ($l' = 1$). This is the left to right sweeping of the algorithm.

5. Form a superblock of size L using $\tilde{H}_{L-l'-2}^L$, two single sites and $\tilde{H}_{l'}^R$. Start with $l' = 1$.

6. Interchanging the role of $\tilde{H}_l^L$ and $\tilde{H}_{l'}^R$, carry out 5-6 of the infinite-system algorithm to obtain $\tilde{H}_{l'+1}^R$. Store it.

7. Repeat steps 5-6 until $l = 1$. This is the right to left sweeping of the algorithm.

8. Repeat starting with step 2 and $l = 1$.

If reflection symmetry is present, one only needs to run the left to right sweeping. The right to left sweeping is identical to the left to right.

Now the question is: How much can the sweeping procedure improve the accuracy? White and Noack [38] investigated the ground-state energy of the one-dimensional Hubbard model, compared with the exact solution obtained from the Bethe Ansatz. They showed that the improvement of the accuracy depends not only on the iteration, but also on the number m of states one uses. With more kept states, the sweeping procedure can increase the precision more easily through the iteration. For some other systems such as inhomogeneous chains and the two-dimensional lattices, the sweeping is absolutely needed. The sweeping can lower the inaccuracy caused by the unsymmetry of the systems in the infinite-system algorithm.

2.3 Density-Matrix Spectra

In this section I would like to emphasize the importance of the density-matrix spectra. From Eqn. (2.9), one can see that the problem whether DMRG can give a good accuracy depends on the reduced density-matrix spectra. The spectra determine how many states one can leave out in the calculation. For example, if the spectrum for a system drops rapidly, one can use relatively few states to achieve a good accuracy in the calculation. The reason is that then most states have relative small eigenvalues and influence the calculation barely. On the other hand, for a slowly decreasing spectrum, many more states have to be used. Such systems will cause computational problems.

Using the spectra, one can explain some aspects of DMRG. For example, the calculations for critical systems are more difficult than those for systems far from the critical points. Computing the density-matrix spectra, those for critical systems fall more slowly than the systems not in the critical point. Another example is the periodic boundary condition. The reason why in the DMRG calculation open boundary conditions are used more than periodic ones is that one needs to use almost quadratically more states in the calculations for the PBC than for the OBC to reach the same precision. Though this is known that in the PBC one has two cuts with the environment instead of one cut in the OBC [39], but the corresponding density-matrix spectra were not shown. With these spectra, one can easily explain such phenomena.

Some authors have tried to use DMRG to calculate the two-dimensional systems [33, 34, 36, 35] but by now only small systems can be reached. The most difficult problem one has met is that a very large number of kept states have to be used. For example, for a $t - J$ models with 12×12 lattice, White used 4000 states to obtain better results [33]. This difficulty

will be reflected in the density-matrix spectra. The spectra will decrease much more slowly than one-dimensional systems. We can conclude that if one tries to check the density-matrix spectra in the calculation one can obtain an impression on how difficult the calculation will be.

For some solvable models, the density-matrix spectra can be calculated not only numerically but also analytically. In the next three chapters I would like to show the analytical density-matrix spectra of solvable models in the different situations mentioned above. The most important is that one can also obtain the spectra for two-dimensional systems such as coupled oscillators and tight-binding models. Those spectra will give us some hints for computing the two-dimensional quantum systems. I will discuss these aspects in detail in the next chapters.

Chapter 3

Coupled Oscillators

Boson systems are a challenge for the DMRG because they differ from spin and fermion systems in that the full Hilbert space is infinite, even for a single site. Therefore, it is necessary to start with a truncation, which is analogous to the DMRG procedure by choosing infinite local bases via the density matrix for one site [25]. Nevertheless, a nontrivial quantity with an infinite number of eigenstates must be treated. It is thus interesting to find the desired properties in a solvable case. In this chapter, I will consider interacting oscillators [40, 41].

The Hamiltonian of interacting oscillators can be written as

$$H = \sum_i \left(-\frac{1}{2} \frac{\partial^2}{\partial u_i^2} + \frac{1}{2} \omega_0^2 u_i^2 \right) + \sum_{i,j} \frac{1}{2} k_{ij} (u_i - u_j)^2, \qquad (3.1)$$

where u_i is the coordinate of the i-th oscillator and ω_0 its frequency. The masses are all equal to unity and the oscillators are coupled by springs of strength k_{ij}. One can diagonalize H with two methods: The first one is using normal coordinates, with which one can immediately write down the ground-state function. The second one is using the bosonic operators and the Bogoliubov transformation. In this chapter I will concentrate on the coordinate representation and on the ground-state properties. In the next chapter, I will consider more general results for the excited states using the bosonic operators.

In section 3.1 the density matrix ρ_{sg} for one oscillator is first considered. As will be seen, ρ_{sg} can be written as the exponential of the Hamiltonian of a (new) harmonic oscillator. In section 3.2 I consider the reduced density matrix ρ_1 for an arbitrary division of subsystem block and environment block. This is shown to have an exponential form consisting of the same number of bosonic operators as the system block.

In the first four sections I discuss an important example,namely open chains of nearest-neighbor coupled oscillators. In this case we will use the form $\omega_0 = 1 - k$, so that for $k = 0$ there is no dispersion, while for $k \to 1$ the system becomes acoustic and has infinite correlation length,

that means, the system is critical. In section 3.2 the density matrix ρ_h for one half chain is obtained. I discuss here also the difference between periodic and open boundaries. The result in the thermodynamic limit is derived in section 3.3 by relating the chain to a massive two-dimensional Gaussian model and its corner transfer matrices (CTMs). The result is similar to the spin chains, considered by Peschel *et al.* in [42], which gives an exponential form consisting of fermionic operators instead of bosonic ones. In section 3.4 I first discuss the squeezed states which are related to the eigenstates of ρ_{sg} and use them in the numerical calculations to obtain the spectra of ρ_h. We can see in this section, how the squeezed(optimal) states emerge in the spectra.

Since the method discussed here can be applied to harmonic oscillators with any kind of interaction and in an arbitrary dimension , we can extend it to various physically interesting phonon systems. In section 3.5 I discuss oscillators with next-nearest-neighbor couplings and exponential ones. DMRG calculations in two dimensions have been discussed in several papers [33, 34, 36, 35]. It is found that one has to keep many more states to obtain a certain accuracy. Section 3.6 contains the two-dimensional density-matrix spectra and a discussion of the reason for the difficulties in the two-dimensional systems.

3.1   Density Matrix for One Oscillator

3.1.1   Density Matrix for Ground State

At the beginning we consider the case where one oscillator is singled out and all others form the environment. The previous authors have numerically determined the corresponding density matrix in the study of an electron-phonon system [25], however, here it can be obtained analytically.

We consider now a system with L oscillators. The coordinate representation of the ground state of H in (1) can be written as

$$
\begin{aligned}
\Psi(\boldsymbol{u}) &= \langle \boldsymbol{u} \mid \Psi \rangle \\
&= C \cdot \exp\left(-\frac{1}{2}\sum_{ij} A^g_{ij} u_i u_j\right),
\end{aligned} \qquad (3.2)
$$

where u_i is the coordinate of the ith oscillator and $\boldsymbol{u} = (u_1, u_2, \cdots, u_L)$. The matrix

$$
A^g_{ij} = \sum_q \omega_q \phi_q(i) \phi_q(j) \qquad (3.3)
$$

is determined by the frequencies ω_q and the eigenvectors $\phi_q(i)$ of the normal modes. From the definition of the total density matrix

$$
\rho = \mid \Psi \rangle \langle \Psi \mid, \qquad (3.4)
$$

one can form matrix elements in the coordinate space

$$\begin{aligned} \rho(\boldsymbol{u},\boldsymbol{u}') &= \langle \boldsymbol{u} \mid \rho \mid \boldsymbol{u}' \rangle \\ &= \Psi(\boldsymbol{u})\Psi(\boldsymbol{u}'). \end{aligned} \tag{3.5}$$

Then the reduced density matrix for oscillator l can be found by integrating over all other coordinates $u_i = u'_i$. This can be done explicitly since (3.2) is a quadratic form in the u_i and leads to

$$\begin{aligned} \rho_{sg}(u_l, u'_l) &= C_{sg} \exp\left(-\frac{1}{2}(a-b)u_l^2\right) \exp\left(-\frac{b}{4}(u_l - u'_l)^2\right) \\ &\times \exp\left(-\frac{1}{2}(a-b)u_l'^2\right) \end{aligned} \tag{3.6}$$

with the constants

$$\begin{aligned} a &= A^g_{ll} \\ b &= \sum_{i,j \neq l} A^g_{li} \, [A^g_{(l)}]^{-1}_{ij} \, A^g_{jl}, \end{aligned} \tag{3.7}$$

where $A^g_{(l)}$ is the matrix obtained from A^g by deleting the l-th row and column.

The operator form of the reduced density matrix ρ_{sg} can be constructed in the following way. The left and right parts of the Eqn. (3.6) are merely the same exponential form with coordinate operator u_l because the matrix elements are formed between two coordinate eigenstates. On the other hand, the second exponential can be transformed into a differential operator using the relation

$$\sqrt{\frac{b}{2}} \exp\left(-\frac{b}{4}(u_l - u'_l)^2\right) = \langle u_l \mid \exp\left(\frac{1}{b}\frac{\partial^2}{\partial u_l^2}\right) \mid u'_l \rangle \tag{3.8}$$

which can be obtained by differentiating the δ function $\langle u_l \mid u'_l \rangle$ of Eqn. (3.8) in the Fourier space and integrate it out (for the details and some other aspects see the appendix A). Thus ρ_{sg} can be found as

$$\rho_{sg} = C_2 \cdot \exp\left(-\frac{1}{4}\omega^2 y^2\right) \exp\left(\frac{1}{2}\frac{\partial^2}{\partial y^2}\right) \exp\left(-\frac{1}{4}\omega^2 y^2\right) \tag{3.9}$$

where $y^2 = bu_l^2/2$ and $\omega^2/4 = (a/b - 1)$. In terms of the Bose operator

$$\alpha = \sqrt{\frac{\omega}{2}}y + \frac{1}{\sqrt{2\omega}}\frac{\partial}{\partial y}, \qquad \alpha^\dagger = \sqrt{\frac{\omega}{2}}y - \frac{1}{\sqrt{2\omega}}\frac{\partial}{\partial y}, \tag{3.10}$$

ρ_{sg} reads

$$\begin{aligned} \rho_{sg} = C_3 \cdot &\exp\left(-\frac{\omega}{8}(\alpha + \alpha^\dagger)^2\right) \\ &\exp\left(\frac{\omega}{4}(\alpha - \alpha^\dagger)^2\right) \exp\left(-\frac{\omega}{8}(\alpha + \alpha^\dagger)^2\right). \end{aligned} \tag{3.11}$$

One can diagonalize ρ_{sg} with a proper Bogoliubov transformation

$$\beta \;=\; \cosh\theta \cdot \alpha \;+\; \sinh\theta \cdot \alpha^\dagger, \tag{3.12}$$

where the parameter θ is obtained by the equation

$$e^\theta \;=\; \left(1 + \frac{\omega^2}{4}\right)^{1/4}. \tag{3.13}$$

Finally, ρ_{sg} has the diagonal form

$$\rho_{sg} \;=\; K_{sg} \cdot \exp\left(-\mathcal{H}\right), \tag{3.14}$$

where

$$\mathcal{H} \;=\; \varepsilon\,\beta^\dagger\,\beta \tag{3.15}$$

is the Hamiltonian of a harmonic oscillator with energy

$$\varepsilon \;=\; 2\sinh^{-1}(\frac{\omega}{2}) \;\;=\; 2\sinh^{-1}\left(\sqrt{a/b - 1}\right). \tag{3.16}$$

ε will be called the single-particle eigenvalue for the reduced density-matrix ρ_{sg}. The eigenvalues of ρ_{sg} are then $w_j = K_{sg}e^{-\varepsilon j}, j \geq 0$, where the constant K_{sg} can be found from the sum rule $\mathrm{Tr}(\rho_{sg}) = \sum_j w_j = 1$.

The density-matrix spectrum for one oscillator at a certain site depends only on the ratio a/b, which contains all of the information about the system and can be obtained from the equations (3.7). It is completely general, whatever the system is. For example, we can deal with inhomogeneous oscillating systems as well as homogeneous ones, or oscillators with long-range interactions.

3.1.2 Open Chain

In this subsection, we consider an open chain of next neighbor coupled oscillators with the same coupling k. The Hamiltonian has the form

$$H_1 \;=\; \sum_{i=1}^{L}\left(-\frac{1}{2}\frac{\partial^2}{\partial x_i^2} + \frac{1}{2}\,\omega_0^2\,x_i^2\right) + \sum_{i=1}^{L-1}\frac{1}{2}\,k\,(x_{i+1} - x_i)^2. \tag{3.17}$$

The simplest case is one for the two couple oscillators, where single-particle eigenvalue reads

$$\varepsilon \;=\; 2\sinh^{-1}\left(\sqrt{4\omega_1\omega_2/(\omega_1 - \omega_2)^2}\right), \tag{3.18}$$

or, equivalently,

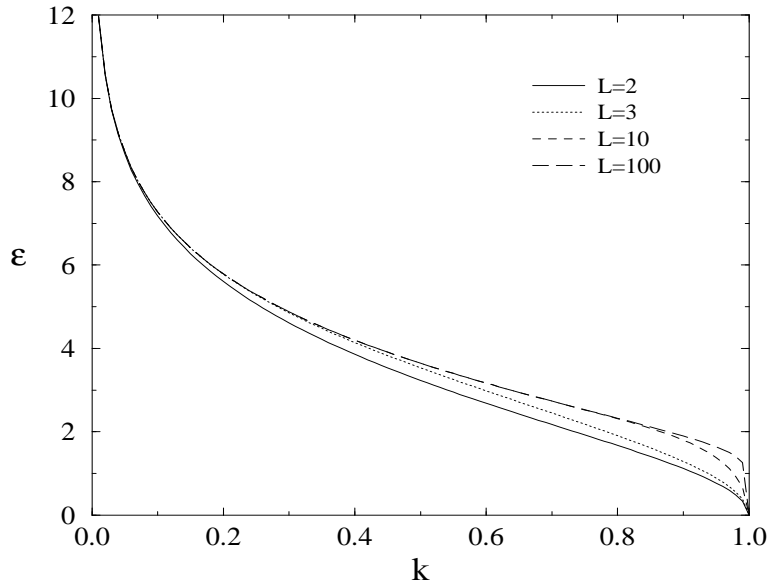$$\varepsilon \;=\; \ln\left(\coth^2(\frac{\eta}{2})\right), \tag{3.19}$$

Figure 3.1: Eigenvalue ε in the density matrix for an oscillator at the end of a chain, as a function of k for different lengths L and $\omega_0 = 1 - k$

where $\omega_1 = \omega_0$, $\omega_2 = \sqrt{\omega_0^2 + 2k}$ are the two eigenfrequencies and $e^{2\eta} = \omega_2/\omega_1$. This is the result obtained in [43] in a different way.

In Fig. 3.1, ε calculated at the end of a chain with size L is plotted as a function of k, putting $\omega_0 = (1 - k)$. Displayed are the calculated curves with different sizes L. The two limits $k \to 0$ and $k \to 1$ are physically interesting. In the case of $k \to 0$, ε diverges logarithmically and all eigenvalues of ρ_{sg} except one go to zero, which represents the fact that the oscillators decouple from each other. In this limit, $|\Psi\rangle$ becomes a product state composed of only one-oscillator state with the frequency ω_0 at different sites. Integrating out the variables at the other sites, which gives only a constant, a one-oscillator state is left and it has only one non-zero eigenvalue $w_0 = 1$. On the other hand, if $k \to 1$, ε goes to zero as $\sqrt{1-k}$ and the eigenvalues w_n decrease very slowly, which corresponds to the systems with strong couplings. At this critical point, the ground-state eigenfunction is independent of the center of mass motion, and this is a synchronized mode, thereby giving an unnormalized eigenfunction. The density matrix therefore is also unnormalized. This singularity gives $\varepsilon = 0$. For the cases $L = 2$ and $L = 3$, one can obtain the features analytically, however, all other cases also own the same features. In Fig. 3.1, two addition cases, $L = 10$ and $L = 100$ are shown. One should note that the difference between $L = 10$ and $L = 100$ is very small in the beginning, but it becomes larger as k exceed 0.8. This results from the relative larger correlation length compared with the size L as $k \to 1$.
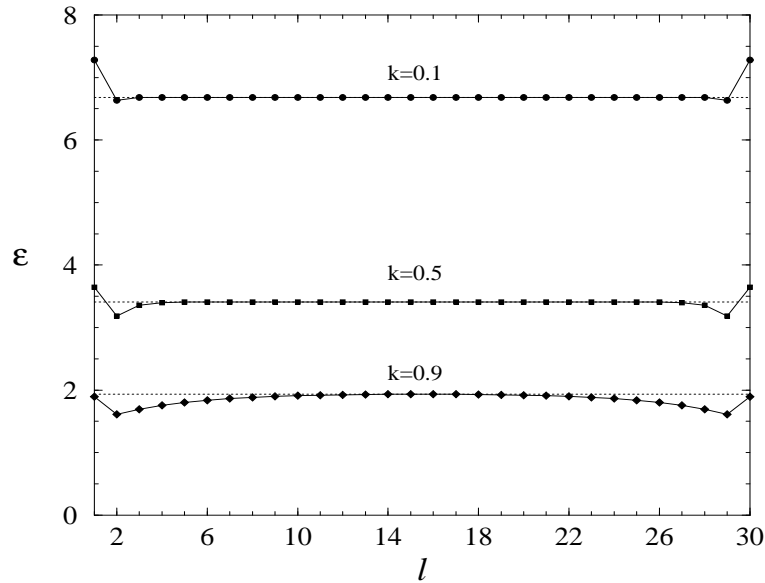
Figure 3.2: Eigenvalue ε as a function of the position of the oscillator, for a chain of $L = 30$ sites and three different values of k.

However, the limit $L \to \infty$, which is approached exponentially in L with the correlation function, is indistinguishable from $L = 100$ on the given scale.

The relation between ε and the position along the chains is investigated in Fig. 3.2, where different curves with various k are plotted. ε is relatively larger at the end, which reflects the fact that the influence of the surrounding here is smaller. It drops at the second site but rises to the bulk values. How fast it rises depends on the value of k. If k is small, it raises rapidly to the expected values, on the other hand, if k becomes larger, the approach slows down owing to the increased correlation length. The overall differences in the ε-values are not very large, though, as seen in Fig. 3.2.

The result which we obtain here can be used to construct the optimal bases for the numerical calculation. What we should do is to squeeze the uncoupled states in order that one can efficiently carry out the DMRG calculation only with the first few states. The details will be discussed in section 3.4.

3.2 Density Matrix for Arbitrary Partitions

3.2.1 Diagonalization of the Density Matrix

In the last section, we have considered the density-matrix spectrum for one oscillator under the influence of the other oscillators. In this section, we will describe how to calculate the density-matrix spectra for an arbitrary division subsystem.

Separating the oscillators into two parts, the system part 1 and the environment part 2, and integrating out the environment part of coordinate of the total density matrix ρ in (3.5), one obtains the reduced density matrix

$$\rho_1(\boldsymbol{u}_1, \boldsymbol{u'}_1) = C_4 \; \cdot \exp\left(-\frac{1}{2}\boldsymbol{u}_1^T(\boldsymbol{A} - \boldsymbol{B})\boldsymbol{u}_1\right)$$

$$\exp\left(\frac{1}{4}(\boldsymbol{u}_1 - \boldsymbol{u'}_1)^T\boldsymbol{B}(\boldsymbol{u}_1 - \boldsymbol{u'}_1)\right)\exp\left(-\frac{1}{2}\boldsymbol{u'}_1^T(\boldsymbol{A} - \boldsymbol{B})\boldsymbol{u'}_1\right), \quad (3.20)$$

where the vectors $\boldsymbol{u}_1 = (u_1, u_1, \cdots)$ and $\boldsymbol{u'}_1 = (u'_1, u'_2, \cdots)$ are composed only of the coordinate u_i of the system part 1 and the matrices A, B can be determined by the equations

$$\begin{aligned} \boldsymbol{A} &= a_{11}^g \\ \boldsymbol{B} &= a_{12}^g(a_{22}^g)^{-1}a_{21}^g \end{aligned} \qquad (3.21)$$

with the four submatrices $a_{11}^g, a_{12}^g, a_{21}^g, a_{22}^g$ of A^g in (3.2). The submatrices $a_{\alpha\beta}^g, \alpha, \beta = 1, 2$ contain the matrix elements of matrix A_{ij}^g which i belongs to the part α and j belongs to the part β. In other words, one divides the matrix A^g into four submatrices $a_{\alpha\beta}^g$, according to whether sites i and j belong to the system part 1 or environment part 2. Keeping M system sites in L oscillators, the dimension of the submatrices $a_{\alpha\beta}^g$ are following: a_{11}^g is $M \times M$, a_{12}^g $M \times (L - M)$, a_{21}^g $(L - M) \times M$ and a_{22}^g $(L - M) \times (L - M)$. Owing to the symmetry of the real matrix A^g in the case of coupling oscillators, $\boldsymbol{A}$ and $\boldsymbol{B}$ are all real and symmetric Matrices.

Comparing the Eqn. (3.21) with the Eqn. (3.7), one finds that they are very similar except that the matrices $\boldsymbol{A}$ and $\boldsymbol{B}$ appear rather than the real numbers a, b. Rotating the coordinate twice and transforming the matrix-element representation into an operator form, one can express the reduced density matrix as

$$\begin{aligned} \rho_1 =& C_1 \cdot \exp\left(\sum_l -\frac{1}{2}(\lambda_l - 1)v_l^2\right) \\ & \exp\left(\sum_l \frac{\partial^2}{\partial v_l^2}\right)\exp\left(\sum_l -\frac{1}{2}(\lambda_l - 1)v_l^2\right), \qquad (3.22) \end{aligned}$$

where λ_l are the eigenvalues of the matrix

$$\boldsymbol{B}^{-1}\boldsymbol{A} = \left(a_{12}^g (a_{22}^g)^{-1} a_{21}^g\right)^{-1} a_{11}^g, \tag{3.23}$$

and $\boldsymbol{v} = (v_1, v_2, \cdots)$ is found as

$$\boldsymbol{v} = \boldsymbol{P}^T \boldsymbol{B} \boldsymbol{u}_1 \tag{3.24}$$

with the eigenvector matrix $\boldsymbol{P}$ of the matrix $\boldsymbol{B}^{-1}\boldsymbol{A}$. ρ_1 is merely a product of operators with uncoupled coordinates, therefore one can diagonalize it with the Bogoliubov transformation used in the last section. The diagonalized form of ρ_1 reads

$$\rho_1 = K_1 \cdot \exp\left(-\sum_l \varepsilon_l \mathcal{B}_l^\dagger \mathcal{B}_l\right) \tag{3.25}$$

with Bose operators $\mathcal{B}_l$ and $\mathcal{B}_l^\dagger$. The single-particle eigenvalues ε_l can be found as

$$\varepsilon_l = 2 \cdot \cosh^{-1}\sqrt{\lambda_l}, \tag{3.26}$$

or equivalently,

$$\lambda_l = \cosh^2\left(\frac{\varepsilon_l}{2}\right). \tag{3.27}$$

As a consequence, the eigenvalues of ρ_1 read

$$w_n = K_1 \cdot \exp\left(-\sum_l \varepsilon_l m_l\right), \quad m_l = 0, 1, 2, \ldots, \tag{3.28}$$

where n is determined by ordering such exponential eigenvalues according to their magnitude. The constant K_1 is obtained from the normalization of ρ_1, namely, $\mathrm{Tr}(\rho_1) = 1$.

The result is valid not only for coupled harmonic oscillators with arbitrary kinds of couplings but also for any kind of partition. For example, the density matrix for one oscillator discussed in the last section can be viewed as a special case of the result. The ground-state matrix A^g contains all the information about the oscillators while the submatrices $a_{\alpha\beta}^g$ include the details of the partition. The ε_l can be found from the M eigenvalues of $(a_{12}^g (a_{22}^g)^{-1} a_{21}^g)^{-1} a_{11}^g$ using the relations (3.26) if M oscillators are kept in the system part 1.

3.2.2 Density Matrix for a Half-Chain

Density matrices for a half-chain are of particular interest, because they are used in the infinite-size version of the DMRG. The spectra decide how many truncated states one should take. Therefore, such density-matrix spectra can give us some physical aspects relating to the numerical calculations.

Here we consider again an open chains of coupled oscillators with the Hamiltonian (3.17). Given system of even size $L = 2M$, the single-particle eigenvalues ε_l of the density-matrix can be found from Eqn. (3.23) and Eqn. (3.26), which can be approximated as $\varepsilon_l \sim 2 \ln \sqrt{\lambda_l}$, if λ_l is much larger than 1. In our calculation fourfold precision is applied. That means, one can obtain precise λ_l not larger than 10^{32}. We can thus calculate ε_l only accurate if they are smaller than $\ln(10^{32}) \sim 75$. Sometimes this is not enough for the calculations, especially in the case of systems with large sizes or with smaller couplings.

To improve the range of the calculation, we can use the reflection symmetry of the homogeneous system. With this symmetry the odd and even eigenfunctions of the Hamiltonian with respect to the reflection point in the middle read

$$
\begin{aligned}
\phi_{q_1}(i) &= +\phi_{q_1}(2M + 1 - i) \\
\phi_{q_2}(i) &= -\phi_{q_2}(2M + 1 - i),
\end{aligned}
\tag{3.29}
$$

where q_1, q_2 are the quantum number in the momentum space referring to the even and odd eigenfunctions. Using (3.29) one can define two $M \times M$ matrices *only in the system block 1*

$$
\begin{aligned}
E_{\gamma\delta} &= \sum_{q_1} \omega_{q_1} \phi_{q_1}(\gamma) \phi_{q_1}(\delta) \\
O_{\gamma\delta} &= \sum_{q_2} \omega_{q_2} \phi_{q_2}(\gamma) \phi_{q_2}(\delta),
\end{aligned}
\tag{3.30}
$$

where

$$
1 \le \gamma, \delta \le M.
\tag{3.31}
$$

In this way the four matrices $a_{\alpha\beta}^g$ can be rewritten in terms of the matrices $\boldsymbol{E}$, $\boldsymbol{O}$ and a reflection matrix $\boldsymbol{U}$, is discussed in the Appendix, and the matrix $\boldsymbol{B}^{-1}\boldsymbol{A}$ can be expressed as

$$
\boldsymbol{B}^{-1}\boldsymbol{A} = \left((\boldsymbol{E} - \boldsymbol{O})^{-1} (\boldsymbol{E} + \boldsymbol{O}) \right)^2.
\tag{3.32}
$$

Thus $\boldsymbol{B}^{-1}\boldsymbol{A}$ is the square of the matrix $(\boldsymbol{E} - \boldsymbol{O})^{-1}(\boldsymbol{E} + \boldsymbol{O})$, we can double the precision by calculating the eigenvalues of the latter matrix, or equivalently, the eigenvalues of the matrix $\boldsymbol{O}^{-1}\boldsymbol{E}$. One finds that the eigenvalues ε_l can be obtained from the equation

$$
(\boldsymbol{O}^{-1}\boldsymbol{E})\varphi_l = \tanh^2(\varepsilon_l/4)\varphi_l
\tag{3.33}
$$

with the eigenfunctions φ_l. Therefore, the ε_l are accurate to 150 and the eigenvalues w_n to 10^{-64} with the quartic precision in the calculation.

In Fig. 3.3 the single-particle eigenvalues ε_l are plotted for $L = 20$ and different coupling constants k. For $k = 0.1$ they all lie on a straight line, which shows approximately the relation

$$
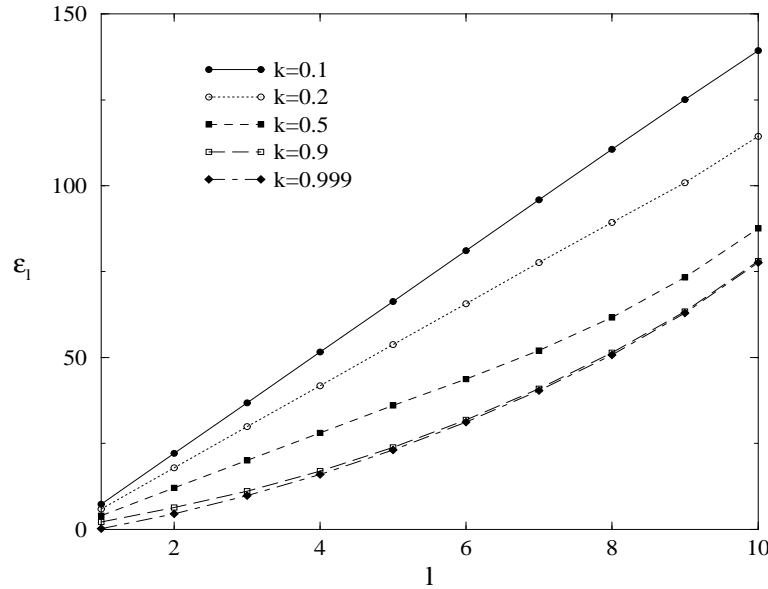\varepsilon_l = (2l - 1)\varepsilon_1,
\tag{3.34}
$$

31

Figure 3.3: Single-particle eigenvalues ε_l for one-half of an oscillator chain, the system is in the ground state, $L = 20$.

which corresponds to the situation one finds in the thermodynamic limit. The phenomenon can be understood if the one-dimensional oscillators are connected to the Gauss model in two dimension and corner transfer matrices , which will be discussed in next section. In the case of $k \ll 1$ i.e. far away from the critical point, the correlation length is much less than L and hence the boundary condition should not influence the spectra much. For next larger coupling, $k = 0.2$, they lie almost on a line except the last ε_l, which shows the boundary effect. Increasing k, the curves bend more and more with increasing correlation lengths. Finally, very close to the critical point ($k = 0.999$), the whole graph is curved. Approaching the critical point, the first eigenvalue ε_1 goes to zero, which tends to 0.2361 in the case of $k = 0.999$.

From the ε_l the actual eigenvalues w_n of ρ_h can be obtained by Eqn. (3.28). The resulting spectra are shown in Fig. 3.4. For relative small k ($k \le 0.5$) , which correlation lengths are small, some step-like degeneracies appear. It results from the relation (3.34) which leads to approximate degeneracies $(1, 1, 1, 2, 2, 3, 4)$ for the first seven levels. In the case of $k = 0.9$, some degeneracies can be seen at the first levels but they stretch out somehow. The reason is that ε_2 is also almost three times of ε_1 but the other ε_l don't obey the rule (3.34) any more. For $k = 0.999$, w_n lie almost on a line because of the small ε_1. In fact, $\varepsilon_2 \cong 19\varepsilon_1$, the first 19 w_n are on a line and the twentieth interrupts the linearity of the spectrum.

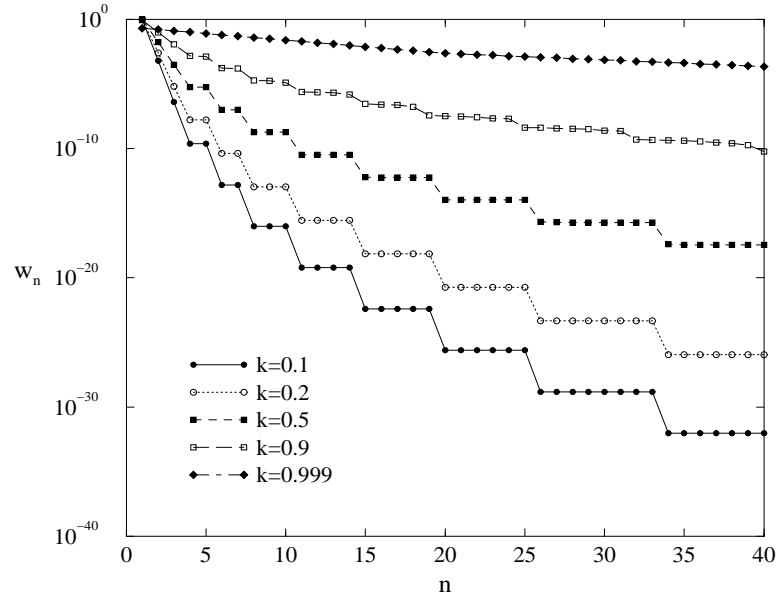We can also obtain the ε_l directly at the critical point. Fig. 3.5 shows

Figure 3.4: Density-matrix eigenvalues w_n, arranged in decreasing order, obtained from the ε_l in Fig. 3.3 and for the same parameters.
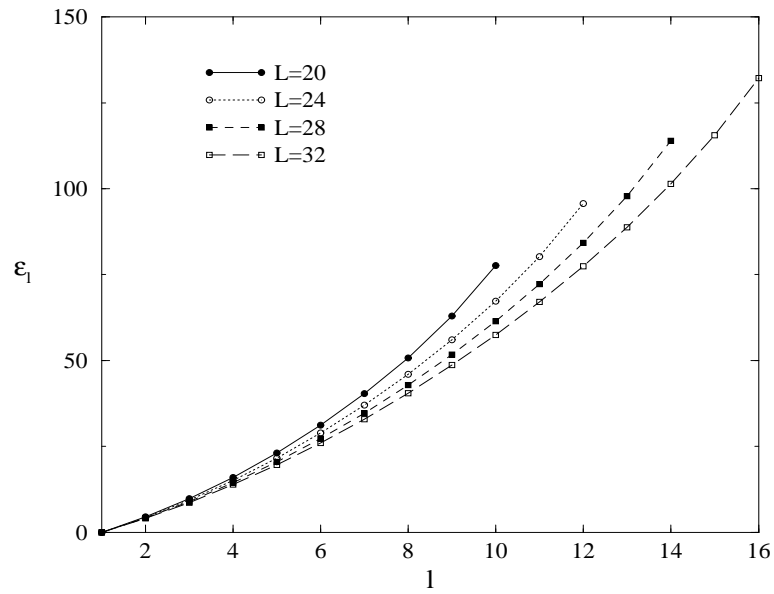

Figure 3.5: Single-particle eigenvalues ε_l for a chain of oscillators at the critical point $k = 1.0$.
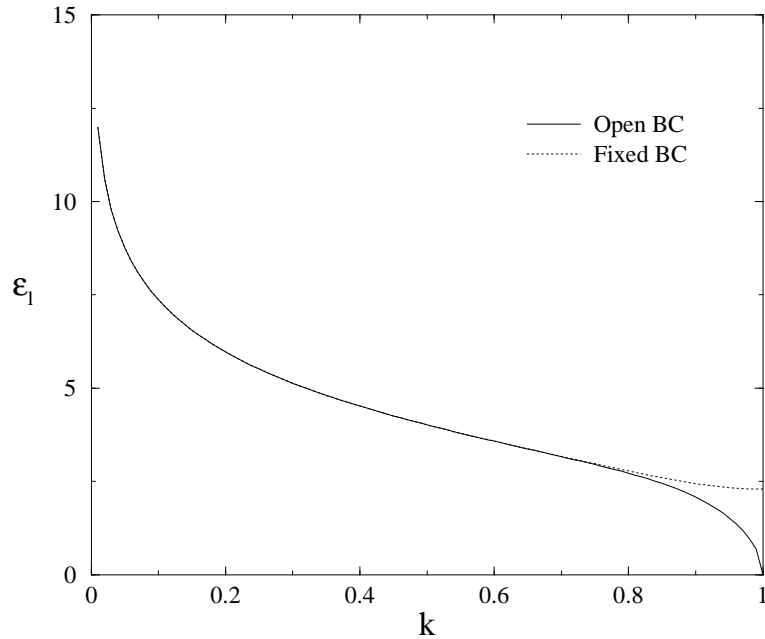
Figure 3.6: The first single-particle eigenvalue for free and fixed boundaries and $L = 16$.

the single-particle spectra for various sizes of the system. Increasing the size L, the curves become flatter, but the curvature remains. In the tails they differ from each other, which shows finite size effects. On the other hand, the other non-critical curves (not shown) converge, as L increases. In these four examples, ε_1 is always zero. We can see the character in Fig 3.1 with $L = 2$, where $\varepsilon = 0$ if $k \rightarrow 1$. Therefore, the w_n are very small and approach zero, because they are infinitely degenerate with $\varepsilon_1 = 0$. I will discuss the reason for this in the next subsection. We do not even know how to normalize them. At the critical point, only ε_1 dominates the spectrum, the other single-particle eigenvalues do not play any role. This causes a catastrophe in the DMRG calculation because we have to use all the Hilbert space, which is infinite, and we cannot truncate the states. Therefore, The situation must be avoided in the numerics. In chapter 4, we will discuss the similar single-particle spectra in the fermionic systems, however, the density-matrix eigenvalues w_n are totally different.

3.2.3   Fixed Boundaries

As mentioned in last subsection, the reduced density matrices at the critical point are unnormalizable. The reason is that due to translation invariance, the system has a zero frequency associated with the center of mass motion. Then the eigenfunction of the ground state is independent of the
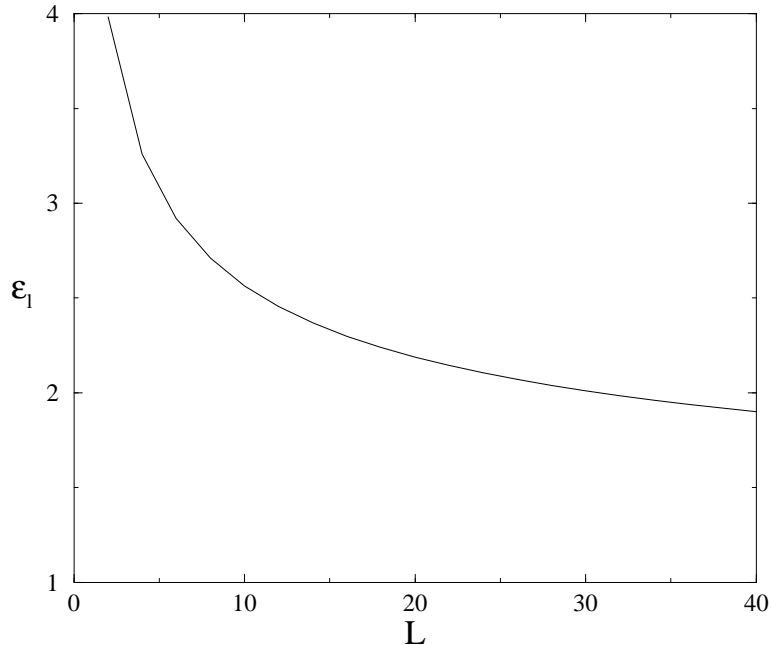
Figure 3.7: The first eigenvalue of the function of the system length L for fixed boundaries and $k = 1$.

center of mass coordinate, and therefore unnormalizable. The reduced density matrices are also unnormalizable.

One can avoid this problem by fixing the ends of the chain. This was done in the study of the DMRG for acoustic phonons by Caron and Moukouri [23]. The fixed boundaries break the translation invariance, and the eigenfunctions are normalizable even for $k = 1$. In Fig. 3.6 the first single-particle eigenvalues for free and fixed boundaries are plotted as a function of k. For small k, where $\xi/L \ll 1$, the two curves coincide, due to the fact that the boundaries do not play any role with a small correlation length. On the contrary, in the region $k > 0.8$, they differ from each other, because the boundaries are much more important with larger correlation lengths. At the critical point, $\varepsilon_1 = 2.30$ for fixed boundaries, whereas $\varepsilon = 0$ for open ones. Fig. 3.7 shows the dependence of ε_1 on the system size L. One can see that ε_1 drops to zero slowly. Unfortunately I cannot calculate ε_1 for larger systems due to numerical limitations, but one can extrapolate it. For $L = 100$ ε_1 is still larger than 1. This explains why Caron and Moukouri could obtain the ground-state energy for $L = 99$ with sufficient accuracy.

The benefit of using fixed boundaries near the critical point is shown in Fig. 3.8. In this figure ε_l and w_n of one-half of a chain with open and fixed boundaries are shown for $k = 0.999$. The fixed boundaries are larger by a factor of 2 than those for open ones, and $\varepsilon_1 = 2.19$ for the
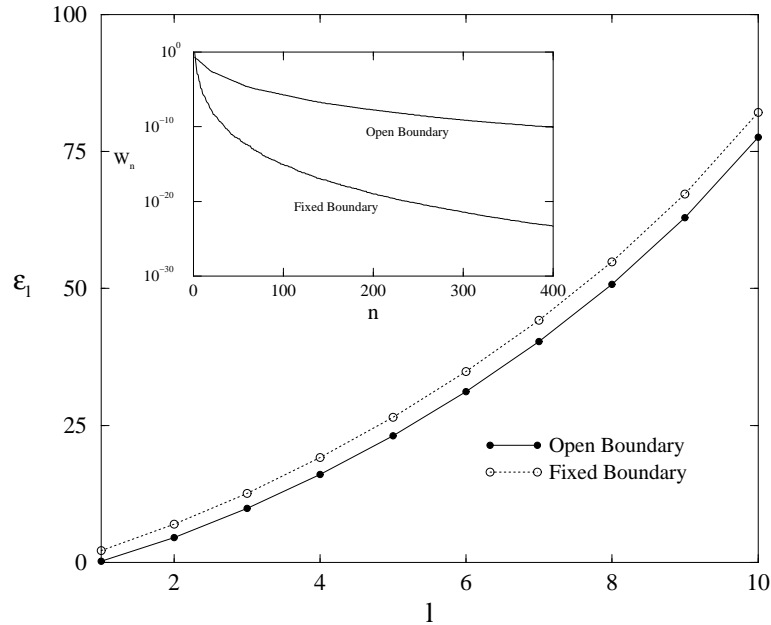
Figure 3.8: Single-particle eigenvalues ε_l of one-half of an oscillator chain with open
and fixed boundaries. The system is in the ground state, $k = 0.999$ and $L = 20$;
the w_n obtained from them are plotted in the inset.

fixed boundaries and $\varepsilon_1 = 0.26$ for the open chain. Therefore, the w_n for
fixed boundaries plotted in the inset drop twice as fast as those of the
open chain. In the DMRG calculations, in this case, one needs only half
as many kept states to reach the same precision.

3.2.4   Open vs. Periodic Conditions

In DMRG calculations one prefers open boundary conditions over periodic
ones, as mentioned already in early papers on the method [3]. The reason
is, roughly speaking, that for periodic boundary condition each block has
two ends which interact with the rest of the lattice. Therefore one needs
twice as many truncation bases as for open boundaries for the same accu-
racy. Using our model, this origin of the different DMRG performance for
open chains and rings can be seen very clearly. Fig 3.9 shows the ε_l and w_n
for open and periodic boundaries. In the case of periodic boundary condi-
tions, the lower ε_l have the same values as for the open chain, but each of
them is approximately two-fold degenerate. Therefore the w_n, which are
plotted in the inset of the figure, are much flatter in the ring than in the
chain. This results in the difficulties for calculating the systems with the
periodic boundaries.

The reason for the degeneracies in the ε_l spectra of rings can be under-
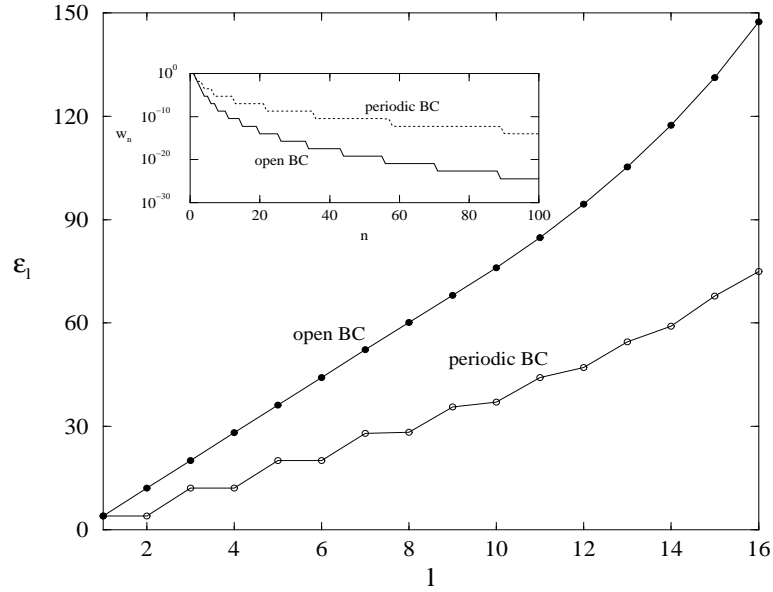stood with Fig. 3.10. The eigenvectors which are obtained by Eqn. (3.24)

Figure 3.9: Single-particle eigenvalues ε_l of one-half of an oscillator chain with open and periodic boundary condition. The system is in the ground state, $k = 0.5$ and $L = 32$; the w_n obtained from them are plotted in the inset.
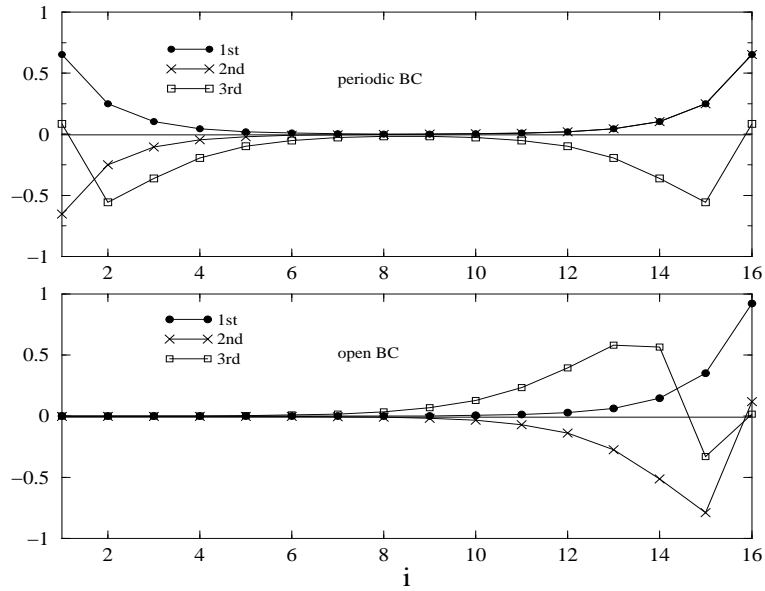

Figure 3.10: Density-matrix eigenstates for the half part of a open chain (lower figure) and a ring (upper figure). Shown are the amplitudes as a function of the position for the lowest three ε_l values for $\omega_0 = k = 0.5$.

are plotted for a ring and an open chain. For the chain, the amplitudes concentrate near the boundary of the end which interacts with the environment part, whereas for the ring, they concentrate at both ends, which causes a symmetric and an antisymmetric eigenvector. Both eigenvectors give the same eigenvalues, as one sees in Fig. 3.9. In other words, the ring, which is cut twice in the DMRG calculation, can be seen as two open chains which interact weakly with each other and then are cut in the middle.

3.3 Thermodynamic Limit

In the calculation for a half open chain, the single-particle spectra in the thermodynamic limit ($L/\xi \gg 1$) are almost linear. Unfortunately we can not find them analytically from our formulae. However, the relation between one-dimensional integrable quantum models and two-dimensional classical models will offer us a different point of view. In fact, in the thermodynamic limit the density matrix for one half chain of the integrable quantum models can be approximated by four corner transfer matrices (CTMs) of classical models. Here we will at first discuss the relation between one oscillator chain and the two-dimensional Gaussian model. In the second subsection we will discuss the corner transfer matrix of the Gaussian model and then give the analytical expression for ε_l, which can be compared with our results from section 3.2.

3.3.1 Relation to the Gauss Model

As a transverse Ising chain is related to the two-dimensional Ising model [18], the Hamiltonian H_1 in (3.17) has a close relation to the transfer matrix of a two-dimensional Gaussian Model (GM). In this model, one has a classical variable x at each lattice site, which takes values between $-\infty$ and ∞. Variables at neighboring sites are coupled by an energy $1/2K(x - x')^2$ (in units of $k_B T$). In order to make the system noncritical, one adds on-site terms $1/2\Delta x^2$. Then the transfer matrix T for a diagonal lattice involves the piece shown in the diagram below:
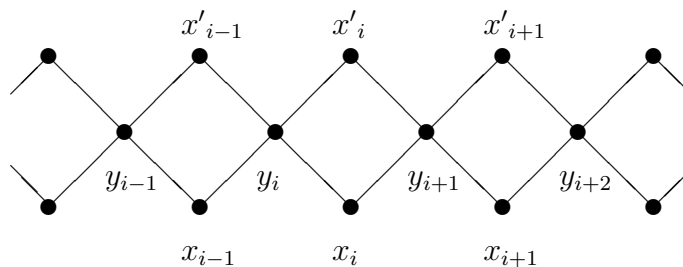
Therefore, T reads[1]

$$
T = \sum_{\{y_i\}} \left(\exp \sum_i \frac{1}{2}\Delta(x_i^2 + x'^2_i + y_i^2) + \frac{1}{2}K(x_{i-1} - y_i)^2 + \frac{1}{2}K(x_i - y_i)^2 \right.
$$
$$
\left. \times \exp \sum_i \frac{1}{2}K(x'_{i-1} - y_i)^2 + \frac{1}{2}K(x'_i - y_i)^2 \right).
$$
(3.35)

By a direct calculation one can show that, for PBC,

$$
[H, T] = 0,
$$
(3.36)

provided that $k = K^2$ and $\omega_0 = \Delta(\Delta + 4K)$. This means that T and H have the same eigenfunctions. Moreover the ground state Ψ in (3.2) gives the maximal eigenvalue for T. As a result, one can also obtain Ψ and ρ_h from the partition function for two dimensional classical systems [18, 44]. For open boundaries condition, one has to modify H at the end to preserve (3.36). However, this boundary term can be neglected, if one considers systems with $L \gg \xi$, where ξ is the correlation length given by $\xi = 2/\ln(1/k)$.

An alternative approach, due to Babudjan and Tetelman [45], is to treat a GM with anisotropic couplings for periodic boundary conditions with the Yang-Baxter equations. They show that the T for different anisotropies commute and obtain H from a proper derivative of T. For this, one parameterizes the two couplings with an Jacobi function sn of module k, for example,

$$
K_1 = -i / \operatorname{sn}(iu, k), \qquad K_2 = i\, k \operatorname{sn}(iu, k).
$$
(3.37)

Using the Yang-Baxter equation, the parameter determines also the on-site energy Δ as well as the correlation length. The parameter u, which specifies the ratio K_1/K_2, varies between 0 and $I(k')$, where I is the complete elliptic integral of the first kind and $k' = \sqrt{1 - k^2}$. In the isotropic case u is equal to $I(k')/2$. The derivative $\partial \ln T/\partial u$ at $u = 0$ gives 3.17 with $\omega_0 = (1 - k)$. This is the reason why we choose this parameterization throughout the thesis.

3.3.2 Corner Transfer Matrix

As discussed in [42], the density matrix ρ_h for a half chain reads

$$
\rho_h = ABCD,
$$
(3.38)

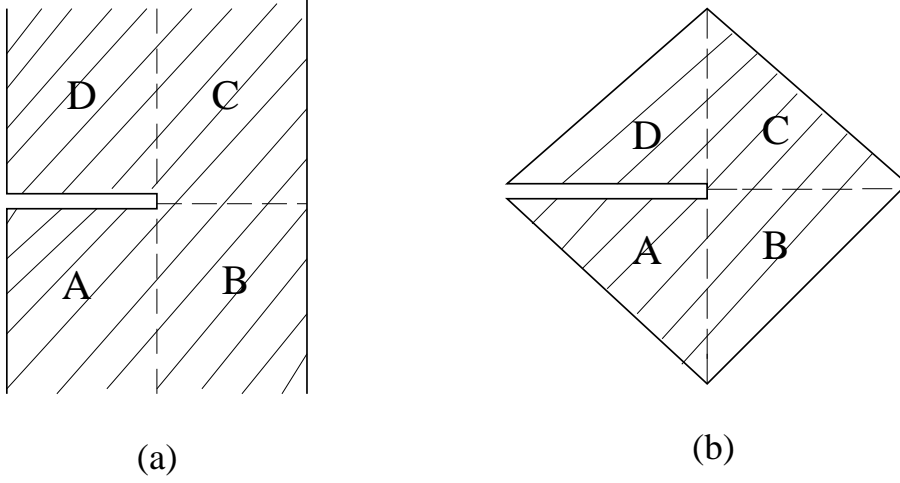[1]through private communication with Professor Peschel

Figure 3.11: The geometry of the CTMs A, B, C, D. (a) four rectangular ones (b) they are approximately four triangular ones in the thermodynamic limit.

where A, B, C, D are four rectangular corner transfer matrices of Ramond type, i.e. without a common central site. They are shown in Fig. 3.11(a). In the case of the thermodynamic limit, where $L \gg \xi$, one can simplify the transfer matrices with triangular ones, as seen in Fig. 3.11(b), by neglecting the marginal effect from the outer triangular for a system away from critical point. Therefore, the products AB and CD are square matrices, and due to the integrability of the Gauss model, i.e. the Yang-Baxter equations, the matrices have the exponential form

$$A \ = \ e^{-u\,\mathcal{H}_{\text{CTM}}} \tag{3.39}$$

and similar for B, C, D, with $\mathcal{H}_{\text{CTM}}$ given by

$$\mathcal{H}_{CTM} = \sum_{n \geq 1} \left\{ -\frac{1}{2}(2n-1)\frac{\partial^2}{\partial x_n^2} + \right.$$
$$\left. \frac{1}{2}(2n-1)(1-k)^2 x_n^2 + \frac{1}{2}2nk(x_{n+1} - x_n)^2 \right\}. \tag{3.40}$$

This operator was studied in [46] in the Hamiltonian limit $u \to 0$ of A. It can be diagonalized with the help of Carlitz polynomials and then becomes the sum of uncoupled harmonic oscillators with eigenvalues $(2l-1)\pi/2I(k')$. Multiplying the four similar operators, $ABCD$, or A^4 in the isotropic model, both give a factor $2I(k')$, so that ρ_h is expressed as

$$\rho_h = K_h \cdot \exp\left(-\sum_{l \geq 1}(2l-1)\varepsilon\mathcal{B}_l^\dagger\mathcal{B}_l \right), \tag{3.41}$$
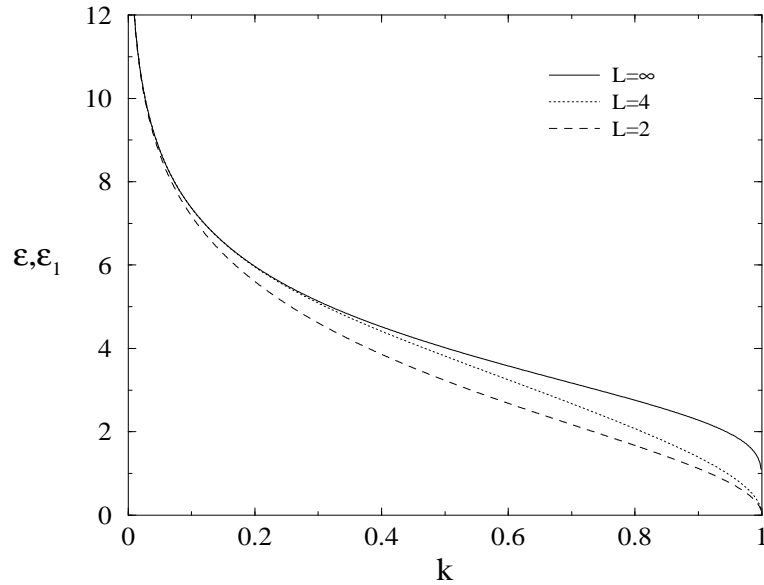
Figure 3.12: Lowest single-particle eigenvalues in the density matrix of a half-chain. Plotted are ε for $L = 2$ and ε_1 for $L = 4$ and $L = \infty$.

where

$$\varepsilon = \pi \frac{I(k')}{I(k)}. \tag{3.42}$$

One sees that ρ_h has exactly the same form as in (3.25) with $\varepsilon_l = (2l-1)\varepsilon$, i.e. the ε_l increase linearly with l.

The parameter $\varepsilon \equiv \varepsilon_1$ is shown in Fig. 3.12 together with the corresponding eigenvalues for short chains. In the case of $k \to 0$, ε is very close to the ε of $L = 2$ and ε_1 of $L = 4$. This corresponds to the fact that the systems with those k have small correlation lengths. For $k \to 1$, the correlation length vanishes only logarithmically, i.e. more slowly than the quantities for finite L.

3.4 Numerics

3.4.1 Optimal States

In order to understand the relation between the density-matrix spectra and DMRG, we will discuss some numerical results of one-dimensional open chains. Since we discuss here a boson system, the most difficult problem one has to face is how many states one must take at one site for a certain precision. Therefore an optimal basis is required to reduce the number of states in one sites. In our case, the best optimal bases are the eigenstates of ρ_{sg} discussed in section 3.1. These are standard oscillator

41

functions of coordinate z

$$z = \frac{1}{\sqrt{2\varepsilon}}(\beta + \beta^\dagger), \tag{3.43}$$

where z is related to x_l by a scale factor

$$z = \sqrt{\frac{\gamma}{\varepsilon}} x_l \tag{3.44}$$

and $\gamma = \sqrt{a(a - b)}$.

One should note that the scale factor hardly changes throughout the chain if the system is not at the critical point (see Fig 3.2). Therefore, we can use the ϵ and γ for the middle of the chain to rewrite the Hamiltonian 3.17

$$H_1 = \sum_i C_1(\beta_i^\dagger \beta_i + 1/2) + C_2(\beta_i^2 + \beta_i^{\dagger 2}) + C_3(\beta_i + \beta_i^\dagger)(\beta_{i+1} + \beta_{i+1}^\dagger), \tag{3.45}$$

where C_1, C_2, C_3 read

$$
\begin{aligned}
C_1 &= \frac{1}{2}(\gamma + \omega_0^2/\gamma + k/\gamma), \\
C_2 &= -\frac{1}{4}(\gamma - \omega_0^2/\gamma + k/\gamma), \\
C_3 &= -\frac{1}{2}(k/\gamma)
\end{aligned}
\tag{3.46}
$$

and $\beta_i, \beta_i^\dagger$ are the creation(annihilation) operators of the eigenstates of ρ_{sg} for each site. We will call such states squeezed states or optimal states. For small k, γ approaches ω_0 and the optimal states coincide with the original ones. Hence the Hamiltonian (3.45) reduces to that with the local basis. Increasing k, the amount of squeezing increases, and it is the advantage one to choose the squeezed states as a local basis.

3.4.2   Numerical Spectra

It is instructive to see how these squeezed states enter the density-matrix spectra in a numerical treatment using a truncated Hilbert space. In Fig.3.13 the analytical density-matrix spectrum for $L = 4$ and $k = 0.5$ is shown. From the Eqn. (3.25) the density matrix ρ_h for the two oscillators in the system part 1 can be expressed as

$$\rho_h = K_h \exp\left\{-\left(\varepsilon_1 \mathcal{B}_1^\dagger \mathcal{B}_1 + \varepsilon_2 \mathcal{B}_2^\dagger \mathcal{B}_2\right)\right\}. \tag{3.47}$$

One can see that the spectrum has a step structure. This is due to the relation $\varepsilon_2 \cong 3\varepsilon_1$. The first degeneracy is caused by $4\varepsilon_1$ and $\varepsilon_2 + \varepsilon_1$. The other
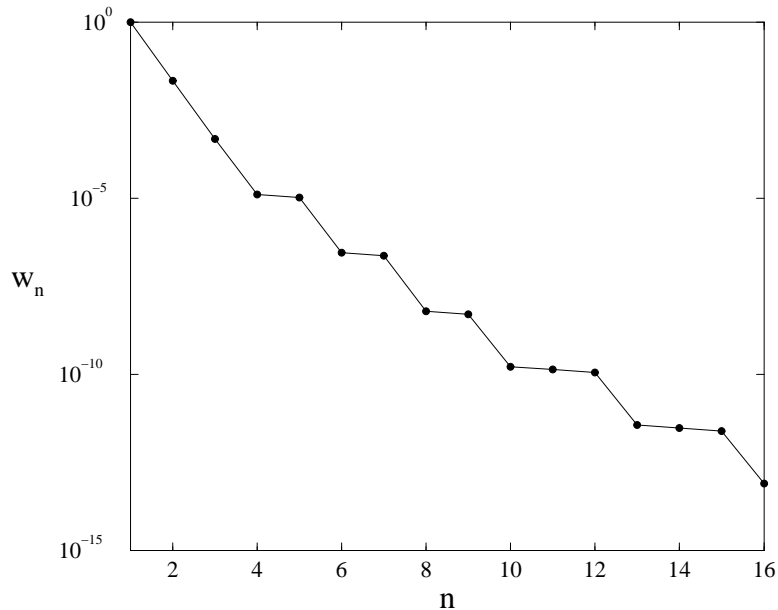
Figure 3.13: The analytical density-matrix spectrum for $L = 4$ and $k = 0.5$.

plateaus can be obtained in the same way, which explains the approximate degeneracies (1,1,1,2,2,2,3). One notes that the steps are not perfect for small w_n because ε_2 is somewhat larger than $3\varepsilon_1$. Fig.3.14 shows the numerical density-matrix spectra for $L = 4$, $k = 0.5$ and $\omega_0 = 0.5$ with different numbers of squeezed states from the exact diagonalization. Choosing r states, the error in the ground-state energy E_0/L is of order 10^{-r}. The spectra look very similar but they have characteristic differences, which concern the degeneracies. If r states are kept, the first r levels (counted from the top) of w_n are the same as for the analytical spectrum. At the next level, states with energy $r\varepsilon_1$ are missing and the corresponding step is absent. In other words, one needs $r + 1$ squeezed states to construct the r level degeneracies. For small w_n, however, the numerical error reduces the precision of the calculation and the spectrum becomes irregular. The tails of the approximate spectra always lie below the exact one.

Carrying out the DMRG calculations, results for $L > 4$ can be obtained as well. Here we used seven squeezed states at each site, a γ which corresponds to $L = 30$ and kept $m = 7$ truncation states per block. In the calculations the error in E_0/L was about 3×10^{-7} for $k = 0.5$. Fig.3.15 shows the corresponding spectra for $L = 6$ and $L = 14$, together with the thermodynamic limit according to (3.41), (3.42). The numerical calculation agrees well with the analytical results. The relative deviations $\delta\varepsilon_l/\varepsilon_l$ for the lowest three levels $\varepsilon_1 = 3.973, \varepsilon_2 = 11.537$ and $\varepsilon_3 = 19.990$ are 6×10^{-6} 7×10^{-5} and 4×10^{-4}. One notices that due to the different ε_l the two curves are similar but not identical. The ε_l for $L = 6$
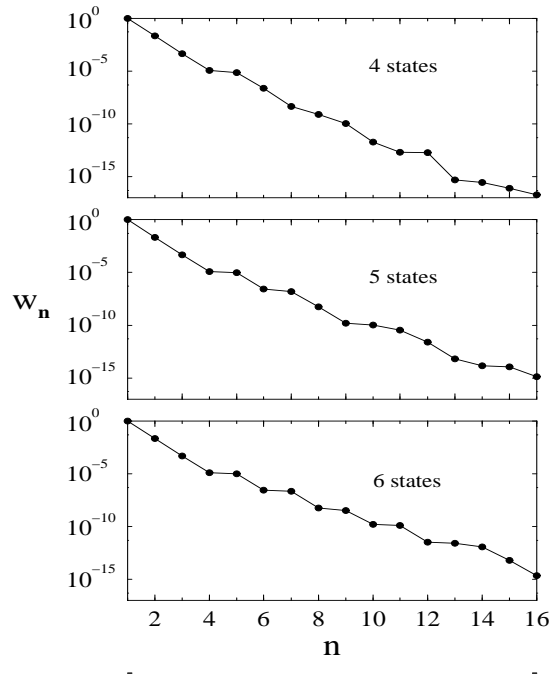
Figure 3.14: Density-matrix spectrum for $L = 4$ and $k = 0.5$, calculated with different numbers of oscillator states.

are smaller than those for $L = 14$. The degeneracies here have changed to $(1, 1, 1, 2, 2, 3, 4)$, which differs from $L = 4$ in the last two eigenvalues. The difference stems from the third eigenvalue $\varepsilon_3 \cong 5\varepsilon$ of ρ_1, which first appears for $L = 6$.

The first two steps of the spectrum for $L = 14$ are almost flat, which indicates that $\varepsilon_2 = 3\varepsilon_1$ as for the infinite system. Indeed, the ε_l from the numerical (DMRG) and analytical (section 3.2) calculations are very close to the large-L limit. For example, ε_1 agrees with the exact result $\varepsilon = 4.0189$ up to three decimal places. This can be understood to be a consequence of the short correlation length $\xi/L \sim 0.11(\xi \sim 3)$ for $k = 0.5$, which makes size effects small.
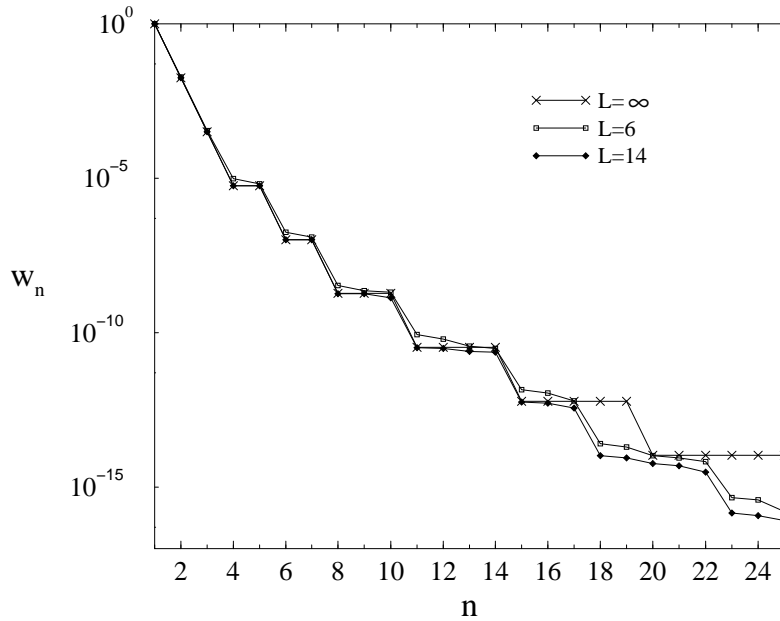
Figure 3.15: Density-matrix spectrum for $k = 0.5$ and two sizes L, calculated with DMRG using 7 states and $m = 7$. Also shown is the analytical result for $L \to \infty$.

3.5 Different Types of Interaction for a Chain

So far we have discussed the density-matrix spectra only for a homogeneous chain the nearest-neighbor coupling. However, using the method described in the section 3.2, the density-matrix spectra for oscillators with arbitrary types of couplings can be determined. The ε_l reveal the nature of the couplings and the properties in the DMRG calculations. It is thus interesting to consider the oscillators with different types of couplings to give us some insight into those systems.

3.5.1 Next-Nearest-Neighbor Couplings

The first example is oscillators not only with nearest-neighbor couplings but also with next-nearest-neighbor ones. The Hamiltonian has the form

$$H_{nn} = \sum_{i=1}^{L} \left(-\frac{1}{2}\frac{\partial^2}{\partial x_i^2} + \frac{1}{2}\omega_0^2 x_i^2 \right) +$$
$$\sum_{i=1}^{L-1} \frac{1}{2}k_1(x_{i+1} - x_i)^2 + \sum_{i=1}^{L-2} \frac{1}{2}k_2(x_{i+2} - x_i)^2. \quad (3.48)$$

Fig. 3.16 shows the ε_l of the systems with different next-nearest-neighbor couplings k_2 for $L = 20, \omega_0 = 0.1$ and $k_1 = 0.1$. The single-particle
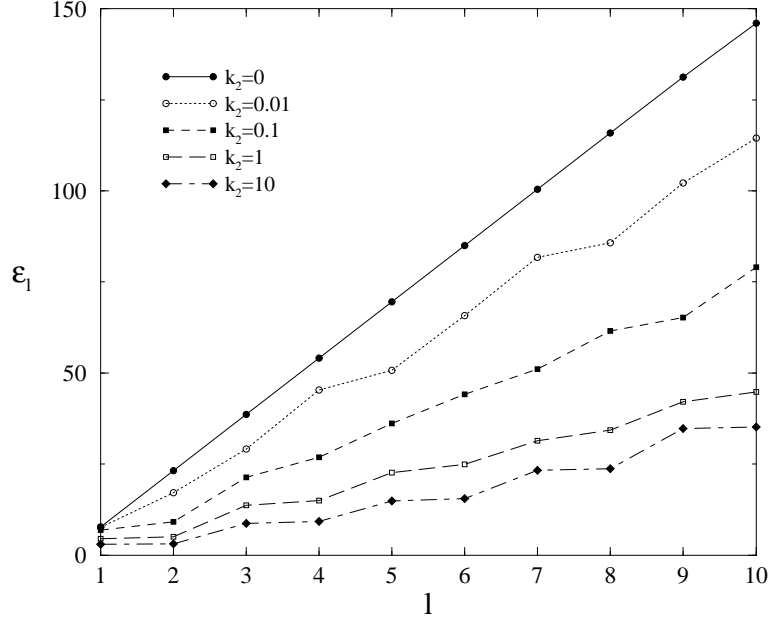
Figure 3.16: The single-particle eigenvalues of oscillators with nearest-neighbor and next-nearest-neighbor coupling. Plotted are ε_l for different k_2 for $L = 20$, $\omega_0 = 1.0$ and $k_1 = 0.1$.

spectra show the competition between the nearest-neighbor interactions and next-nearest-neighbor ones. In the limit $k_2 \to 0$, the system comes back to a system only with the nearest-neighbor couplings, where the ε_l are linear. In the opposite limit, if $k_2 \gg k_1$, the system approach to a chain only with the next-nearest-neighbor couplings, which is made up of two independent chains with size $L/2$. The ε_l are thus two-fold degenerate and the w_n will be flat. Therefore the single-particle spectra become flatter with the increasing k_2 and the zig-zag structure in the spectra shows the competition between the two kinds of interactions.

3.5.2 Exponential Couplings

Oscillators with exponential couplings are interesting to us because so far we have not yet treated systems with long-range interactions. The Hamiltonian for such a system with open boundaries reads

$$H_e = \sum_{i=1}^{L} \left(-\frac{1}{2}\frac{\partial^2}{\partial x_i^2} + \frac{1}{2}\omega_0^2 x_i^2 \right) + \sum_{i<j} \frac{1}{2}ke^{-\lambda|i-j|}(x_i - x_j)^2. \qquad (3.49)$$

The single-particle eigenvalues for different relatively short range of the interaction ($\lambda < 1$), $\omega_0 = 1$ and $k = 1$ are plotted in Fig. 3.17. One should note that the flat curves above 150 are due to the limit of our calculations
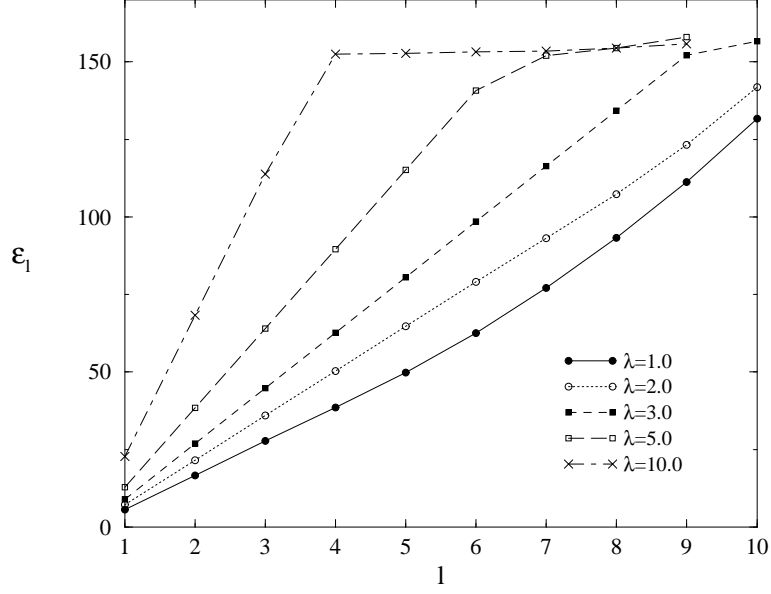
Figure 3.17: The single-particle eigenvalues of oscillators with exponential couplings. Plotted are ε_l with different $\lambda > 1$ for $L = 20$, $\omega_0 = 1.0$ and $k = 1.0$.

discussed in section 3.1. However, we can see the characteristic behavior from the first smaller eigenvalues. For $\lambda = 1$, the first ε_l lie still on a line, but they bend over somewhat. The curve is similar to the spectra for the systems with the nearest-neighbor coupling near the critical point. With increasing λ, the ε_l become larger and straighter, just like the curves for the nearest-neighbor coupled oscillators in the thermodynamic limit. This is due to the fact that the range of the interaction decreases and one approaches the case of nearest-couplings. In the limit $\lambda \to \infty$, the oscillators are completely decoupled which leads to $\varepsilon_l \to \infty$.

In Fig. 3.18, on the other hand, the case of $\lambda > 1$ is shown, where the couplings between the oscillators decay slowly. With decreasing λ, the long-range couplings become more important and the ε_l grow except ε_1, which goes down to a finite limit. The phenomenon can be understood from the limiting case $\lambda \to 0$, where the couplings are all equal among the oscillators. The oscillators have now only two normal frequencies, namely ω_0 and $\omega_1 = \sqrt{\omega_0^2 + Lk}$. One can say that the system has one natural frequency ω_0 and one bulk frequency ω_1 because the oscillators are tied together strongly through the couplings. From Eqn. (3.33), one finds the eigenvalues of the matrix $\boldsymbol{O}^{-1}\boldsymbol{E}$ are all equal to unity except one. Therefore, every single-particle eigenvalue goes to infinity except $\varepsilon_1 = 4 \tanh^{-1}(\sqrt{\omega_0/\omega_1})$, which is equal to 2.026 in the case of $\omega_0 = 1, k = 1$ and $L = 20$. Examining the ε_l in the calculation $\lambda = 0.001$, $\varepsilon_1 = 2.031$, which is very close to the limiting value.
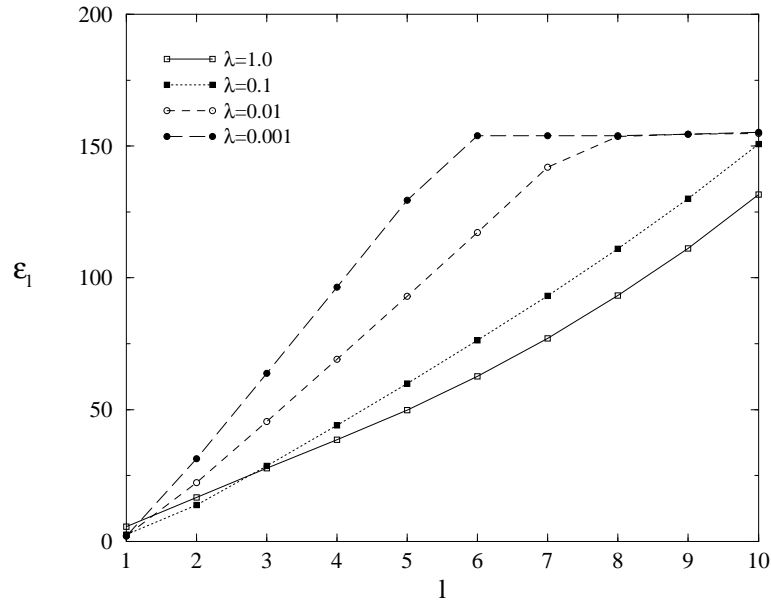
Figure 3.18: The single-particle eigenvalues of oscillators with exponential couplings. Plotted are ε_l with different $\lambda < 1$ for $L = 20$, $\omega_0 = 1.0$ and $k = 1.0$.

3.6 Two-Dimensional Boson Systems

The application of DMRG to some two-dimensional systems, for example, free fermions [35] and the transverse Ising model [36], has been discussed in some detail. From the limit of noninteracting chains, or from numerical calculations, it was derived that the number m of states one needs to keep a certain accuracy grows *exponentially* with the width M_d of the system. However the spectra themselves have not been observed although they are most essential for the problem. In this section, I will determine the density-matrix spectra of two-dimensional arrays of oscillators and then discuss the exponential growing number of truncation states and their origin.

3.6.1 Spectra

In this last part of the section, we consider a two-dimensional square lattice of oscillators with nearest-neighbor couplings k_x and k_y in the two directions. The oscillators are described by one coordinate as in the previous subsections. The shape of the system is a rectangle with $L = N \times M_d$ sites, where N is even. We will treat it with two different methods, which give the same results.

The first treatment method is to numerate the oscillators from 1 to L in such a way that the desired sites of system part 1 come first. For example,

if we want to separate the system into two equal half rectangles, we should count the sites from left up to right down. But if the density matrix for the half triangle is desired, we should diagonally numerate them. In this section we consider only the rectangular partition, whereas we will treat the other kinds of division in the fermionic case (Section 5.3). After the problem is set up in this way, we can use the general formulae (3.23) and (3.26) to obtain the spectrum.

On the other hand, the two-dimensional lattice can be reduced to a one-dimensional problem by introducing normal coordinates in the y-direction. The Hamiltonian now reads

$$H_{2b} = \sum_q \left(\sum_i -\frac{1}{2}\frac{\partial^2}{\partial \phi_i(q)^2} + \right.$$
$$\left. \frac{1}{2}\omega(q)^2\phi_i(q)^2 + \frac{1}{2}k_x(\phi_{i+1}(q) - \phi_i(q))^2 \right), \qquad (3.50)$$

where the $\phi_i(q)$ are normal coordinates in i-th the column and the normal frequencies are

$$\omega(q)^2 = \omega_0^2 + 2k_y(1 - cosq). \qquad (3.51)$$

The vertical momenta q depend on the boundary condition. For open boundaries, as used in the DMRG, they are

$$q = \frac{m}{M_d}\pi, \quad m = 0, 1, 2, \ldots, (M_d - 1). \qquad (3.52)$$

Eqn. (3.50) shows that if we couple the columns via k_x, the different momenta do not mix. Therefore one can separate the system into M_d uncoupled chains which have natural frequencies $\omega(q)$ and coupling k_x.

For each momentum q, one obtains $N/2$ single-particle eigenvalues $\varepsilon_j(q)$ according to Eqn. (3.25). Alternatively one may say that, for fixed j, one has a band of M_d eigenvalues. This band reflects the fact that one now has M_d points of contact between the two halves of the system, instead of only one in the one-dimensional case. In the thermodynamic limit, the $\varepsilon_j(q)$ can be determined by Eqn.(3.41) and (3.42), with the parameter $k = k(q)$ determined from the equation $k_x/\omega(q) = k/(1 - k)$, or, equivalently,

$$k = k_x/[k_x + \omega(q)]. \qquad (3.53)$$

With each q, one finds $\varepsilon_j(q)$ as in the case of one-dimensional systems. Collecting the single-particle eigenvalues for different k and arranging them in an ascending order, the band structure is found again.

Such single-particle spectra, calculated numerically for a 10×10 lattice are shown in Fig. 3.19. Plotted are ε_l for the different transverse coupling k_y. If there are no interactions between chains, one obtains five plateaus, which have the linear relation according to the Eqn. (3.34). Turning
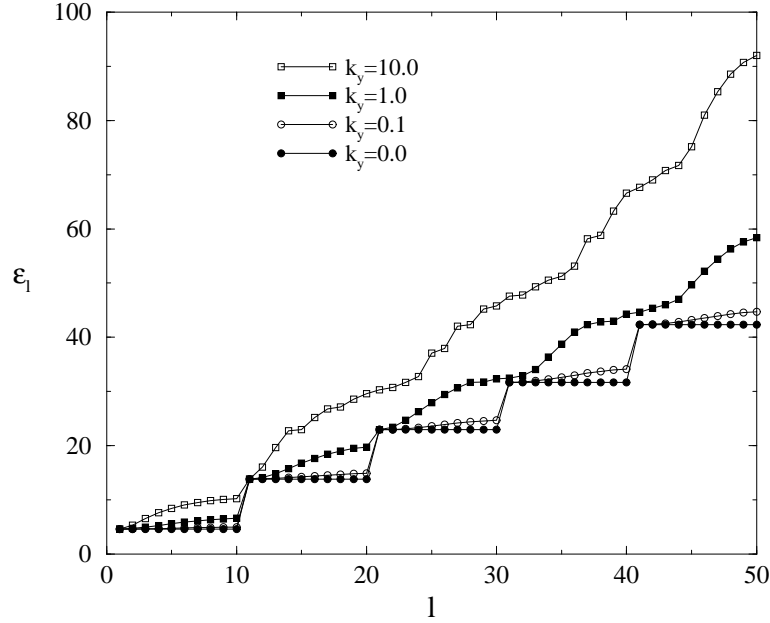
Figure 3.19: Bosonic single-particle eigenvalues $\varepsilon_l(q)$, c.f. Eqn.(3.25), for half of a 10×10 system, arranged in ascending order, for $\omega_0 = k_x = 1.0$ and four values of the coupling k_y.

on $k_y(> 0)$, the eigenvalues increase except $q = 0$ and form real bands. For small k_y, the stair-like structure persists till the end of the spectra, while with large k_y the bands smear out for larger eigenvalues of j due to the factor $(2j - 1)$, and eventually overlap. We can see that for larger k_y, a certain continuous curve develops, which can be approximated by a straight line

$$\varepsilon_l \cong \kappa l \qquad (3.54)$$

with integer l, and $\kappa \cong 2\varepsilon(q = 0)/M_d$ inversely proportional to the width M_d.

Specifying the occupation numbers of the bosonic single-particle levels ε_l in (3.28), one can obtain the eigenvalues w_n of ρ_1. Due to the low band of single-particle eigenvalues ε_l, shown in Fig. 3.20, the spectra decrease slowly and are totally different from those in one dimension. Using the same parameters, these curves are plotted with the ε_l in Fig 3.19. For small k_x, the spectra have also a stair-like structure as the ε_l but with a far larger plateaus, which are caused by combinatorial factors. With increasing k_y, the curves become smoother and the discontinuities in the curves disappear for larger k_y. In all cases, the spectra decay much more rapidly at the beginning, followed by a slower decay for larger n. One can derive an asymptotic formula from Eqn. (3.54), following Ref. [47] which
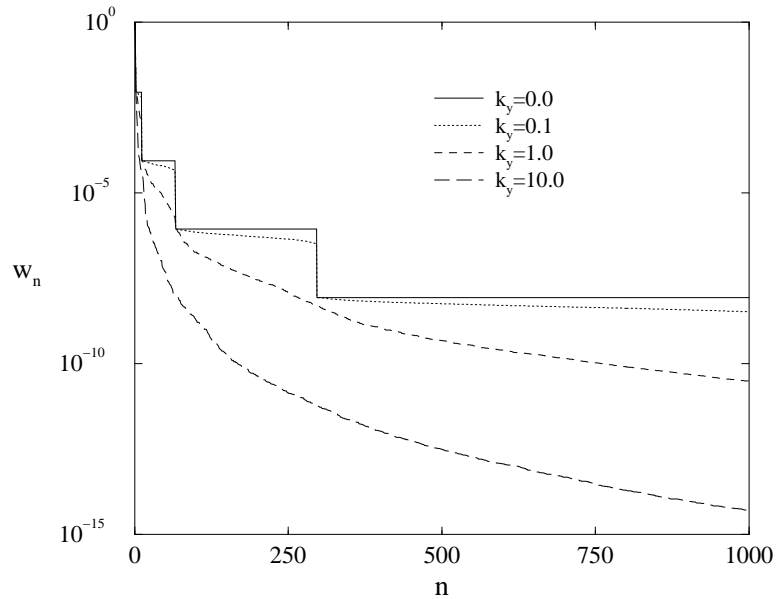
Figure 3.20: Density-matrix eigenvalues w_n, arranged in decreasing order, obtained from the ε_l in Fig.3.19 and for the same parameters

reads

$$w_n \sim \exp\{-(\kappa/(2\,\pi^2/3))\ln^2 n\} \tag{3.55}$$

and which fits reasonable well to the curves. We can calculate also the truncation error, which is much larger than in one dimension due to the slow decay. After $n = 10, 500$, and 1000, it is approximately $10^{-5}, 10^{-7}$ and 10^{-8}, respectively, if $k_x = k_y = \omega_0 = 1.0$.

3.6.2 Difficulties in Two-Dimensional Systems

We have discussed the truncation error in the two-dimensional lattice, and found that many more truncation states are needed to obtain a certain good accuracy for 10×10 lattice. In this subsection we will discuss the difficulties for the DMRG calculation of two-dimensional systems.

At this stage, one can do an experiment to see the change of the curves, as the systems become more two-dimensional. By changing the width M_d from 1 to N, we can calculate the w_n of the $10 \times M_d$ oscillators as before and the corresponding spectra are shown in Fig. 3.21 for the case $k_x = k_y = \omega_0 = 1$. As can be seen, the curves drop more and more slowly with increasing M. This can be explained with Eqn. (3.54) and (3.55). The parameter κ decreases with increasing M and this leads to the flatter structure of w_n.

The result confirms that the situation worsens as the systems become more two-dimensional. At the beginning of the spectra, w_n decay much
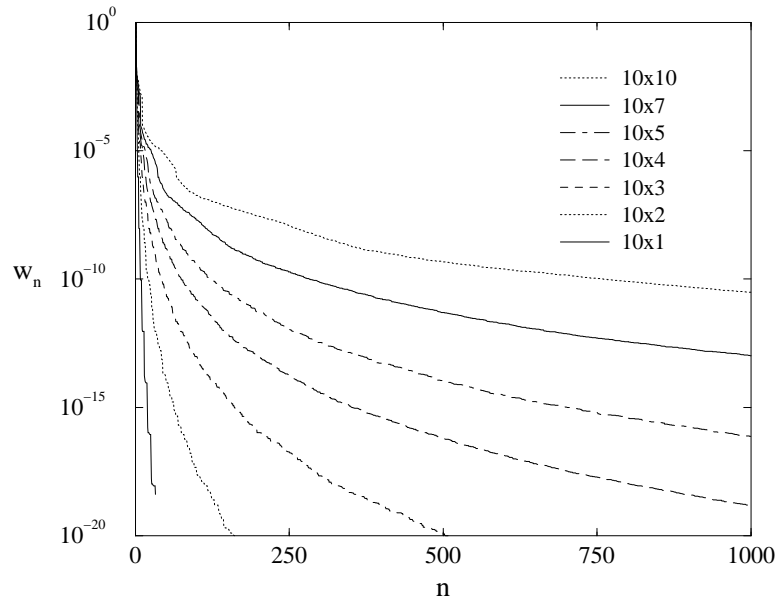
Figure 3.21: Density-matrix eigenvalues w_n for systems of different width M_d and $\omega_0 = k_x = k_y = 1.0$

more rapidly, which helps in numerical calculations. The faster initial decay before the onset of the combinatorial effects helps in numerical calculations. Also the interaction helps here to some extent since the ε-values increase with k_y, but this does not remove the basic $1/M$ dependence in the exponent.

One should mention that we have not treated critical models here, but only systems with a gap. In the critical cases, As discussed in the section 3.2.3, one always obtains a vanishing ε_1 due to the transformation invariance. In order to avoid the zero, one can fix the boundaries as Caron did in Ref. [23]. However one cannot avoid the appearance of a small ε_1. That will be even worse in the two-dimensional critical model due to the band structure of ε_l, because small ε_l will appear M times, causing very flat w_n-spectra.

The difficulties with DMRG calculations for two-dimensional systems are clear here. The problem arises from small ε_l, which result from the intersection between the system part 1 and the environment part 2. Therefore, one should reduce such an interface in the consideration of the partition. Furthermore, one should apply as many symmetries as possible. Whether the momentum-space approach of Ref. [34, 48] can help here is not yet clear. Similar results will be found in the case of fermion systems in section 5.3.

Chapter 4

Coupled Oscillators - Coherent-State Treatment

In the last Chapter I have treated the coupled oscillators with the x-representation wave functions and found the reduced density matrices with many facets for the ground state. On the other hand, one can rewrite the coupled oscillators with Bose operators and directly diagonalize the Hamiltonian, using the method introduced by Bogoliubov [49], which was originally applied to the superfluid. In this approach, coherent states are needed to obtain the reduced density matrices. The advantage of the coherent-state approach is that one can apply the same procedure to the solvable fermion systems, which will be discussed in the next chapter. The main aim of this chapter is to serve as a bridge between the boson and fermion systems.

In this chapter, I will describe the coherent-state treatment of boson systems. In section 4.1 I will introduce the exact diagonalization of solvable Bose systems and the corresponding ground state. In section 4.2, the reduced density matrices will be obtained using the coherent states. In section 4.3 I will treat the coupled oscillators with this approach, the density matrices of ground state and first excited state will be discussed.

4.1 Solvable Bosonic Systems and their Ground State

We consider now the general form of Hamiltonians which are quadratic in Bose operators

$$H_b = \sum_{ij=1}^{L} \left\{ b_i^\dagger A_{ij} b_j + \frac{1}{2} (b_i^\dagger B_{ij} b_j^\dagger + h.c.) \right\}, \qquad (4.1)$$

where the b_j and $b_j^\dagger$ are Bose annihilation and creation operators. Due to the Hermicity of H_b, the matrices $\boldsymbol{A}$ and $\boldsymbol{B}$ are both Hermitian. In the

following we consider only real matrices. One can diagonalize H through
the canonical transformation [49]

$$\eta_k = \sum_i (g_{ki} b_i + h_{ki} b_i^\dagger), \tag{4.2}$$

which leads to

$$H_b = \sum_k \Lambda_k \eta_k^\dagger \eta_k + \text{constant}. \tag{4.3}$$

The quantities Λ_k^2 are obtained from the eigenvalues equations

$$\begin{aligned}
(\boldsymbol{A} + \boldsymbol{B})(\boldsymbol{A} - \boldsymbol{B}) \, \phi_k &= \Lambda_k^2 \, \phi_k, \\
(\boldsymbol{A} - \boldsymbol{B})(\boldsymbol{A} + \boldsymbol{B}) \, \psi_k &= \Lambda_k^2 \, \psi_k
\end{aligned} \tag{4.4}$$

by introducing the two vectors $\phi_{ki} = g_{ki} + h_{ki}$ and $\psi_{ki} = g_{ki} - h_{ki}$. Due
to the fact that the η_k and $\eta_k^\dagger$ are canonical Bose operators that have to
satisfy the commutation relation $[\eta_k, \eta_{k'}^\dagger] = \delta_{kk'}$, one has

$$\sum_i \psi_{ki} \phi_{ik'} = \delta_{kk'}. \tag{4.5}$$

The ϕ_k and ψ_k are both orthogonal, but not necessarily orthonormal.

Consider now the ground state $\mid \Phi_0 \rangle$ of the Hamiltonian (4.1) for an
even number of sites L. Due to the form of H_b, an eigenstate will in
general be a superposition of contributions with an even or an odd number
of particles. Therefore one can make an Ansatz that the ground state has
an exponential form

$$\mid \Phi_0 \rangle = C \, \exp\{\frac{1}{2} \sum_{ij} G_{ij} b_i^\dagger b_j^\dagger\} \mid 0 \rangle, \tag{4.6}$$

where $\mid 0 \rangle$ is the vacuum of the b_i, i.e.

$$b_i \mid 0 \rangle = 0. \tag{4.7}$$

In the next chapter I will use this Ansatz for fermion systems, where
in the exponent Fermi creation operators are used. Such an exponential
form is known from superconductivity, where the BCS wave function (in
momentum space) can be written in this way [50].

In the case of all $\Lambda_k > 0$, the ground state must fulfill the condition

$$\eta_k \mid \Phi_0 \rangle = 0 \quad \text{for all } k \tag{4.8}$$

which leads to (see Appendix)

$$\sum_m g_{km} G_{mn} + h_{kn} = 0 \quad \text{for all } k, n. \tag{4.9}$$

Thus $\boldsymbol{G}$ relates the two matrices $\boldsymbol{g}$ and $\boldsymbol{h}$ of the transformation (4.2). If $\boldsymbol{g}$ is invertible and $\boldsymbol{h} \neq 0$, one obtains G_{ij} from the relation

$$\boldsymbol{G} = -\boldsymbol{g}^{-1}\boldsymbol{h}. \tag{4.10}$$

That means that the Ansatz (4.6) has been proved.

If $\boldsymbol{g}$ is not invertible or $\boldsymbol{h} = 0$, G_{ij} has no solution or is equal to zero, the situation is more tricky. Assume that the system does not have isolated sites which do not interact with the other ones. Not being able to obtain a reasonable G_{ij} in this case, the Ansatz (4.6) fails. Nevertheless, one can use the symmetry between b_i and $b_i^\dagger$ to generate another exponential ground state. By interchanging creation and annihilation operators of some sites, for example $b_i \leftrightarrow b_i^\dagger$, one constructs a new set of creation and annihilation operators, provided $\boldsymbol{g}$ in this new bases is invertible or $\boldsymbol{h} \neq 0$. With this new set of operators, G_{ij} may be found and the Ansatz (4.6) holds again.

Having a look at the exponential form with the old set of the operators, the ground state does not only consist of creation operators, but also the annihilation at the i-th operator-interchanged sites, where the vacuum $| 0' \rangle$ reads

$$
\begin{aligned}
b_j \, | 0' \rangle &= 0, \quad \text{for } j \neq i, \\
b_i^\dagger \, | 0' \rangle &= 0.
\end{aligned}
\tag{4.11}
$$

This vacuum has infinite number of bosons for the operator-interchanged sites but no bosons in the other sites. In the case of fermions, the interchange $c \leftrightarrow c^\dagger$ is known as particle-hole transformation, because one has only two states for every site.

4.2 Density Matrix and Coherent States

Using Eqn. (4.6) the total density-matrix $\rho_0 = | \Phi_0 \rangle \langle \Phi_0 |$ can be explicitly obtained in an exponential form

$$\rho_0 = |C|^2 \exp\left(\frac{1}{2} \sum_{ij} G_{ij} b_i^\dagger b_j^\dagger \right) | 0 \rangle \langle 0 | \exp\left(\frac{1}{2} \sum_{ij} G_{ij} b_i b_j \right). \tag{4.12}$$

Dividing the total system into two parts (system and environment), one is searching for the reduced density-matrix in subsystem 1. This is obtained by taking the trace over subsystem 2

$$\rho_1 = \text{Tr}_2 \left(\rho_0 \right). \tag{4.13}$$

Different from the approach in the last chapter, one does not have the coordinate representation for the density matrix but an operator form (4.12).

Therefore an another set of variables used to integrate out the degree of freedom in part 2 is needed. To accomplish this, one should introduce coherent states. Coherent states are eigenstates of the annihilation operator b_i, which satisfies the eigenvalue equations [51]

$$b_i \mid \phi_1 \cdots \phi_L \rangle = \phi_i \mid \phi_1 \cdots \phi_L \rangle. \tag{4.14}$$

Such states can be built from the vacuum with the operators $b_j^\dagger$ and complex numbers ϕ_i

$$\mid \phi_1 \cdots \phi_L \rangle = \exp\left(\sum_i \phi_i b_i^\dagger\right) \mid 0 \rangle. \tag{4.15}$$

Using this, one can write the trace of an operator O as

$$\mathrm{Tr}\, O = \int \prod_\alpha \frac{d\phi_\alpha^* d\phi_\alpha}{2\pi i} e^{-\sum_\alpha \phi_i^* \phi_i} \langle \phi \mid O \mid \phi \rangle. \tag{4.16}$$

After forming a general matrix element of ρ_0 with such states and taking the trace over the environment with (4.16), one obtains, if part 1 consists of M sites

$$\langle \phi_1 \cdots \phi_M \mid \rho_1 \mid \phi_1' \cdots \phi_M' \rangle$$
$$= C_1 \int \prod_{i=M+1}^{L} d\phi_i^* d\phi_i e^{-\sum_i \phi_i^* \phi_i} \langle \phi_1 \cdots \phi_M$$
$$\phi_{M+1} \cdots \phi_L \mid \rho_0 \mid \phi_1' \cdots \phi_M' \phi_{M+1} \cdots \phi_L \rangle. \tag{4.17}$$

Inserting Eqn. (4.12) leads to an integrand which contains only quadratic forms of complex numbers in the exponents. By rotating and displacing the variables, the matrix element (4.17) can be expressed as

$$\langle \phi_1 \cdots \phi_M \mid \rho_1 \mid \phi_1' \cdots \phi_M' \rangle$$
$$= C_2 \exp\left(\frac{1}{2}\sum_{ij} \alpha_{ij} \phi_i^* \phi_j^*\right) \exp\left(\sum_{ij} \beta_{ij} \phi_i^* \phi_j'\right)$$
$$\times \exp\left(\frac{1}{2}\sum_{ij} \alpha_{ij} \phi_i' \phi_j'\right), \quad i,j \leq M. \tag{4.18}$$

The $M \times M$ matrices α and β appearing here are defined as follows. One divides $\boldsymbol{G}$ into four submatrices a^{11}, a^{12}, a^{21} and a^{22}, according to whether the sites i, j belong to part 1 or part 2. In terms of these

$$\begin{aligned}
\alpha &= a^{11} + a^{12}(1 - a^{22})^{-1} a^{22}(1 + a^{22})^{-1} a^{21}, \\
\beta &= a^{12}(1 - a^{22})^{-1}(1 + a^{22})^{-1} a^{21}.
\end{aligned} \tag{4.19}$$

As shown in the Appendix one can reconstruct the operator form of ρ_1 from the matrix elements (4.18). This gives

$$
\begin{aligned}
\rho_1 \;=\;& C_2 \exp\left(\frac{1}{2}\sum_{ij}\alpha_{ij}b_i^\dagger b_j^\dagger\right) \exp\left(\sum_{ij}[\ln\beta]_{ij}b_i^\dagger b_j\right) \\
& \times \exp\left(\frac{1}{2}\sum_{ij}\alpha_{ij}b_i b_j\right), \quad i,j \le M.
\end{aligned} \tag{4.20}
$$

In the end, since the Bose operators appear quadratic in the exponents, ρ_1 can be diagonalized by calculating the Heisenberg operators $\rho_1 b_j \rho_1^{-1}$ and $\rho_1 b_j^\dagger \rho_1^{-1}$. Due to the form of ρ_1, they are linear combinations of the b and $b^\dagger$. Inserting a Bogoliubov transformation, one arrives at the form,

$$
\rho_1 = K \ \exp\left(-\sum_{l=1}^{M}\varepsilon_l \mathcal{B}_l^\dagger \mathcal{B}_l\right) \tag{4.21}
$$

with new Bose operators $\mathcal{B}_l^\dagger, \mathcal{B}_l$. The single-particle eigenvalues ε_l can be obtained from the equation

$$
(\beta + \beta^{-1} + \beta^{-1}\alpha - \alpha\beta^{-1} - \alpha\beta^{-1}\alpha)\,\chi_l = 2\cosh\varepsilon_l\,\chi_l. \tag{4.22}
$$

Typically, the matrix has elements varying exponentially over a large range. The normalization factor K is fixed by the sum rule $\mathrm{Tr}(\rho_1) = 1$. In this way, one can calculate the density-matrix spectra numerically for an arbitrary part of a finite system with Hamiltonian (4.1).

In practice, there are some difficulties in using (4.22) to obtain the ε_l. The matrix on the left has a symmetric part $(\beta + \beta^{-1} - \alpha\beta^{-1}\alpha)$ and an antisymmetric one $(\beta^{-1}\alpha - \alpha\beta^{-1})$. Therefore one cannot use the usual routines for symmetric matrices. I have used programs from the NAG library, but these work at most with double precision which limits the ε-values one can calculate to $\varepsilon_l \le 40$. Therefore one cannot treat systems which are too large or with rapidly increasing ε_l. From a numerical point of view, the real space method discussed in the last chapter is much better. Nevertheless, I have introduced this method because one can obtain the reduced density matrices for fermion systems only with the coherent states and the ground states of such solvable models have given more insight with the pairing as in the superconductivity.

4.3 Ground State of Coupled Oscillators - Coherent-State Treatment

In the preceding sections I have described the general method to obtain the reduced density matrices for solvable boson systems. Since the Hamiltonian (3.1) for coupled oscillators can be rewritten into one in quadratic

Bose Operators, one can treat them in the same way. Due to the fact that
$(\boldsymbol{A} - \boldsymbol{B})(\boldsymbol{A} + \boldsymbol{B})$ and $(\boldsymbol{A} + \boldsymbol{B})(\boldsymbol{A} - \boldsymbol{B})$ both equal the potential matrix
in Eqn. (3.1), the eigenvalues Λ_k are, as expected, equal to the normal
frequencies ω_k and ϕ_k are the eigenvectors of normal modes. In addition,
the ψ_k are linearly related to the ϕ_k

$$\psi_k = \frac{\omega_0}{\omega_k}\phi_k. \tag{4.23}$$

This follows from the general relation

$$(\boldsymbol{A} - \boldsymbol{B})\ \phi_k = \omega_k\psi_k, \tag{4.24}$$

and the fact that $(\boldsymbol{A} - \boldsymbol{B}) = \omega_0\boldsymbol{1}$ for the coupled oscillators. Due to the
condition (4.5), which implies that the ϕ_k are not normalized, one can
introduce a new set of vectors ϕ'_k which are the orthonormal eigenvectors
of $(\boldsymbol{A} + \boldsymbol{B})(\boldsymbol{A} - \boldsymbol{B})$ and are related to ϕ_k by

$$\phi_k = \sqrt{\frac{\omega_k}{\omega_0}}\phi'_k. \tag{4.25}$$

Thus ψ_k can be expressed as

$$\psi_k = \sqrt{\frac{\omega_0}{\omega_k}}\phi'_k \tag{4.26}$$

Therefore, the canonical transformation (4.2) reads

$$\eta_k = \frac{1}{2}(\sqrt{\frac{\omega_k}{\omega_0}} + \sqrt{\frac{\omega_0}{\omega_k}})B_k + \frac{1}{2}(\sqrt{\frac{\omega_k}{\omega_0}} - \sqrt{\frac{\omega_0}{\omega_k}})B_k^\dagger, \tag{4.27}$$

where

$$B_k = \sum_i \phi'_{ki}b_i. \tag{4.28}$$

Since B_k $(B_k^\dagger)$ are obtained by an orthonormal transformation from b_i $(b_i^\dagger)$,
they are also Bose annihilation(creation) operators.

Consider now the ground state of the coupled oscillators. As shown in
the last section, it has an exponential form in the creation operators $b_j^\dagger$,
and therefore also in the $B_k^\dagger$. Following the condition (4.8), it reads

$$\frac{1}{2}(\sqrt{\frac{\omega_k}{\omega_0}} + \sqrt{\frac{\omega_0}{\omega_k}})B_k + \frac{1}{2}(\sqrt{\frac{\omega_k}{\omega_0}} - \sqrt{\frac{\omega_0}{\omega_k}})B_k^\dagger \mid \Psi_0\rangle = 0. \tag{4.29}$$

As discussed in appendix B, the operator B_k play a role as $\partial/\partial B_k^\dagger$, thereby
the ground state has the form as

$$\mid \Psi_0\rangle = C_1 \exp\left(-\frac{1}{2}\sum_k \frac{\omega_0 - \omega_k}{\omega_0 + \omega_k}B_k^{\dagger 2}\right) \mid 0\rangle. \tag{4.30}$$

How can one understand Eqn. (4.30)? Let us consider one oscillator with a frequency ω_0. I denote $|\omega_0\rangle$ and $B^\dagger(B)$ as the ground state and the creation (annihilation) operator for the oscillator. Now I change the frequency ω_0 to ω, thereby the ground state changes to $|\omega\rangle$. According to the reference [52], $|\omega\rangle$ is given by

$$|\omega\rangle = C \exp\left\{-\frac{1}{2}\frac{(\omega_0 - \omega)}{(\omega_0 + \omega)}B^{\dagger 2}\right\}|\omega_0\rangle. \tag{4.31}$$

The state $|\omega\rangle$ is called a squeezed state of $|\omega_0\rangle$. Back to our Eqn. (4.30), since coupled oscillators can be treated as L independent oscillators with frequencies ω_k in the normal modes and $|0\rangle$ is the ground state of the L oscillator with frequencies all equal to ω_0 in these normal modes, $|\Psi_0\rangle$ is then a squeezed state of $|0\rangle$. According to (4.31), $|\Psi_0\rangle$ is given by Eqn. (4.30).

Transforming the Bose operators $B_k^\dagger$ into $b_j^\dagger$ with Eqn. (4.28), G_{ij} can be expressed as

$$G_{ij} = -\sum_k \phi_{ik}\left(\frac{\omega_0 - \omega_k}{\omega_0 + \omega_k}\right)\phi_{kj}. \tag{4.32}$$

Instead of using Eqn. (4.10), one obtains G_{ij} directly from the frequencies and the eigenvectors of normal modes. According to the discussion of last section, the reduced density-matrix spectra can be calculated from the submatrices of $\boldsymbol{G}$. I have calculated coupled oscillators with $L = 6$, $k = 0.5$ and $\omega_0 = 0.5$ and found that the ε_l are identical with those in the last chapter. This indicates that the method in this chapter is equivalent to that in the last chapter, though I cannot yet give a rigorous proof.

Chapter 5

Solvable Fermionic Systems

In the last chapters I have emphasized the importance of the density-matrix spectra for the bosonic systems. One should ask whether the spectra can be obtained explicitly for some solvable fermionic models. For some non-critical systems this is possible by using the relation between the density matrices of quantum chains and the corner transfer matrices (CTM's) [17] of the corresponding two-dimensional classical problems (see Ref.[44]). In this way, the spectra for the transverse Ising chain [18] and the XXZ Heisenberg chain [18] could be determined in the thermodynamic limit and compared with DMRG calculations. In all these cases, one finds simple analytic expressions and, apart from degeneracies, a strict exponential behavior. But the CTM approach is limited to large noncritical systems, therefore an alternative approach is necessary by which one can treat solvable fermion systems of arbitrary size. In the last chapter I described how boson systems can be treated with coherent states. A similar approach can be used for fermions [53].

The solvable fermionic models I want to consider have a general Hamiltonian

$$H_f \;=\; \sum_{ij=1}^{L} \left\{ c_i^\dagger A_{ij} c_j + \frac{1}{2}(c_i^\dagger B_{ij} c_j^\dagger + h.c.) \right\}, \qquad (5.1)$$

where the c_i's and $c_i^\dagger$'s are Fermi annihilation and creation operators. Due to the Hermiticity of H_f, the matrix $\boldsymbol{A}$ is Hermitian and $\boldsymbol{B}$ is antisymmetric. In the following I consider only real matrices. One can diagonalize H through a canonical transformation [54], analogously to the procedure in the chapter 4. The sole difference is that the η_k and $\eta_k^\dagger$ are Fermi operators, leading to

$$\frac{1}{2} \sum_i \phi_{ki}\phi_{ik'} + \psi_{ki}\psi_{ik'} = \delta_{k,k'}, \qquad (5.2)$$

instead of (4.5). Therefore one can choose ϕ_k and ψ_k as orthonormal bases [54].

The way to find the eigenvalues w_n of the reduced density matrices is also similar to the bosonic case, therefore I will not describe the details here, but in appendix C. One should use here coherent states of fermions composed of fermionic operators and Grassmann variables. However, α and β are the same as in the Eqn (4.19) and reduced density matrices ρ_1 has the form

$$\rho_1 = K \, \exp\left(-\sum_{l=1}^{M} \varepsilon_l f_l^\dagger f_l\right), \tag{5.3}$$

where f_l and $f_l^\dagger$ are here Fermi operators and ε_l are still the eigenvalues of the Eqn. (4.22). The normalization factor K is fixed by the sum rule $\mathrm{Tr}(\rho_1) = 1$. In this way, one can calculate the density-matrix spectra numerically for an arbitrary part of a finite system with Hamiltonian (5.1).

In the following section 5.1 I apply the method to the transverse Ising chain and discuss the resulting spectra for a number of situations, including the critical case, the first excited state and related row transfer matrices. Section 5.2 deals with the other one-dimensional problems, namely the spin one-half XX and XY chain. The XX spin chain can be transformed into the tight-binding model in one dimension and gives us a good example for treating the two-dimensional TB model. The spin one-half chain in a field is interesting because it has a disorder point where the density-matrix spectrum collapses. In section 5.3 we turn to the physically most important case of a tight-binding model which we discuss in two dimensions. We present spectra for systems of various sizes and shapes, as well as truncation errors showing the difficulties in this case. Section 5.4, finally, contains a summary and some additional remarks.

5.1   Transverse Ising Chain

As a first example, we consider in this section the transverse Ising chain with open boundaries described by

$$H = -\sum_{i=1}^{L} \sigma_i^z - \lambda \sum_{i=1}^{L-1} \sigma_i^x \sigma_{i+1}^x, \tag{5.4}$$

where the σ^α are Pauli spin matrices and the transverse field has been set equal to one. In the thermodynamic limit, this system has a quantum critical point at $\lambda = 1$ and long-range order in σ^x for $\lambda > 1$. In terms of spinless fermions H reads

$$H = -2\sum_{i=1}^{L} (c_i^\dagger c_i - 1/2) - \lambda \sum_{i=1}^{L-1} (c_i^\dagger - c_i)(c_{i+1}^\dagger + c_{i+1}) \tag{5.5}$$

and thus has the form (5.1). In the following we discuss the reduced density matrix ρ_1 for one half of the chain, i.e. $M = L/2$.
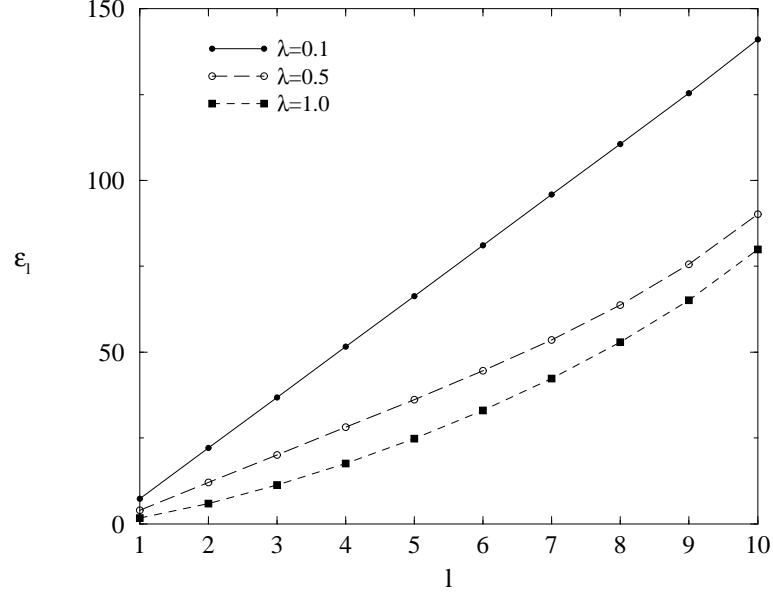
Figure 5.1: Single-particle eigenvalues ε_l for one-half of a transverse Ising chain, arranged in ascending order. The system is in the ground state, $L = 20$ and $\lambda < 1$.

5.1.1 Density-Matrix Spectra for One Half Chain

We first consider the ground state. Before discussing the density-matrix spectra of different λ, those of the thermodynamic limit should briefly be mentioned in order that one can compare the results. Namely, the transverse Ising chain can be related to the two-dimensional Ising model. Using the CTM, the reduced density matrix ρ_h for one-half chain reads [18]

$$\rho_h = K \exp\left\{-\sum_l \varepsilon_l f_l^\dagger f_l\right\}, \tag{5.6}$$

where $f_j^\dagger$ and f_j are Fermi operators and the single particle energies

$$\varepsilon_l = \begin{cases} (2l+1)\varepsilon, & \text{for } \lambda < 1 \\ 2l\varepsilon, & \text{for } \lambda > 1 \end{cases} \tag{5.7}$$

where $l = 0, 1, 2, \ldots$ and ε is given by

$$\varepsilon = \pi \frac{I(k')}{I(k)}. \tag{5.8}$$

Here $I(k)$ denotes the complete elliptic integral of the first kind, $k' = \sqrt{1-k^2}$ and the parameter k with $0 \leq k \leq 1$ is related to λ by

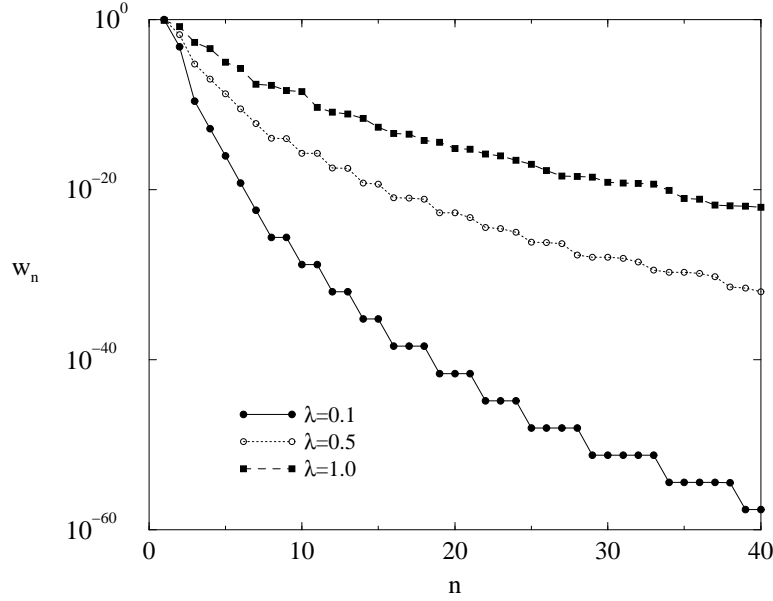$$k = \begin{cases} \lambda, & \text{for } \lambda < 1 \\ 1/\lambda, & \text{for } \lambda > 1. \end{cases} \tag{5.9}$$

Figure 5.2: Density-matrix eigenvalues w_n, arranged in decreasing order, obtained from the ε_l in Fig. 5.1 and for the same parameters.

In the case $\lambda > 1$, one always obtains $\varepsilon_0 = 0$, which generates twofold degeneracies in the density-matrix spectra due to the long-rang order. One can find the details in the paper by Peschel *et al.* [18].

We now turn to our results and first discuss the disordered phase. In Fig. 5.1, the single-particle eigenvalues ε_l are plotted for $L = 20$ and different coupling constants λ. For $\lambda = 0.1$ they all lie on a straight line, which corresponds to Eqn. (5.7) in the thermodynamic limit. This is what one expects since the correlation length is much less than L and hence boundary and finite-size effects should be small. One can also check the values are exactly those obtained by Eqn. (5.7) and (5.8). It seems that difficult, however, to derive this formula directly from our equations. For larger coupling, $\lambda = 0.5$, only the first ε_l follow a linear law, and the curve bends upwards. This is similar to the behavior one finds in the finite-size CTMs [55], though the geometry there is different. At the same time, the initial slope decreases. Finally, at the critical point, the whole graph is curved.

One can derive w_n of ρ_1 from the ε_l by specifying the occupation numbers $f_l^\dagger f_l$ equal to zero or one in Eqn. (5.3). The resulting spectra are shown in Fig. (5.2) in a semi-logarithmic plot. Note that not all w_n are shown (the total number is 2^M), however they are correctly normalized to one. Similar results, but for a smaller number of w_n, were obtained in Ref. [18] via DMRG calculations. For $\lambda = 0.1$, where $\varepsilon_l = \varepsilon, 3\varepsilon, 5\varepsilon, \ldots$, the w_n take all values proportional to $e^{-n\varepsilon}$ except $e^{-2\varepsilon}$. The first degeneracy
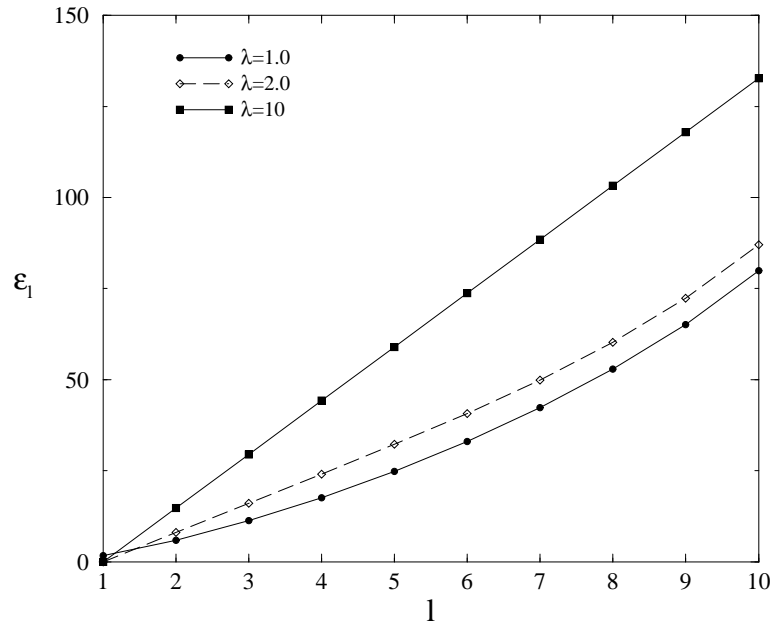
Figure 5.3: Single-particle eigenvalues ε_l for one-half of a transverse Ising chain, arranged in ascending order. The system is in the ground state, $L = 20$ and $\lambda > 1$. Notice that the ε_l for $\lambda = 10$ are obtained by the Eqn. (5.7).

occurs for the eigenvalue $e^{-8\varepsilon}$ because it can be obtained from $3\varepsilon + 5\varepsilon$ or $\varepsilon + 7\varepsilon$. The other degeneracies follow in the same way. The spectrum for $\lambda = 0.5$ has a similar structure, except that in the smaller w_n the degeneracies are lifted due to the fact that the bigger ε_l do not lie on the same straight line any more. For the critical point ($\lambda = 1$), the degeneracies disappear, stemming from the curved spectrum. Due to the relatively large values of the ε_l there is a rather rapid decay (note the vertical scale) so that the system can be treated very well by DMRG [56, 57]. This holds even at the critical point, where the decay is slowest.

Spectra for the ordered phase ($\lambda > 1$) are shown in Fig. 5.3. The two lowest curves are numerical results. However, for $\lambda > 2.5$, ε_0 is very small (almost 0) and ε_{L-1} is large. This difference caused the computational problem because any small inaccuracy compared with ε_{L-1} will cause large inaccuracy compared with ε_0. Therefore I used the analytical result (5.7) for the case $\lambda = 10$. One sees that if one moves away from the critical point, the ε_l straighten out again and ε_0 decreases to 0. For $\lambda = 2$ ($k = 0.5$), one has $\varepsilon_1/2 = 4.01895$, whereas $\varepsilon = 4.01892$ from the elliptic function (5.8). Therefore the numerical and analytical results coincide. However, the higher other eigenvalues differ more and more from the analytical result due to boundary effects. The analytical ε_l obeying the linear rule (5.7) show us the thermodynamic limit in the ordered phase.

The w_n for $\lambda > 1$ obtained from the ε_l are shown in Fig. 5.4. In
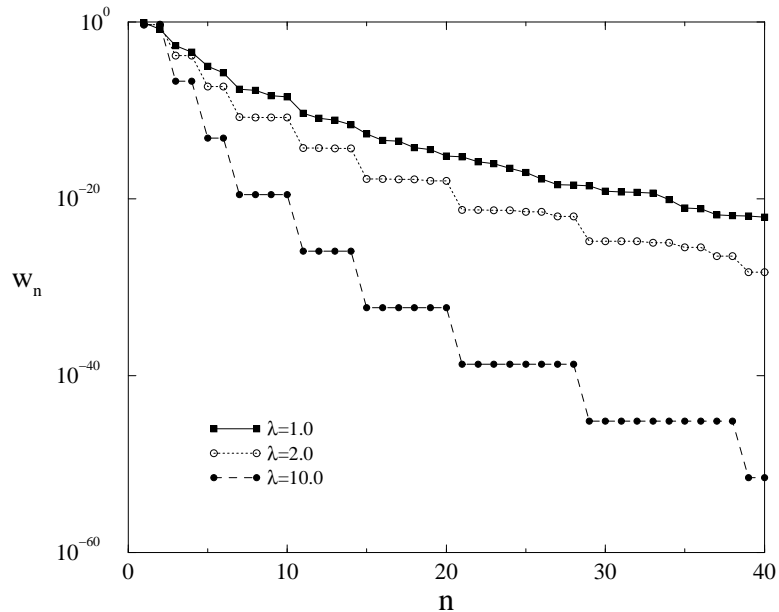
Figure 5.4: Density-matrix eigenvalues w_n, arranged in decreasing order, obtained from the ε_l in Fig. 5.3 and for the same parameters.

contrast to those in the case of disordered region, the w_n are at least doubly degenerate, due to the small ε_0. Therefore they are flatter than those for $\lambda < 1$ with the same k. However, they also drop so rapidly that one can also treat the system very well by DMRG.

The situation at the critical point $\lambda = 1$ is presented in more detail in the next figures. Fig. 5.5 shows the ε-spectra for various sizes of the system. As L increases, the number of ε increases, the curves become flatter, but the curvature remains. There is no sign of a linear region related to conformal invariance on this scale (compare Ref. [55]). The w_n spectra are plotted in Fig. 5.6. Because of the form of the ε, there are few degeneracies and the curves have the typical, relatively smooth shape found also for other critical systems [2, 16]. As can be seen, the w_n decrease more slowly with increasing size, and they do not converge at this stage. The fan-shaped tails essentially show finite-size effects.

Comparing the ε_l of ρ_h for $\lambda \leq 1(k \leq 1)$ with those for the coupled oscillators in the section 3.2, one sees that they are very similar, but not the same. Moreover, the single-particle spectra for fermions and for bosons go to the same thermodynamics limits. However, the w_n for fermions (5.3) and bosons in Eqn. (3.25) differ from each other because of the different statistics. In the case of bosons, the w_n decrease more slowly than fermions. Furthermore, the reduced density matrices for bosons are un-normalizable in the critical point $k = 1.0$, while for fermions ($\lambda = 1.0$) they are normalizable. The reason is that one state can be occupied by

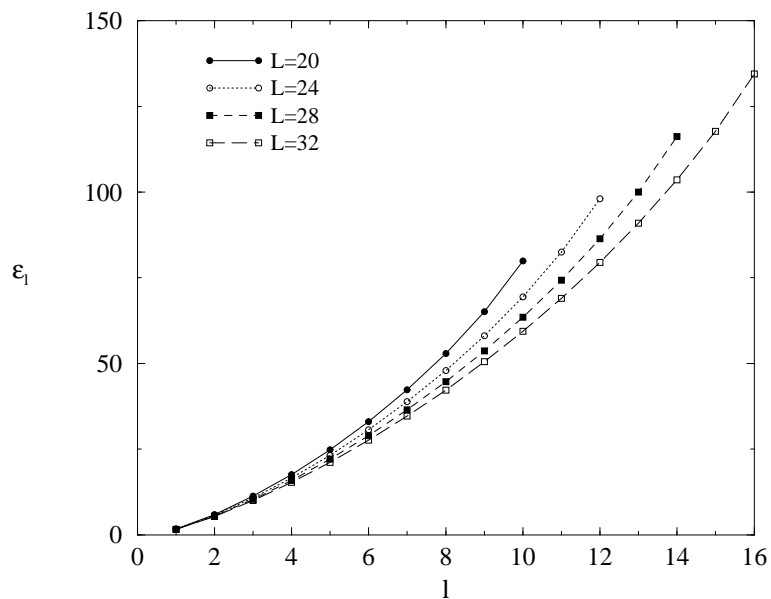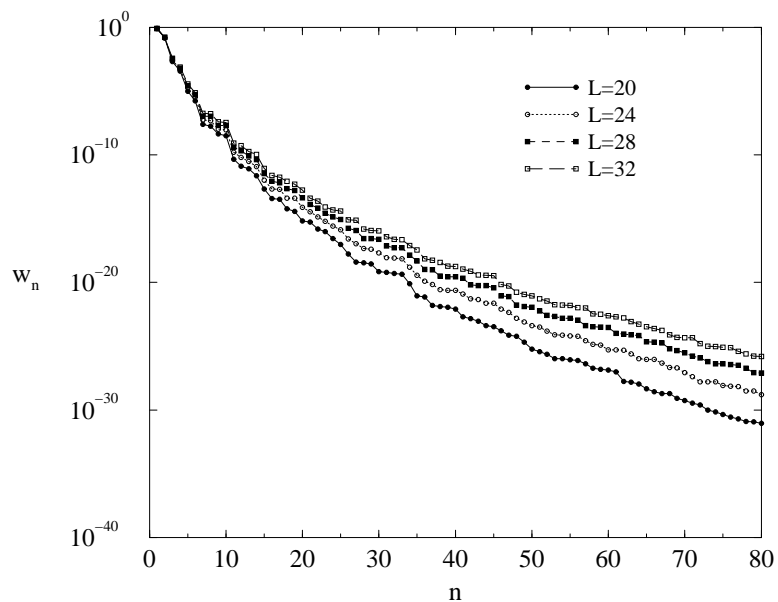**Figure 5.5:** Single-particle eigenvalues ε_l for critical transverse Ising chains in the ground state.

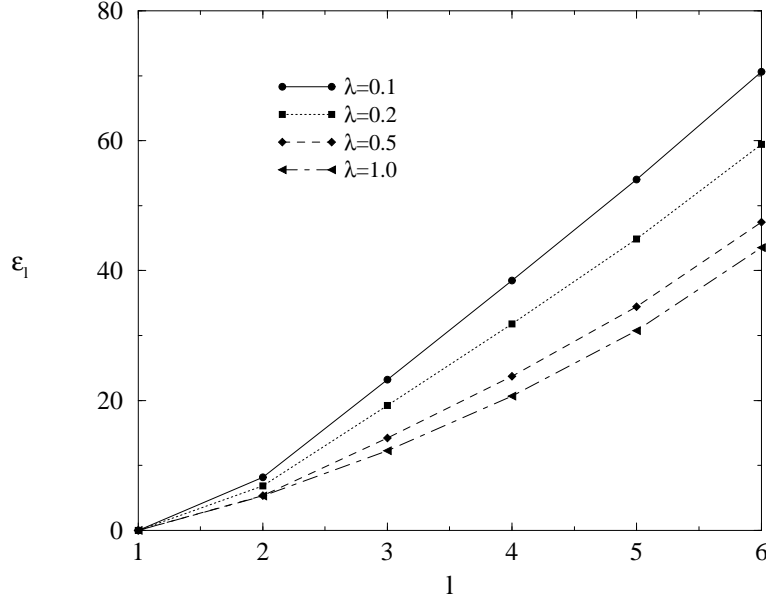**Figure 5.6:** Density-matrix eigenvalues w_n for transverse Ising chains at the critical point obtained from the ε_l in Fig. 5.5.

Figure 5.7: Single-particle eigenvalues ε_l for critical transverse Ising chains in the ground state.

an arbitrary number of bosons, but only by one fermion. If some single-particle eigenvalues are small, the spectra w_n for bosons will be rather flat and one zero single-particle eigenvalue makes the density unrenormalizable. For fermions, on the contrary, the situation is much less dramatic.

5.1.2 First Excited State

So far, we have treated the ground state, but one can also determine the density matrices for the first excited state $| \Phi_1 >$. This state contains an odd number of fermions. To apply the formalism here, one can perform a particle-hole transformation at one site, e.g. $c_1^\dagger \leftrightarrow c_1$. Then $| \Phi_1 >$ appears in the even subspace and can be written in the form (4.6). With the help of the relations

$$
\begin{aligned}
\eta_1^\dagger \, | \, \Phi_1 > &= 0 \\
\eta_k \, | \, \Phi_1 > &= 0 \quad \text{for } k \geq 2,
\end{aligned} \tag{5.10}
$$

one can then derive the corresponding equation for the matrix G_{ij}. This procedure to obtain G_{ij} has been addressed in the last chapter in the bosonic case. Before particle-hole transformation, one can find g_{ij} and h_{ij} from Eqn. (5.10). Unfortunately, g_{ij} is not invertible, which reflects the fact that the first excited state has an other particle configuration than ground state, i.e. it has only odd number of fermions. Therefore, one has
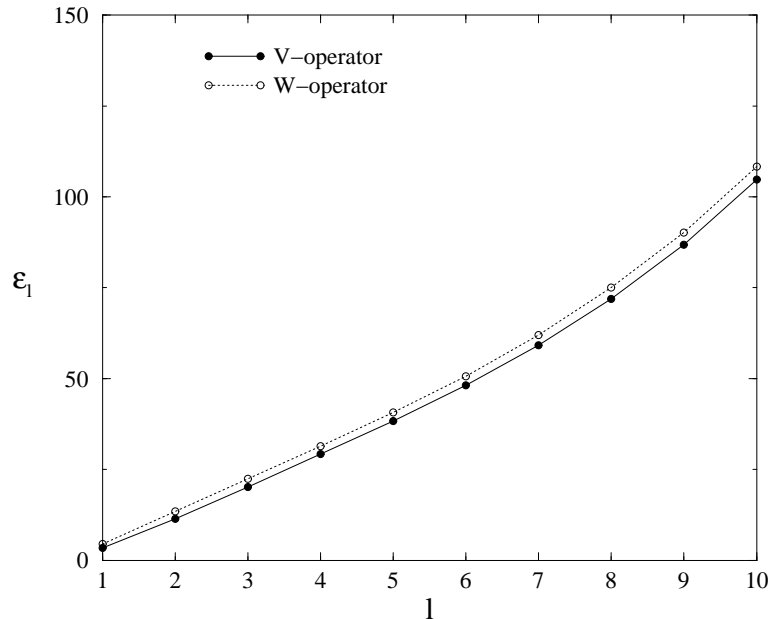
Figure 5.8: Single-particle eigenvalues ε of the two different row-to-row matrices V and W.

to make a particle-hole transformation on one site. One obtains the same results, on whichever site one makes it.

In this way, the single-particle eigenvalues ε_l shown in Fig. 5.7 were obtained. In contrast to the case of the ground state, the first eigenvalue is zero here. This reflects the fact that, in the original representation, the fermion number is odd, while the number of sites is even. The other eigenvalues are very similar to those for the ground state. In particular, one has a linear spectrum away from $\lambda = 1$ and a curved one at the critical point. The vanishing of ε_1 causes all eigenvalues w_n of ρ_1 to be at least doubly degenerate.

5.1.3   Two-Dimensional Ising Model

The closely related problem of the row-to-row transfer matrices for the two-dimensional Ising model can be studied in the same way. For a square lattice with the couplings $K_1(K_2)$ in the vertical (horizontal) direction one can consider two symmetrized version (see Fig. 6.2 without defects), namely

$$V = V_2^{1/2}V_1V_2^{1/2}; \quad W = V_1^{1/2}V_2V_1^{1/2} \tag{5.11}$$

where, for open boundaries

$$V_1 = \exp\left[K_1^* \sum_{i=1}^{L} \sigma_i^z\right], \tag{5.12}$$

69

$$V_2 = \exp\left[K_2 \sum_{i=1}^{L-1} \sigma_i^x \sigma_{i+1}^x\right].$$

(5.13)

The σ_i^α are Pauli matrices and K_1^* denotes dual coupling of K_1, $\tanh K_1^* = \exp(-2K_1)$. In terms of Fermi operators $c_i, c_i^\dagger$ via the Jordan-Wigner transformation they read

$$V_1 = \exp\left[K_1^* \sum_{i=1}^{L} (2c_i^\dagger c_i - 1)\right],$$

(5.14)

$$V_2 = \exp\left[K_2 \sum_{i=1}^{L-1} (c_i^\dagger - c_i)(c_{i+1}^\dagger + c_{i+1})\right].$$

(5.15)

Both represent fermionic quantum chains and can be diagonalized [58, 59] with the Bogoliubov transformation. DMRG calculations using the operator V have already been done [60]. In the last chapter, I will discuss the two-dimensional Ising plane with various defects, where the DMRG calculations for the pure Ising plane are needed.

Following Ref. [59] one can find the g_{ij} and h_{ij} for the eigenvector with maximal eigenvalue, which is needed for the thermodynamics. From g_{ij} and h_{ij}, G_{ij} is obtained using Eqn. (4.10) and the ε_l follow. The spectrum of the ε_l in the isotropic case $K_1 = K_2$ is very similar to that found above in Fig. 5.1. This also holds for the magnitude of the ε_l and the problem can therefore be treated equally well by DMRG. An example for $K_1 = K_2 = 0.3$ is shown in Fig. 5.8. For W, the ε-spectrum is strictly linear at the lower end and described by a formula containing elliptic integrals as in Eqn. (5.7), while for V the values are somewhat smaller and there is a deviation from linearity for the first ε_l. This reflects the different of the geometrical representation of the two transfer matrices: W can directly be related to two multiplied CTMs, while in order to form V one has to multiply a row-to-row TM between two CTMs.

5.2 XX- and XY-Spin Chain

In this section I will consider XX and transverse XY spin chains. The two spin chains have some interesting properties, the most important is that they have different ground-state structure than the transverse Ising chains. I want to discuss these ground states and thereby to generalize the ansatz (4.6).
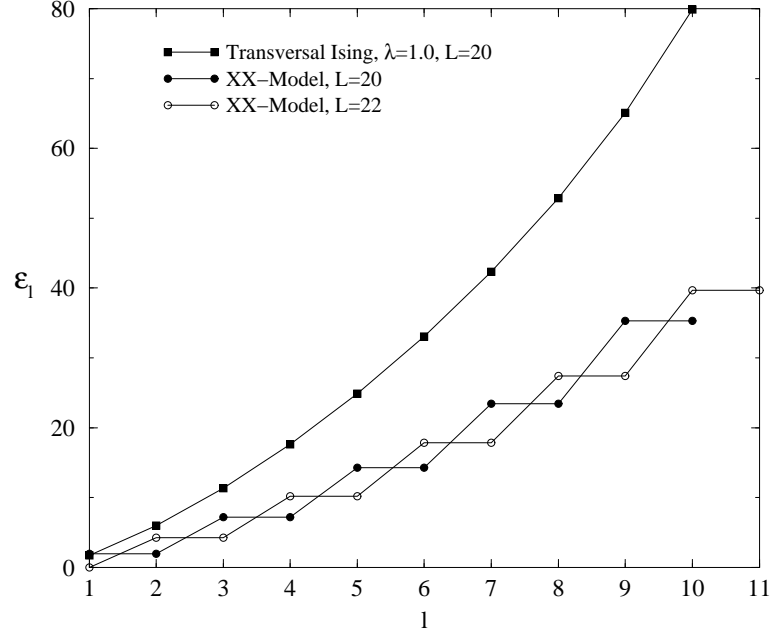
Figure 5.9: The single-particle eigenvalues ε_l for one half of an XX spin chain with two different lengths compared with a critical transverse Ising chain.

5.2.1   XX-Spin Chain

The XX-spin chain with open boundaries reads

$$H_{XX} = -J/2 \sum_{i=1}^{L-1} \left(\sigma_i^x \sigma_{i+1}^x + \sigma_i^y \sigma_{i+1}^y \right). \qquad (5.16)$$

Through the Jordan-Wigner transformation, the Hamiltonian (5.16) can be expressed in term of fermions as

$$H_{XX} = -J \sum_{i=1}^{L-1} \left(c_i^\dagger c_{i+1} + c_{i+1}^\dagger c_i \right). \qquad (5.17)$$

This shows that the XX spin chain with open boundaries is identical with the tight-binding (TB) model in one dimension. Therefore I want to treat it as an introduction of two-dimensional TB model in the next section.

After a Fourier transformation, Eqn. (5.17) can be expressed as

$$H_{XX} = -J \sum_k 2 \cos k \, c_k^\dagger c_k, \quad k = \frac{\pi}{L+1} n, \quad n = 1, 2, \ldots, L, \quad (5.18)$$

where $c_k (c_k^\dagger)$ are the annihilation (creation) operator in momentum space. Compared with Eqn. (C.3), $\Lambda_k = -2 \cos k$. For even L, i.e. $L = 2M$, one

has M negative single-particle Energies if $n = 1, \ldots, M$. Thus the ground state contains $M = L/2$ single particles with negative Λ_k. For odd L, i.e. $L = 2M + 1$, one has M negative single-particle energies if $n = 1, \ldots, M$ and $\Lambda_k = 0$ if $n = M + 1$. This zero energy will not affect the total energy, thus the ground states are two-fold degenerate, containing M or $M + 1$ particles, respectively. Because of the algorithm of DMRG, I will only consider even L.

The ground state here is different from that in the transverse Ising models. One can see from Eqn. (C.4) that our Ansatz for the ground state is not particle conserved, while the ground state for the tight-binding model has conserved particles. One can consider this mathematically. Because H only contains hopping, $B = 0$ in Eqn. (5.1), the fermion number is fixed and the ground state does not have the form (C.4). Formally, this manifests itself in the fact that $h_{ij} = 0$ so that the matrix G_{ij} cannot be found. However, as discussed in the last chapter, one has to perform enough particle-hole transformations to obtain G_{ij}. In the present case, one exchanges the creation and annihilation operators on $L/2$ sites, for example on every second one, by which the effective g_{ij} is invertible and $h_{ij} \neq 0$. One should notice that the results are the same, on whichever $L/2$ sites one performs the transformation due to the fact that the ground state is unique for an open XX spin chain if L is even. In terms of new operators, $| \Phi_o \rangle$, which originally contains $L/2$ particles, becomes a superposition of terms with particle numbers ranging from 0 to L and can again be written in form (4.6). If one transforms the ground state back into the original operators, it gives

$$| \Phi_0 \rangle = C_f \exp \{ \frac{1}{2} \sum_{ij} G_{ij} c_i^\dagger c_j \} | 0, 1, 0, 1, \cdots \rangle, \qquad (5.19)$$

where $| 0, 1, 0, 1, \cdots \rangle$ denotes the state without particles on the sites $i = 1, 3, 5, \cdots$ and with one particle on the sites $i = 2, 4, 6, \cdots$. $G_{ij} \neq 0$ only if $i(j)$ takes even (odd) number. The exponential operator in the ground state (5.19) annihilates a particle and creates another particle at the same time, thereby conserving the particles. In the same way, an arbitrary n-particle eigenstate of H could be handled by exchanging particles and holes at n sites. The density-matrix spectrum is not affected by such local transformations.

In Fig. 5.9, I show the single-particle eigenvalues ε for $L = 20$ and $L = 22$. Because the XX model is critical, one can compare the results with those for the critical transverse Ising chain. As can be seen, the eigenvalues ε for XX chain and $L = 20$ are all two-fold degenerated, while those for $L = 22$ are two-fold degenerate, except when $\varepsilon_1 = 0$. Because of these degeneracies, the single-particle spectrum for XX chain increases more slowly than that in the critical transverse Ising chain with the same size. The density-matrix spectra w_n obtained from the ε_l in Fig. 5.9 are
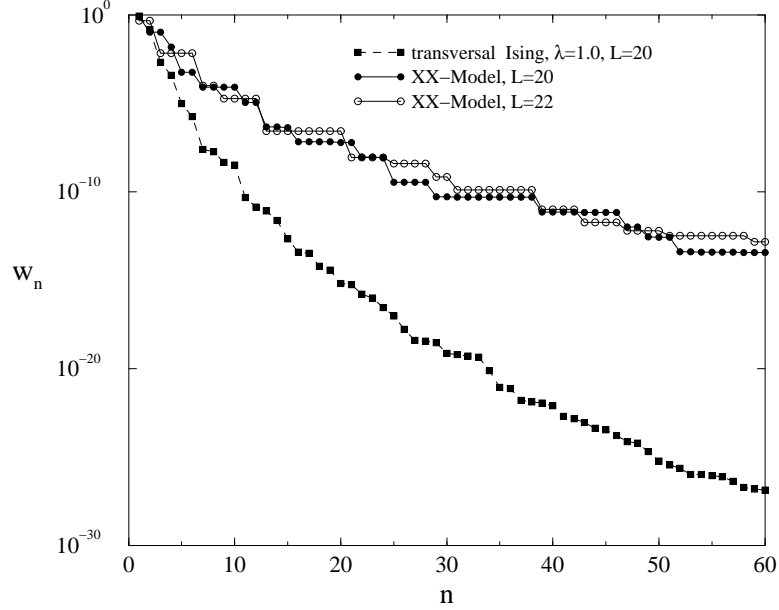
Figure 5.10: Density-matrix eigenvalues w_n, arranged in decreasing order, obtained from ε_l in Fig. 5.9.

shown in Fig. 5.10. Due to the flatter ε spectra, the w_n for the XX model drop much more slowly than for the transverse Ising chain. Their step-like structure for the XX chains is a consequence of the degeneracies of the ε.

For $L = 22$, the w_n are always two-fold degenerate due to the fact that $\varepsilon_1 = 0$, while for $L = 20$ this is not the case. We can understand the phenomenon using the particle-hole symmetry. The ground state for $L = 2M$ can be separated into two states

$$\mid \Phi_0 \rangle = \mid P \rangle + \mid H \rangle, \tag{5.20}$$

where the state $\mid P \rangle$ contains $M, M-1, \ldots, [M/2]$ particles in the system part 1 ($[x]$ is equal to the integer part of x) and $\mid H \rangle$ is its particle-hole symmetric state. For odd M, where $[M/2] = (M-1)/2$, one finds that

$$\mathrm{Tr}_2 \mid P \rangle \langle H \mid = \mathrm{Tr}_2 \mid H \rangle \langle P \mid = 0 \tag{5.21}$$

because $\mid P \rangle$ always contains less particles in the environment than $\mid H \rangle$ and hence they are orthogonal with respect to the bases of the environment. Thereby the reduced density matrix $\rho_h = \mathrm{Tr}_2 \mid \Phi_0 \rangle \langle \Phi_0 \mid$ for the one-half chain reads

$$\begin{aligned} \rho_h =& \mathrm{Tr}_2 \left(\mid P \rangle + \mid H \rangle \right) \left(\langle P \mid + \langle H \mid \right) \\ =& \mathrm{Tr}_2 \left(\mid P \rangle \langle P \mid \right) + \mathrm{Tr}_2 \left(\mid H \rangle \langle H \mid \right). \end{aligned} \tag{5.22}$$

Since $\mid H \rangle$ is merely the particle-hole symmetric state, the density matrix spectra for this state are the same with them from the state $\mid P \rangle$, therefore
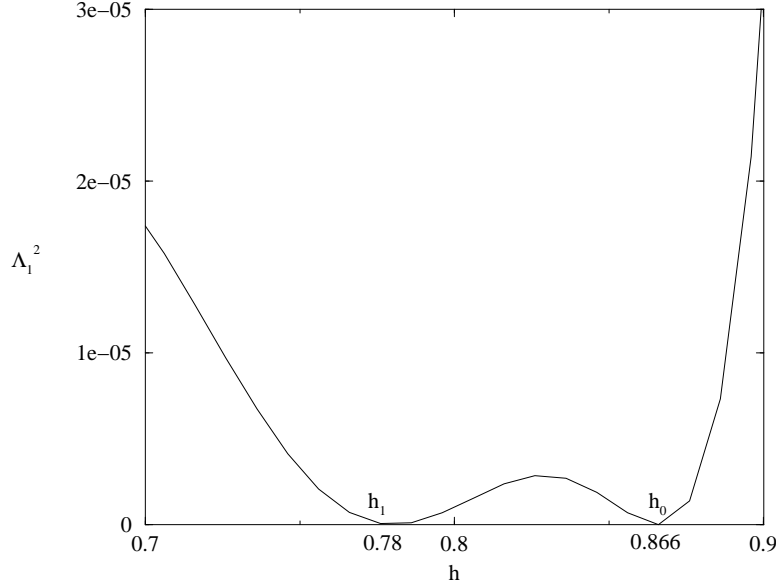
Figure 5.11: The first single-particle eigenvalue Λ_1 of the Hamiltonian 5.23 for the XY chain in a transverse field. The anisotropy is $\gamma = 0.5$, the length $L = 8$.

the density-matrix spectra for ρ_h are at least two-fold degenerate. On the contrary, for even M, where $[M/2] = M/2$, $\mid P \rangle$ is not orthogonal with $\mid H \rangle$ because they both contain the state composed of $M/2$ particles in the surrounding. The density matrices are not always degenerate.

In spite of the difference of degeneracies the two w_n-curves for odd and even M are very similar. Though they drop much slowly than those in the critical transverse Ising chain, they do not create any difficulties in the DMRG calculation. With 60 truncated states one can obtain the truncation error less than 10^{-10}.

5.2.2 Transverse XY-Spin Chain

In this subsection I consider an anisotropic XY chain with a transverse magnetic field described by the Hamiltonian

$$H_{XY} = -J/2 \sum_{i=1}^{L-1} \left\{ (1+\gamma)\sigma_i^x \sigma_{i+1}^x + (1-\gamma)\sigma_i^y \sigma_{i+1}^y + \right.$$
$$\left. h(\sigma_i^z + \sigma_{i+1}^z) \right\} \tag{5.23}$$

which reads in terms of fermions

$$H_{XY} = -J \sum_{i=1}^{L-1} \left\{ (c_i^\dagger c_{i+1} + \gamma c_i^\dagger c_{i+1}^\dagger + h.c.) \right.$$
$$\left. + h(c_i^\dagger c_i + c_{i+1}^\dagger c_{i+1} - 1) \right\}. \tag{5.24}$$
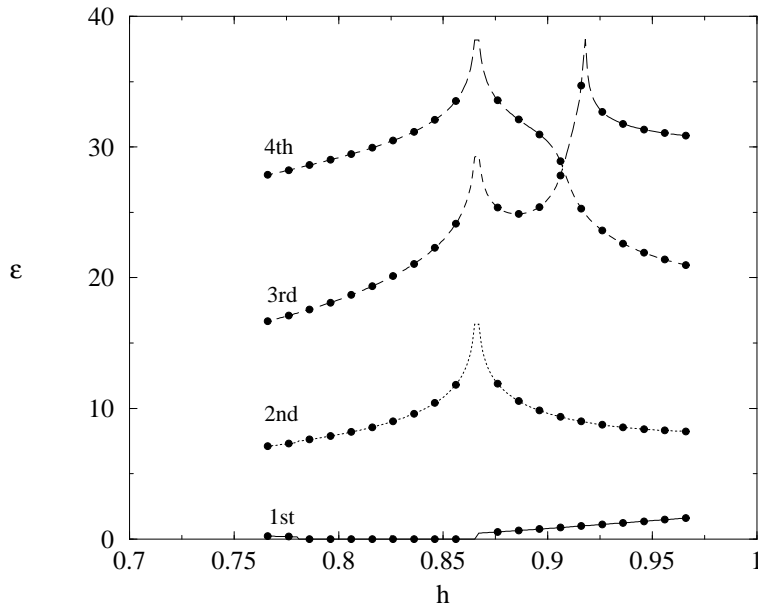
Figure 5.12: The four lowest single-particle eigenvalues ε for an XY spin chain in a field h. The anisotropy is $\gamma = 0.5$, the length $L = 8$. Lines result from the analytical method, solid circles from a DMRG calculation.

Although similar to the transverse Ising chain, this system has a special feature. For

$$\gamma^2 + h^2 = 1 \qquad (5.25)$$

the ground state simplifies and also becomes two-fold degenerate. In the spin language, one has two simple product states [61]. Moreover, the behavior of correlation functions changes from monotonic to oscillatory [62] and thus (5.25) represents a "disorder line" [63]. On this line, H describes also a stochastic reaction-diffusion model [64] equivalent to Glauber's kinetic spin model.

The appearance of a simple ground state can be observed in the density-matrix spectrum, namely in this disorder line there are only two nonzero eigenvalues for the reduced density matrices. This phenomenon has been seen in DMRG calculations for certain other models (see Sec. 3.1 in Ref. [3]). That means, one will find only one non-infinite eigenvalue ε in the single-particle spectrum along this line. For the XY chain, this can be investigated very well in the fermionic approach.

So far I have studied the ground states of the transverse Ising model, which always had an even number of particles. However this is not the case for all models. It is known that H_{XY} commutes with the transverse Ising model for $\gamma^2 + h^2 > 1$. Thereby the ground states in this region also have an even number of particles. On the contrary, in the order oscillating phase $\gamma^2 + h^2 < 1$, the situation is quite different. Fig (5.11) shows the

first single-particle energy Λ_1 of H_{XY} as a function of the parameter h in the region $0.7 \leq h \leq 0.9$ for fixed anisotropy $\gamma = 0.5$ and $L = 8$. One can see that they oscillate and cross zero twice, once at the disorder line $h_0 = 0.866$, once at the point $h_1 = 0.78$. At h_0 and h_1, $\Lambda_1 = 0$ the ground states are two-fold degenerate, because $|\Phi_0\rangle$ and $\eta_1^\dagger|\Phi_0\rangle$ have the same energy. These two ground states correspond to an even and an odd number of particles in the state. Therefore the configuration of the ground state must change from evenness to oddness, or vice versa, provided the system crosses a point with zero Λ_1. For $h > h_0$, since the ground state has the same configuration as the transverse Ising model, one can directly treat it, while for $h_1 < h < h_0$, where the ground state contains an odd number of particles, one has to perform a particle-hole transformation at one site as for the excited states in the subsection 5.1.2. Crossing h_1, the system change again the configuration. A detailed discussion for the periodic boundaries can be seen in Ref. [65].

Fig. 5.12 shows the lowest ε_l values as a function of h for $\gamma = 0.5$. One can see that, coming from larger values of h, all ε_l except the lowest one diverge as one approaches h_0 due to the fact that H_{XY} has a simplified ground state at h_0. For $h < h_0$ they become finite again. Note that in the region $h_1 < h < h_0$ ε_1 is always zero, which reflects the fact that an odd number of particles is on the even sites, as discussed in the last subsection. One can check the curves in the figure by performing direct DMRG calculations. The dots in the figure representing the DMRG results agree completely with the curves. At the next crossing h_1, however, as seen from the figure, the higher ε_l do not show such effects, indicating that the ground state of H_{XY} does not simplify there. At h_0, the divergence of the ε_l for $l \geq 2$ together with the value $\varepsilon_1 = 0$ lead to the density-matrix eigenvalues $w_1 = w_2 = 1/2$, while all other w_n are zero, i.e. the spectrum collapses at this point. For larger systems, there are further crossings at smaller values of h. This effect could be a tool in the search for simple ground states by DMRG.

5.3   Two-Dimensional Tight-Binding Model

As the last, but most important example we consider a tight-binding model with open boundaries described by

$$H_{TB} = - \sum_{<\mathbf{i},\mathbf{j}>} \left(c_\mathbf{i}^\dagger c_\mathbf{j} + c_\mathbf{j}^\dagger c_\mathbf{i} \right), \tag{5.26}$$

where the brackets $< \mathbf{i}, \mathbf{j} >$ denote nearest-neighbor sites. This model is critical and solvable in all dimensions. We treat it here for the case of a square lattice and we assume that the system also has the shape of a square with $L = N^2$ sites where N is even. This problem has has served as a DMRG test case some time ago [35].

5.3.1 Ground States of the TB Model

The ground states of the two-dimensional TB model is not as simple as that of the one-dimensional because it is multiply degenerate. To see this, one transforms the Hamiltonian (5.26) into the Fourier space, which leads to the form

$$H_{TB} = -\sum_{k_x,k_y} 2\cos\left(\frac{k_x - k_y}{2}\right)\cos\left(\frac{k_x + k_y}{2}\right)c^\dagger(k_x, k_y)c(k_x, k_y), \quad (5.27)$$

and where

$$k_\alpha = 2\pi n_\alpha/N_\alpha, \quad n_\alpha = 0, \ldots, N - 1 \ (\alpha = x, y) \quad (5.28)$$

due to the open boundaries. $c^\dagger(k_x, k_y)$ and $c(k_x, k_y)$ are the representative fermionic creation and annihilation operators for the momentum space. Therefore the single-particle energies have the form

$$\Lambda_k = -2\cos\left(\frac{k_x - k_y}{2}\right)\cos\left(\frac{k_x + k_y}{2}\right). \quad (5.29)$$

They are zero in case $n_x + n_y = 0$ or N. In this case, one has N solutions, giving 2^N degeneracies in the 2^{N^2} states. The degenerate states have different number of particles. In the most interesting half-filled ground states, they are also $\binom{N}{N/2}$-fold degenerate. Therefore one should choose one representative state to demonstrate the character of ground states of the tight-binding model.

I have mentioned in the section 5.2.1 that one can make particle-hole transformations on arbitrary $L/2$ sites in the Hamiltonian and obtains the same results due to the uniqueness of the ground state. But the situation in the two-dimensional TB model is different because of the degeneracies. A certain configuration of the particle-hole transformation will decide a ground state differing from those from the other configurations. One can already see it from a 2×2 lattice. Exchanging the creation and annihilation operators on every second site with some chosen ϕ and ψ (usually by computer), the vacuum state of η_k for the transformed Hamiltonian corresponds to a half-full ground state of the TB model. On the other hand, one can totally inverse the particles and holes on the lattice to obtain the other vacuum, which corresponds to another half-full ground state. Both states are orthonormal and give the same density-matrix spectra for the half plane. The density-matrix spectra in the next two subsections will be obtained with the same method. Namely, I made particle-hole transformations for the Hamiltonian on every two sites and calculated the corresponding vacuum. The ground states will have a form similar to Eqn. (5.19).
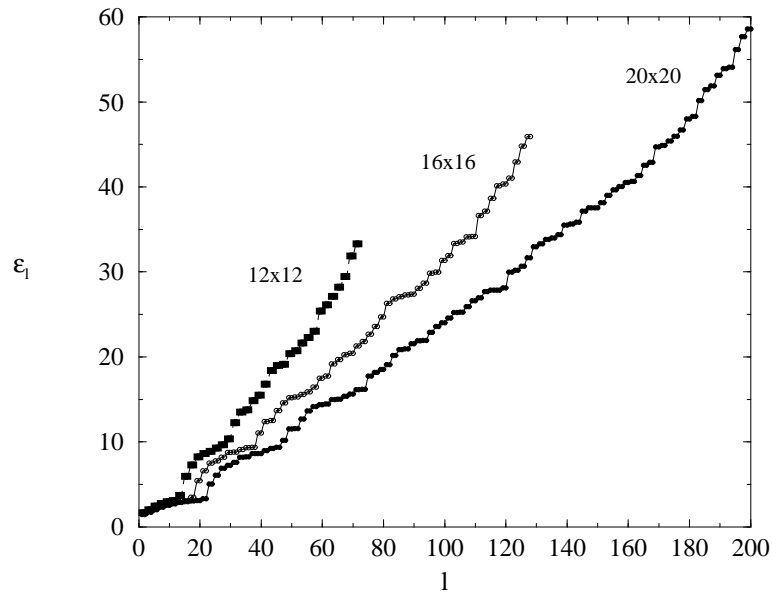
Figure 5.13: Single-particle eigenvalues ε_l for two-dimensional tight-binding models of different sizes. The ε_l are for one half of the system.
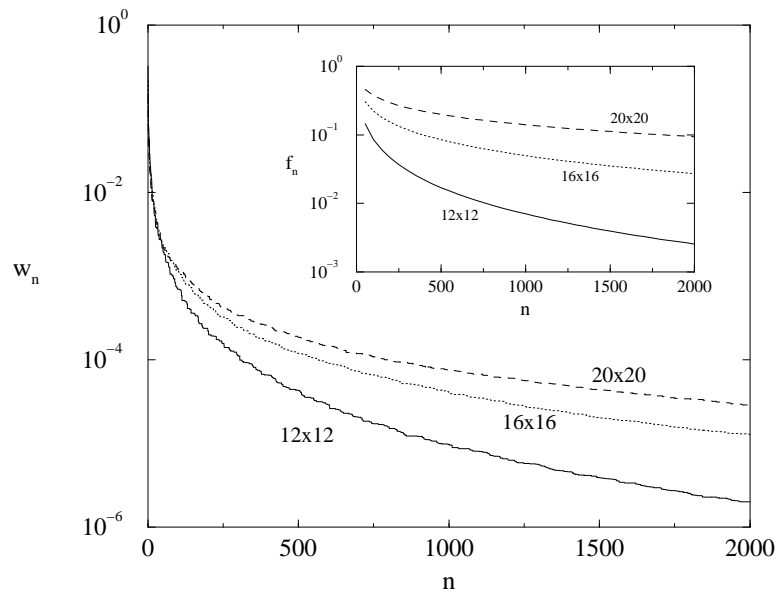

Figure 5.14: Density-matrix eigenvalues w_n of two-dimensional tight-binding models, obtained from the ε_l in Fig. 5.13. The inset shows the truncation error (see text).

5.3.2 Density Matrices for One Half Plane

In this subsection I will consider the density matrices for one half plane of the square $N \times N$ lattice, providing N is even. To carry out the calculation, one makes the problem formally one-dimensional by numbering the sites from 1 to L (in this case $L = N^2$.) in such a way that the desired partition into two parts arises naturally. For example, a meander-like numbering as in [35] permits a division of the square into two halves.

In figure 5.13, the single-particle eigenvalues ε_l for such a half-system and three different sizes are shown. One notices two features which are in contrast to the one-dimensional results: a "foot" of low-lying ε_l and a much smaller slope of the curves (note the scales). Both are strongly size-dependent. The number of ε_l in the foot is equal to N, which indicates that these states are closely connected with the interface between system and environment.

Fig. 5.14 shows the first 2000 eigenvalues w_n which result. Due to the small ε_l, they decrease very slowly and the situation worsens as the system is enlarged. The tails of the curves can be described qualitatively by $\ln(w_n) \sim -\ln^2(n)$ as in [21, 41]. The effect of these tails shows up even more in the truncation error f_n, which is defined as the sum of all w's beyond n. This quantity is given in the inset of the figure. With $n = 2000$ it is approximately 5×10^{-2}, 5×10^{-1} and 10^{-1}, respectively. Thus the situation is not only much worse than for one-dimensional systems, but also worse than for the two-dimensional system with a gap as discussed in section 3.6 and in Ref. [41]. Standard DMRG calculations using, say, 2000 states would be limited to sizes below 12×12, and even then the accuracy would be much less than the one obtained in quantum chains.

Let me mention that one can also include spin in H and thereby treat the Hubbard model in the $U = 0$ limit. Then the operators f_l, $f_l^\dagger$ in ρ_1 acquire a spin label, too, and all single-particle levels become doubly degenerate. Fig. 5.15 shows the first 3000 eigenvalues w_n for the model compared with the TB model with the same size. One sees at the tails of the w_n-curves even flatter than in the spinless case due to the degeneracies. However, the curves are also pulled down by smaller normalization factors which leads to a faster initial decay.

5.3.3 Density Matrices for A Quarter

One can also calculate the density-matrix spectra for other shapes of the selected subsystem. As an illustration, we show in Fig. 5.16 results for one quarter of a quadratic system (for example the upper right one). Note that the sizes indicated there refer to the whole system. One sees again some small eigenvalues, but fewer than for the half-system, while there are further higher-lying plateaus and additional short steps. Obviously

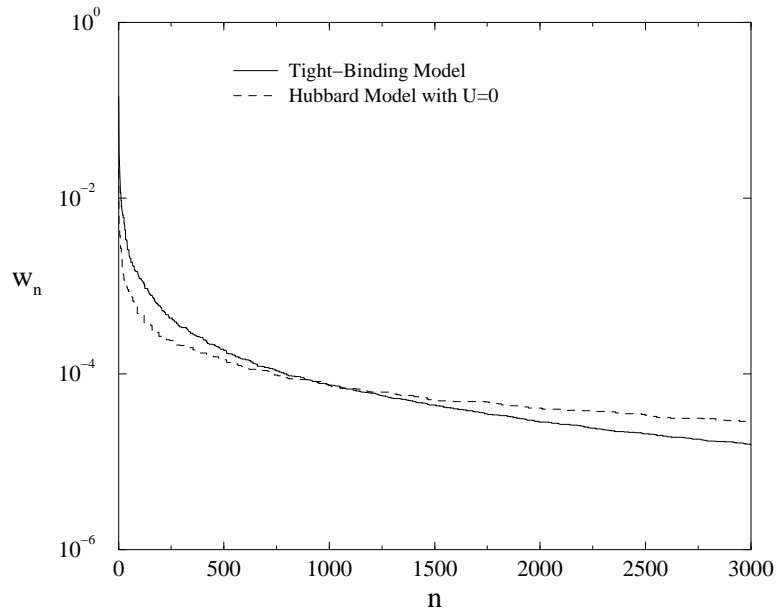**Figure 5.15:** Density-matrix eigenvalues w_n for Hubbard model with $U = 0$ and two-dimensional tight-binding models. The w_n are for one half of the system, the width $N = 20$.
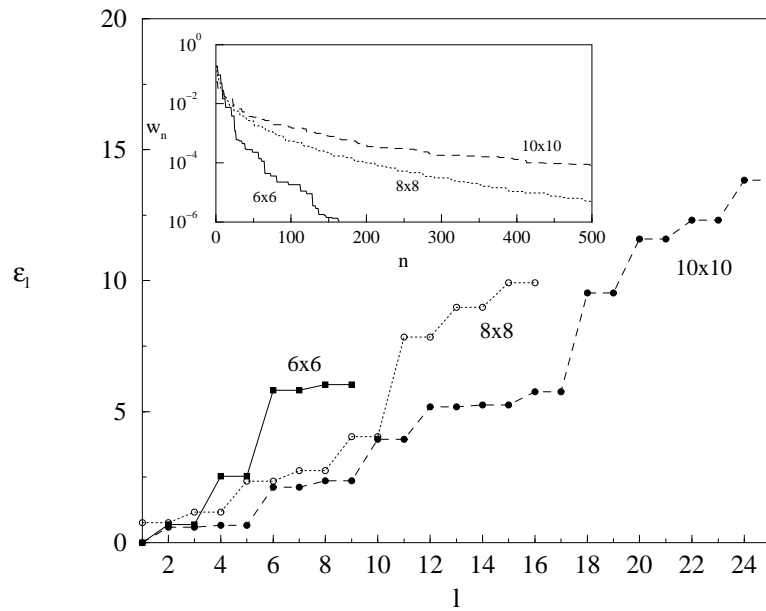

Figure 5.16: Single-particle eigenvalues ε_l of two-dimensional tight-binding models. The ε_l are for a quarter of the system, the w_n obtained from them are plotted in the inset.
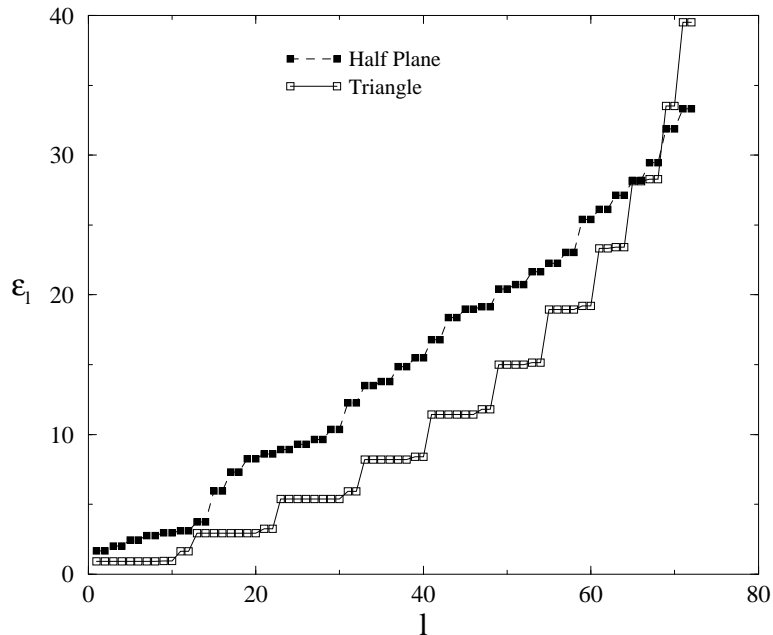
Figure 5.17: Single-particle eigenvalues ε_l of two-dimensional tight-binding models. The ε_l are for a triangle and for a half plane, the width $N = 12$.

this reflects the particular interface with a corner. For the 10×10 system, for example, the two lowest plateaus contain 9 states which is just the number of sites along the interface. The eigenvalues w_n are plotted in the inset of the figure. They are similar to those for the half-system but some more steps persist for small n. In the same way, one can investigate cases where one cuts the square diagonally at various positions. Such partitions appear in a recent new DMRG algorithm [66]. I will discuss the resulting spectra in the next subsection.

5.3.4   Density Matrices for A Triangle

Finally, I will consider density matrices for a half diagonal triangle. This kind of partition is interesting because in Ref. [66]. Xiang *et al.* used these density matrices to study the two-dimensional Heisenberg model. To treat the problem, one can numerate the lattice along the diagonal direction as made in this Ref. In Fig. 5.17 the single-particle spectra ε_l for a 12×12 lattice of such a partition are shown, compared with those for the one-half plane. As can been seen, the ε_l have some steps and are flatter. One should be cautioned that they are actually only two-fold degenerate, though in the figure they seem to have more degeneracies. These small values of ε_l can be understood from the cut between the system and the environment. In the case of one-half plane, the sites along the cut only lose the couplings
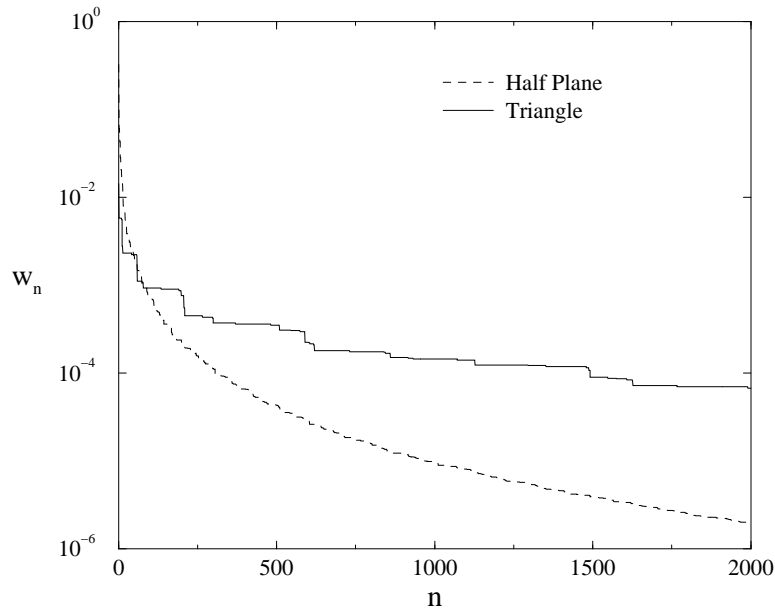
Figure 5.18: Density-matrix eigenvalues w_n of two-dimensional tight-binding models, obtained from the ε_l in Fig. 5.17

of the x-direction by dividing the lattice into two parts, whereas in the case of the triangle, most sites along the cut lose the couplings of the both x- and y-directions. These loss of coupling constants results in the small values of ε_l.

Fig. 5.18 shows the w_n derived from those ε_l. As expected, the small step-like structure generates the flat density-matrix spectrum. Compared with the eigenvalues for one-half plane, they drop faster at the beginning due to a larger normalization factor, then decrease much more slowly and form some plateaus. In fact, the spectra are related to DMRG calculations. In Ref. [66], the authors enlarge $(N-1) \times (N-1)$ lattice to $N \times N$ one using the triangular density matrices, therefore there should exist some problems with larger systems.

5.4   Brief Summary

I have studied the reduced density matrices for non-interacting fermions on a lattice. The key ingredient for the calculation was a simple representation of the (ground) state. This led rather directly to the exponential Boltzmann-like form of the density matrices. The only really numerical step involved was the calculation of the single-fermion eigenvalues appearing in the exponent. With these, we discussed a number of cases in one and two dimensions with characteristic differences. We focused on the eigen-

values, but one can also investigate the single- fermion eigenfunctions. One then sees that they are concentrated near the interface between the two parts of the system. This explains the decisive role of the connectivity for the spectra.

One should mention that fermionic density matrices have been studied before, e.g. in quantum chemistry [67, 68]. However, in this case the systems are continuous and the Hilbert space is infinite. Then already the single-particle density matrices have infinitely many eigenstates [69]. Our systems are discrete, but we are interested in density matrices for arbitrarily large subsystems. These are non-trivial even for non-interacting fermions. From the experience with other models, one can expect that the results are roughly representative also for more complicated systems.

For this reason, the two-dimensional case is particularly important. With our formulae, we could treat the tight-binding model for arbitrary partitions of the system. This allows to make much more detailed statements than a previous, purely numerical investigation of this system [35]. In particular, one can see the very slow decay of the spectra and of the truncation errors directly. Basically, it is connected with the existence of long boundaries between the two parts of the system. In the current DMRG procedures, these appear necessarily at some point of the calculation. Therefore it is not yet clear whether a recent new algorithm [66] can really overcome this problem.

Chapter 6

Ising Plane with Defects

In the previous chapters, I have presented the theory of DMRG and compared some results with the numerical calculations. In this chapter I want to introduce a precise application of DMRG, namely the transfer-matrix DMRG (TDMRG), for the planar Ising model with linear defects [70].

The planar Ising model with line-like defects is a peculiar system, because it shows non-universal magnetic exponents. This is connected with the values $\nu = 1$ and $x_s = 1/2$ of the exponents for the correlation length and the surface magnetization of the pure system, respectively. A one-dimensional, energy-like perturbation then is marginal and can change the critical behavior continuously. For this reason, the system has been the topic of various studies [71], with the focus most recently on a conformal treatment [72] and on random systems [73]. While the simple chain and ladder defects considered by Bariev are solvable free-fermion problems, the other cases we study are not integrable and one has to use numerical methods. Since with the transfer matrices (TMs) the Ising plane is an one-dimensional problem, DMRG is a good method to solve them, as pointed out by Nishino [7, 44]. In the following I will use the TDMRG to obtain the quantity of direct physical interest, the local magnetization at or near the defect lines.

In section 6.1 I will follow reference [44] and introduce the principle of TDMRG and the infinite algorithm. In section 6.2 the correlation functions and the magnetization of the Ising plane with different defects will be discussed. From these, the local critical exponents β_l will be obtained.

6.1 Transfer-Matrix DMRG

6.1.1 Transfer Matrix and Density Matrices

I consider now the transfer matrix of the square anisotropic homogeneous Ising model on a cylinder, i.e. with periodic boundary conditions in the y-direction and open boundaries in the x-direction. The lattice is assumed to
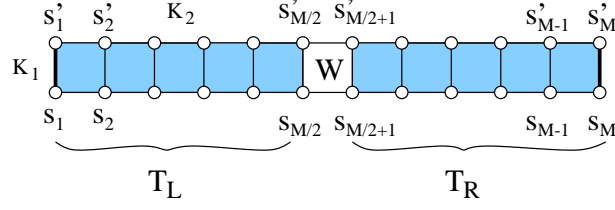
Figure 6.1: Division of the transfer matrix $T^{(M)}$ into the half-row transfer matrices T_L and T_R, and a Boltzmann weight W.

consist of $M \times N$ sites (M denotes the width in the x-direction and N in the y-direction.) I label the spins in a row from left to right as $s_1, s_2, \ldots, s_M$, and occasionally use the vector notation $\boldsymbol{s} = (s_1, s_2, \ldots, s_M)$ for simplicity. The vertical (horizontal) couplings between the nearest neighbors will be denoted by $K_1(K_2)$. The partition function has the form

$$Z = \text{Tr} \left\{ T^{(M)}(\boldsymbol{s}' \mid \boldsymbol{s})^N \right\}, \qquad (6.1)$$

where

$$T^{(M)}(\boldsymbol{s}' \mid \boldsymbol{s}) = \exp \left\{ \frac{K_2}{2} \sum_{i=1}^{M-1} (s_i' s_{i+1}' + s_i s_{i+1}) + K_1 \sum_{i=1}^{M} s_i' s_{i+1}' \right\} \qquad (6.2)$$

is the symmetrized transfer matrix which corresponds to quantity V in (5.11) in the last chapter. One can define an elementary building block

$$W(s_i' s_{i+1}' \mid s_i s_{i+1}) = \exp \left\{ \frac{K_1}{2} (s_{i+1} s_{i+1}' + s_{i+1}' s_i) + \frac{K_2}{2} (s_i s_{i+1} + s_i' s_i') \right\}, \qquad (6.3)$$

which contains the Boltzmann weights of one square (actually half of them since the blocks have common edges). In terms of the Ws, the transfer matrix for a strip can be expressed as

$$T^{(M)}(\boldsymbol{s}' \mid \boldsymbol{s}) = \exp \left(\frac{K_1}{2} s_1 s_1' \right) \left\{ \prod_{i=1}^{M-1} W(s_i' s_{i+1}' \mid s_i s_{i+1}) \right\} \exp \left(\frac{K_1}{2} s_M s_M' \right), \qquad (6.4)$$

where the additional two terms complete the Boltzmann weights at the boundaries. Following the convention of the quantum DMRG, one can divide the spin row into left and right parts (see Fig. 6.1). Decompose $T^{(M)}$ into three factors

$$T^{(M)}(\boldsymbol{s}' \mid \boldsymbol{s}) = T_L(\boldsymbol{s}_L' \mid \boldsymbol{s}_L) W(s_i' s_{i+1}' \mid s_i s_{i+1}) T_R(\boldsymbol{s}_R' \mid \boldsymbol{s}_R), \qquad (6.5)$$

where $T_L(\boldsymbol{s}'_L \mid \boldsymbol{s}_L)$ and $T_R(\boldsymbol{s}'_R \mid \boldsymbol{s}_R)$ are the half-row TMs

$$T_L(\boldsymbol{s}'_L \mid \boldsymbol{s}_L) = \exp\left(\frac{K_1}{2}s_1 s'_1\right), \prod_{i=1}^{M/2-1} W(s'_i s'_{i+1} \mid s_i s_{i+1})$$

$$T_R(\boldsymbol{s}'_R \mid \boldsymbol{s}_R) = \prod_{i=M/2}^{M} W(s'_i s'_{i+1} \mid s_i s_{i+1}) \exp\left(\frac{K_1}{2}s_M s'_M\right), \qquad (6.6)$$

where the total spin tensor indices are expressed as $\boldsymbol{s}= (\boldsymbol{s}_L \boldsymbol{s}_R)$, where $\boldsymbol{s}_L = (s_1 \ldots s_{M/2})$ and $(\boldsymbol{s}_R = (s_{M/2+1} \ldots s_M)$

For quantum chains, one is usually interested in the ground state. Here, the eigenstate of the transfer matrix with the largest eigenvalue is relevant since it determines the thermodynamic behavior. I denote this state by $\Phi_0^{(M)}(\boldsymbol{s})$ and its eigenvalue by $\lambda_0^{(M)}$, i.e. $T^{(M)}\Phi_0^{(M)}(\boldsymbol{s}) = \lambda_0^{(M)}\Phi_0^{(M)}(\boldsymbol{s})$. Therefore the reduced density matrices for the left and right halves of systems are defined as

$$\rho_L(\boldsymbol{s}'_L \mid \boldsymbol{s}_L) = \sum_{\boldsymbol{s}_R} \Phi_0^{(M)}(\boldsymbol{s}'_L \boldsymbol{s}_R)\Phi_0^{(M)}(\boldsymbol{s}_L \boldsymbol{s}_R),$$

$$\rho_R(\boldsymbol{s}'_R \mid \boldsymbol{s}'_R) = \sum_{\boldsymbol{s}_L} \Phi_0^{(M)}(\boldsymbol{s}_L \boldsymbol{s}'_R)\Phi_0^{(M)}(\boldsymbol{s}_L \boldsymbol{s}_R). \qquad (6.7)$$

They have the diagonal form

$$\rho_L(\boldsymbol{s}'_L \mid \boldsymbol{s}_L) = \sum_{\xi} V_L(\boldsymbol{s}'_L \mid \xi)\, \omega_\xi^2\, V_L(\boldsymbol{s}_L \mid \xi),$$

$$\rho_R(\boldsymbol{s}'_R \mid \boldsymbol{s}_R) = \sum_{\zeta} V_R(\boldsymbol{s}'_R \mid \zeta)\, \mu_\zeta^2\, V_R(\boldsymbol{s}_R \mid \zeta) \qquad (6.8)$$

with the descending eigenvalues ($\omega_1^2 \geq \omega_2^2 \geq \cdots \geq 0$ and $\mu_1^2 \geq \mu_2^2 \geq \cdots \geq 0$) and matrices of eigenvectors V_L, V_R.

As described in the last chapter, the eigenvalues of density matrices decay exponentially, therefore one can choose the $m \leq 2^M$ the important eigenstates, corresponding to the m largest eigenvalues, to simplify the calculations. I choose the same symbols V_L and V_R to denote the truncated eigenvectors matrices, which only contain the m eigenvectors, Due to the truncation they are rectangular with dimension $(2^{M/2} \times m_t)$. An operator $O_L(\boldsymbol{s}'_L, \boldsymbol{s}_L)$ in the left part can be expressed under such a truncated transformation as

$$\tilde{O}_L(\xi', \xi) = \sum_{\boldsymbol{s}'_L \boldsymbol{s}_L} V_L(\boldsymbol{s}'_L \mid \xi')O_L(\boldsymbol{s}'_L, \boldsymbol{s}_L)V_L(\boldsymbol{s}_L \mid \xi). \qquad (6.9)$$

Therefore $\tilde{O}$ is an $m \times m$ matrix. The situation for operators on the right side is similar. The transformation for transfer matrices will be discussed in the next subsection.

6.1.2 Infinite-System Algorithm

The infinite-system algorithm begins with the smallest size. i.e. $M = 4$, and constructs renormalized transfer matrices $\tilde{T}^{(6)}, \tilde{T}^{(8)}, \ldots, \tilde{T}^{(M)}$ for arbitrary M. For the four-site system, the transfer matrix is

$$T^{(4)}(s_1's_2's_3's_4' \mid s_1s_2s_3s_4) = T_L(s_1's_2' \mid s_1s_2)W(s_2's_3' \mid s_2s_3)T_R(s_3's_4' \mid s_3s_4). \tag{6.10}$$

Following the procedure described in the last subsection, one diagonalizes $T^{(4)}$ and finds the eigenstate $\Phi_0^{(4)}$ for the largest eigenvalue. From the eigenvectors of the reduced density matrices $\rho_L(s_1's_2' \mid s_1s_2)$ and $\rho_R(s_1's_2' \mid s_1s_2)$ one can find the matrices $V_L(s_1s_2 \mid \xi)$ and $V_R(s_3s_4 \mid \zeta)$.

To enlarge the system from $M = 4$ to $M = 6$, one should find the new $\tilde{T}_L$ and $\tilde{T}_R$ under the RG transformation

$$\tilde{T}_L(\xi's_3' \mid \xi s_3) = \sum_{s_1's_2's_1s_2} V_L(s_1's_2' \mid \xi')T_L(s_1's_2' \mid s_1s_2)$$

$$W(s_2's_3' \mid s_2s_3)V_L(s_1s_2 \mid \xi),$$

$$\tilde{T}_R(s_4'\zeta' \mid s_4\zeta) = \sum_{s_5's_6's_5s_6} V_R(s_5's_6' \mid \zeta')W(s_4's_5' \mid s_4s_5)$$

$$T_L(s_5's_6' \mid s_5s_6)V_L(s_5s_6 \mid \zeta). \tag{6.11}$$

Here $s_5', s_6's_5s_6$ are used because they correspond to the system $M = 6$. The Greek indices ξ and ζ take at most m values. One notices that the largest eigenvalue increases exponentially if one enlarges the system, i.e. $\ln(\lambda_0^{(M)}) \sim M$ which causes computational problems. To avoid that, I divide the $\tilde{T}_L$ and $\tilde{T}_R$ by the largest eigenvalue $\sqrt{\lambda_0'^{(M)}}$ of the renormalized TMs $\tilde{T}^{(M)}$ after the RG transformation

$$\hat{T}_L = \frac{\tilde{T}_L}{\sqrt{\lambda_0'^{(M)}}}, \qquad \hat{T}_R = \frac{\tilde{T}_R}{\sqrt{\lambda_0'^{(M)}}}. \tag{6.12}$$

At this step one has to divide them by $\lambda_0'^{(4)}(= \lambda_0^{(4)})$. Carrying TMs in (6.11) to the next iteration, the renormalized transfer matrix for $\tilde{T}^{(M)} = 6$ is given by

$$\tilde{T}^{(6)}(\xi's_3's_4'\zeta' \mid \xi s_3s_4\zeta) = \hat{T}_L(\xi's_3' \mid \xi s_3)W(s_3's_4' \mid s_3s_4)\hat{T}_R(s_4'\zeta' \mid s_4\zeta). \tag{6.13}$$

Using the DMRG algorithm and iteration, one obtains all renormalized TMs $\tilde{T}^{(M)}$.

The eigenstates of the transfer matrices are not influenced by the division but the eigenvalues are. One finds that the largest eigenvalue $\lambda_0^{(M)}$ of T^M is related to all $\lambda_0'^{(2i)}, i \leq M/2$

$$\lambda_o^{(M)} = \prod_{i=2}^{M/2} \lambda_0'^{(2i)}. \tag{6.14}$$

From this relation, one can find the true eigenvalue and hence the free energy of the Ising plane.

In order to improve the result further, one could carry out the sweeping process of the finite-system algorithm. Because our results from the infinite-system algorithm had very good accuracy compared with the analytical results, however, I did not use it in the following calculations and therefore will not describe the procedure. One can find the details in reference [44, 3].

6.2 Planar Ising Model with Line-like Defects

In this section I will discuss some line-like defects (see Fig. 6.2 and Fig. 6.4) on the Ising surface. In next subsections I will introduce the defects in detail, here I want to follow the discussion by Iglói, Peschel and Turban [71] to consider how the dimensionality of systems and defects and the surface scaling dimensions affect the local critical behavior.

One can first consider the line-like defects as perturbation on a homogeneous Ising plane. For convenience I denote dimension of the Ising plane as $d(=2)$ and that of the defects as $d^*(=1)$. The line-like coupling perturbation reads

$$\delta H_\epsilon = \delta K \int d^{d^*}r \; \epsilon(r), \tag{6.15}$$

where $\epsilon(r)$ denotes the bulk density energy and equals $\langle \sigma_{M/2}(r)\sigma_{M/2+1}(r)\rangle$ for the ladder defect and $\langle \sigma_{M/2}(r)\sigma_{M/2}(r)\rangle$ for the chain defect. $\delta K = K' - K$ denotes the difference of couplings between Ising plane and defects. Under a scaling transformation $r' \to r/b$ $(b > 1)$, the perturbation (6.15) can be expressed as

$$\delta H_\epsilon = \delta K b^{d^*-x_\epsilon} \int d^{d^*}r' \; \epsilon(r'). \tag{6.16}$$

Therefore the coupling perturbation has a scaling dimension $d^* - x_\epsilon$. If $d^* - x_\epsilon > 0$, the coupling increases under rescaling and the defect is relevant. On the contrary, if $d^* - x_\epsilon < 0$, the defect is irrelevant. A defect is marginal if $d^* = x_\epsilon$. From the scaling analysis of correlation length, on the other hand, x_ϵ has the form

$$x_\epsilon = d - 1/\nu. \tag{6.17}$$

In the case of the two-dimensional Ising model, $d = 2$ and $\nu = 1$, therefore the line-like defects are marginal, which gives the non-universal local critical behavior.
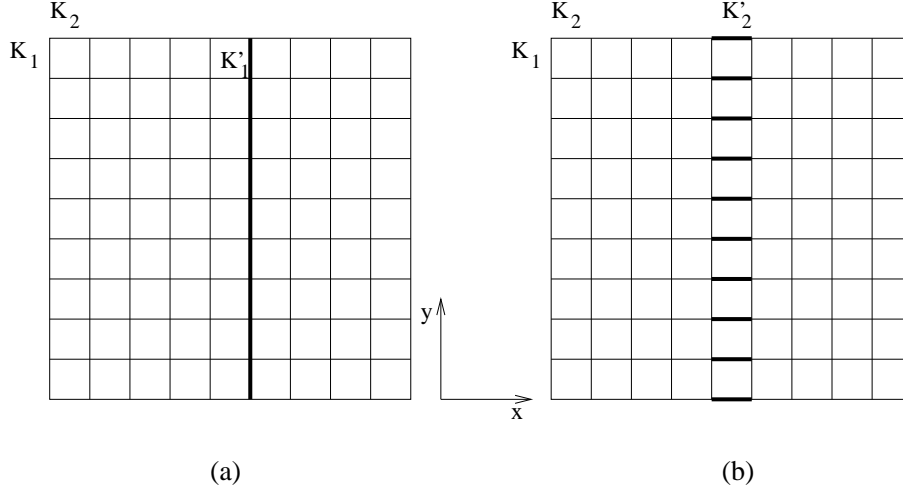
Figure 6.2: Ising square lattice with two kind of defect lines; (a)chain defect, (b)ladder defect

One can also start with two independent Ising planes and couple them with K'. The perturbation reads now

$$\delta H_{K'} = K' \int d^{d^*} r \, \langle \sigma_1(r) \rangle \langle \sigma_2(r) \rangle, \qquad (6.18)$$

where σ_1 and σ_2 are the surface spins, which belong individually to the left and right Ising planes. Under a scaling transformation, the perturbation (6.18) is given by

$$\delta H_{K'} = K' b^{d^* - 2x_s} \int d^{d^*} r' \, \langle \sigma_1(r') \rangle \langle \sigma_2(r') \rangle \qquad (6.19)$$

with the surface exponent x_s. In this case, the scaling dimension is $d^* - 2x_s$. If $d^* - 2x_s > 0$, the defect is relevant. The defect is irrelevant provided $d^* - 2x_s < 0$. Non-universal local critical behavior is expected when the perturbation is marginal i.e. when $d^* = 2x_s$. In the case of Ising model, $x_s = \beta_s/\nu = 1/2$ because $\beta_s = 1/2$ and $\nu = 1$. Therefore the line-like defects on the Ising plane, in accordance with the analysis of the bulk perturbation, are marginal and expected to give the local varying exponents at or near the defects.

6.2.1   Analytic results - Bariev's Treatment

According to the scaling arguments a defect line in the two dimensional Ising model, is expected to lead to continuously varying local exponents. This problem was first investigated by Bariev [37] who deduced the local magnetization, as a function of the perturbation strength and distance to the defect, from the asymptotic behavior of the two-spin correlation

function below the critical temperature. This was followed by a detailed study of the two-spin correlation function by McCoy and Perk [74]. These calculations used the fact that even with such a defect the model is a solvable free-fermion problem.

Bariev studied the two kinds of perturbation shown in Fig. 6.2. The chain defect has modified couplings K_1' parallel to the defect line, whereas, for the ladder defect, perturbed couplings K_2' are in the perpendicular direction. The local magnetization has the form

$$\langle \sigma(x) \rangle \sim t^{\beta_l} x^{\beta_l - \beta}, \tag{6.20}$$

where $t = |1 - T/T_c|$ and when the distance x to the defect line is much smaller than the bulk correlation length ξ. In the Ising plane $\beta = 1/8$ is the bulk magnetization exponent and the local magnetization exponents β_l vary continuously with K_1' or K_2'. They can be expressed as

$$\beta_l = \frac{2}{\pi^2} \arctan^2 \kappa_1, \quad \kappa_1 = \frac{\tanh K_1'^*}{\tanh K_1^*} \quad \text{chain defect}, \tag{6.21}$$

$$\beta_l = \frac{2}{\pi^2} \arctan^2 \kappa_2^{-1}, \quad \kappa_2 = \frac{\tanh K_2'}{\tanh K_2} \quad \text{ladder defect}, \tag{6.22}$$

where the bulk couplings take their critical values related by

$$\sinh 2K_1 \sinh 2K_2 = 1 \tag{6.23}$$

and the asterisk denotes dual variables (for example, $\tanh K_1^* = \exp(-2K_1)$).

Fig. 6.3 shows the resulting local exponents. The chain defect exponent decreases continuously from $\beta_l = 1/2$ when $K_1' \to -\infty$ to $\beta_l = 0$ when $K_1' \to \infty$. In the case of $K_1' \to -\infty$, the spins along the defects are forced into antiparallel configurations. Nearby spins decouple the defects and the total spins vanish near the defects. The local exponents then takes the free surface value. In the other limit the magnetization does not vanish even if $t \to 0$ owing to the infinity couplings. When $K_1' = 0$, the inner spins along the vanishing defect line decouple in the y-direction. Thereby one can sum out the inner spin and the chain defect becomes a ladder with strength given by $\tanh K_2' = \tanh^2 K_2$. Then (6.21) and (6.22) give identical results since $\sinh 2K_1 \sinh 2K_2 = 1$ on the critical line.

For a ladder defect the local exponent is invariant under the change $K_2' \to -K_2'$ because one can invert signs of the spins for one half of the system to restore the original defect coupling. When $K_2' = 0$, the plane is separated into two parts and β_l takes the free surface value i.e. $\beta_l = 1/2$. If $K_2' \to \pm\infty$, the couplings force the spins along the defects to be pulled together and form a chain defect with $K_1' = 2K_1$. With the appropriate values of the perturbed couplings, the two formulae give identical results.
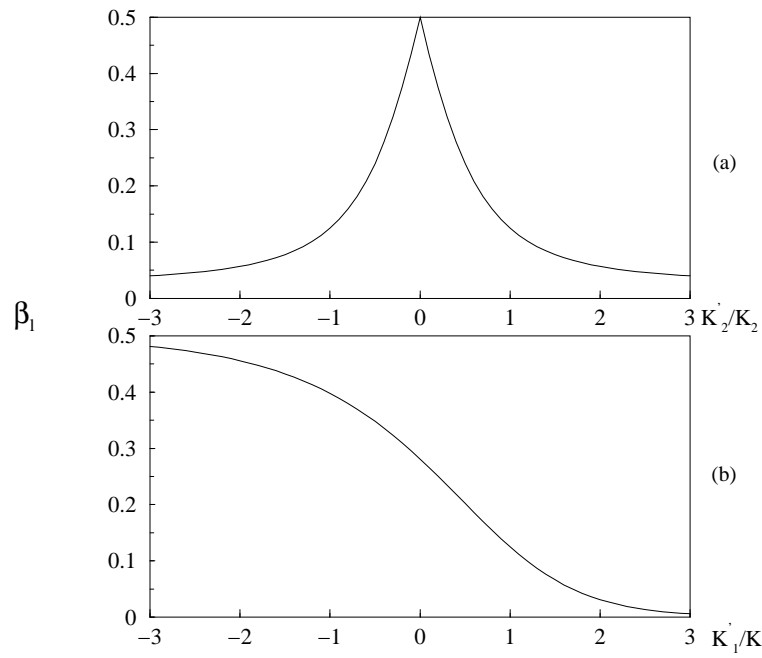
Figure 6.3: Local magnetization exponent β_l against defect strength in the Bariev model for (a)chain defect, (b)ladder defect
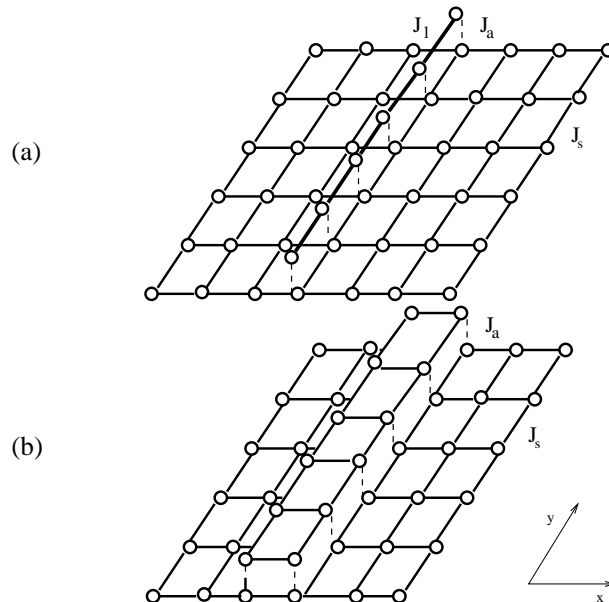

Figure 6.4: Geometry and interactions of Ising models with two different line-like imperfections (a) one additional line of spins, (b)pair of adjacent line of spins.

92

6.2.2 Numerics - TDMRG Treatment

In the last subsection I have discussed the chain and ladder defects, for which the magnetization critical exponents can be obtained analytically. On the other hand, one can use the TDMRG to determine them numerically. The benefit of using TDMRG is that one can obtain β_l also for other kinds of defects which do not belong to the free fermionic models and therefore cannot be determined analytically. For example, one can consider an additional chain or two neighboring chains on the Ising plane as shown in Fig. 6.4. Such lines of adatoms can be produced artificially and have been the topic of various studies in recent years [71]. In this subsection I only consider three kinds of perturbations.

- one additional line, varying vertical couplings J_a, Fig. 6.4a

- one additional line, varying horizontal couplings J_l, Fig. 6.4a

- two neighboring lines, varying vertical couplings J_a, Fig. 6.4b

The other couplings are kept equal to J_s. These Ising model are also expected to have non-universal behavior i.e. continuously varying critical exponents.

One can use TDMRG to obtain the local magnetization at or near the defects lines and thereby determine the non-universal critical exponent β_l. To achieve this, I used the transfer matrix running along the direction of the defect. In this way one is treating an infinitely long strip of width M with the defect located in the middle. After enlarging the system step by step until a certain desired size is reached, one can insert different defects. This makes the calculations very convenient. Here the infinite algorithm was used, no further sweeps to optimize were made, since tests on the ladder defects gave very good coincidence with the analytical results (6.22), which I will discuss below. Most calculations were done with 64 truncated states and a truncation error around 10^{-15}.

To find the local magnetization, one can study the Ising plane with or without boundaries. For the free boundary, the magnetization is normally zero for finite sizes, while, for $T < T_c$, the spontaneous magnetization will occur for large systems ($L \gg \xi$) due to symmetry breaking by some fluctuation appearing in the calculation. Therefore one can calculate it from the spin operator on the defect sites

$$m_d = \langle \Phi_0 \mid \sigma_d \mid \Phi_0 \rangle, \tag{6.24}$$

where $\mid \Phi_0 \rangle$ is the eigenfunction of the transfer matrix with the largest eigenvalue obtained from TDMRG and σ_d denotes the spin operator near or at the defects. This method has been used by some authors [75, 76] however, it seems not to be reliable because the fluctuation appears randomly. A more reliable method to obtain the magnetization is to calculate
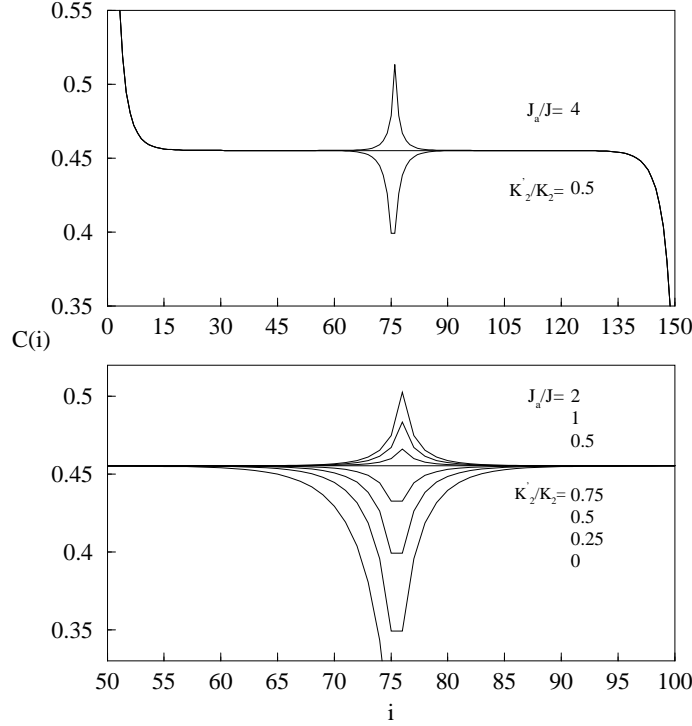
Figure 6.5: Spin correlation function $C(i)$ for a strip of width $M = 150$ with ladder defects (below the plateau) or one additional line of spins (above the plateau) on an isotropic Ising plane ($K_1 = K_2 = J_s$), as obtained from DMRG calculations at the reduced temperature $t = 0.072$. The defect strengths K_2'/K_2 and J_a/J_s are indicated. Upper part: total view, lower part: central region.

the correlation function $C(i) = \langle \sigma_1 \sigma_i \rangle$ for free boundaries. Since in this case one has to obtain all the information on the local spins and the spin correlations, it costs a lot of time to obtain the data. Since one has to reach large systems and calculate a lot of data for magnetization, therefore it is not favorable to calculate the β_l in this way.

A direct and simple way to overcome the problem is to add boundary magnetic fields, or equivalently, to fix the boundary spins in order to break the symmetry. Using (6.24) the magnetization can always be found for an arbitrary size. The width was always larger than the correlation length and varied between $M = 100$ and $M = 5000$ for the temperature range studied ($0.001 < t < 0.1$, where $t = 1 - T/T_c$ is the reduced temperature). The (absolute) error in m_d, determined by compared with analytical results most 10^{-4} for a system at $t = 0.001$, cut in the middle by a ladder defect. For less severe modifications and larger values of t it was even smaller.

In figure 6.5 the correlation function $C(i)$ across the strip for a ladder defect (Fig. 6.2b) and for an additional line using TDMRG (Fig. 6.4a) is shown. The upper part gives an overall picture, while the lower one shows
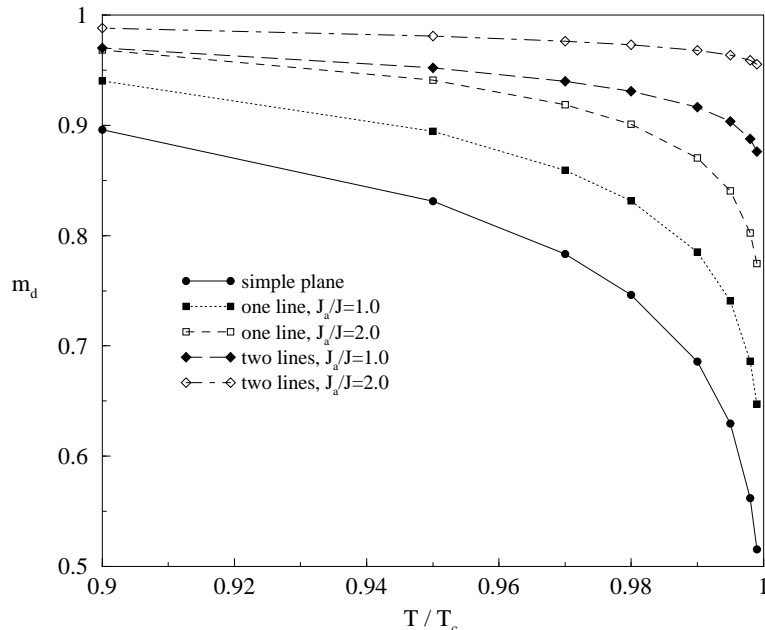
Figure 6.6: Local magnetization m_d of the spins below one or two additional lines as a function of temperature, for three values of the coupling ratio J_a/J_s. The lowest curve is the Onsager result for the perfect Ising model.

the defect region in more detail. For ladder defects the strength K_2' of the defect bonds was varied, whereas for an additional line it was the coupling J_a between the line spins and the substrate.

Since $C(i)$ here is obtained for large distances, one can use the relations

$$C(M/2) = m_s m_d,$$
$$C(M) = m_s^2 \qquad\qquad (6.25)$$

to obtain the magnetization at the defect (m_d) and at the boundary (m_s) One can see how m_d increases or decreases near the defect, depending on the sign of the perturbation. (similar curves were obtained in [Szalma,Igloi] for a random system). For the ladder defects and when $K_2' < K_2$, the magnetization is smaller than the bulk one due to the weak interaction between the spins along the defects. Cutting the ladder bonds with $K_2' = 0$, one obtains the boundary magnetization (m_s^2) of the homogeneous model in the middle of the strip. Compared with the analytical result by McCoy and Wu [77]

$$m_s = \left[\frac{\cosh 2K_1 - \coth 2K_2}{\cosh 2K_1 - 1} \right]^{1/2}, \qquad\qquad (6.26)$$

the error of the numerical calculation is about 10^{-6}, when the size is larger than the correlation length and 32 kept states are used. For $t =$

0.01, the surface magnetization is reached to the error 10^{-6} with the size $L \sim 700$, using kept 64 states. One can see that in this extreme case, the TDMRG achieved good results without sweeps compared with the analytical magnetization (6.26). Therefore one can trust the method to calculate the other defects. For line defects, m_d being always larger than that in the homogeneous system, characterizes the additional spin effects. The possible increase of m_d depends on the details of the defect. Letting J_a go to infinity, the effect is equivalent to a chain defect in the plane with merely doubled bond strength. Therefore m_d is limited in this case.

The temperature dependence of m_d is shown in Fig. 6.2.2 for the spins in the plane situated below one or two additional lines. One can see how it is increased over the Onsager value by increasing the coupling J_a. As expected, the effect is even stronger for two additional lines. In this case, m_d has already twice the undisturbed value for the smallest shown t. Quantitatively, this enhancement is described by a decrease of the exponent β_l, the local critical exponent which describes the vanishing of the magnetization near the additional line of magnetic adatoms.

To obtain β_l, one can analyze the temperature behavior of m_d in terms of an effective (critical) exponent β_{eff}, defined by [78, 79, 80]

$$\beta_{\text{eff}}(t) = \ln(m_d(t_i)/m_d(t_{i+1}))/\ln(t_i/t_{i+1}) \qquad (6.27)$$

with $t = (t_i + t_{i+1})/2$ (alternatively, one could choose t to be the geometric mean $t = \sqrt{t_i t_{i+1}}$). As one approaches the critical point, $t \to 0$, this quantity converges to the true local exponent β_l. It is also a very sensitive indicator for the numerical accuracy of a calculation.

I give here some typical results in figure 6.7 for one additional line and four values of the ratio J_l/J_s of the couplings in the line. For $J_l = 0$, one is treating a homogeneous plane with an independent chain, and the Onsager result $\beta = 1/8$ is recovered with high accuracy. In the other cases, to achieve better results, the exponents both for the spin in the line and the one below it are analyzed. One see that the two curves have different slopes, but approach the same limit for $t \to 0$. The limit can determine the values β_l accurately to at least three digits. For the case $J_a/J_l \gg 1$ which, as mentioned, is equivalent to a line defect in the plane, it was checked explicitly by comparing with the analytical result (6.21). In the figure, also a negative J_l is shown, which leads to a reduction of m_d and an increase of β_l over the Onsager value . In this case, a limiting value 0.142 is approached rapidly for $J_l/J_s < -1$. This is the same effect as for a chain defect in the plane with strong antiferromagnetic couplings Igl93. In that case, the exponent is increased up to the value 0.5 of the free surface. The sign of J_a, on the other hand, has no influence on the exponent.

The results for β_l are collected in Table 1 and in figure 6.8, where the exponent is plotted as a function of the varied couplings (keeping the
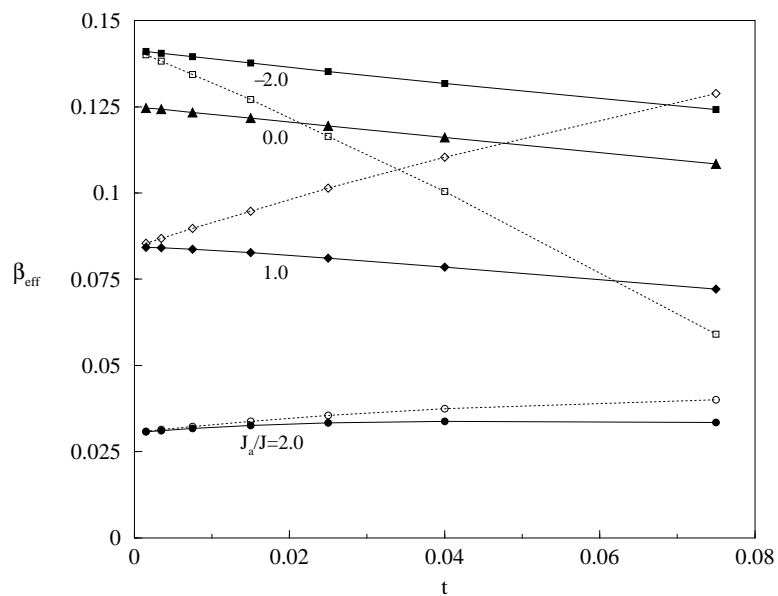
Figure 6.7: Effective exponent β_{eff} as function of the reduced temperature t for one additional line and three different coupling ratios J_l/J_s. Full: Spins located below the line, dotted: spins in the line.

Table 6.1: Numerical values for the local exponent β_l of an Ising plane with one and two additional lines of spins.

lines	1	1	2
λ	J_a/J_s	J_l/J_s	J_a/J_s
0.0	0.125	0.125	0.125
0.25	0.121	0.118	0.098
0.5	0.111	0.109	0.056
1.0	0.084	0.084	0.018
2.0	0.051	0.031	0.005
4.0	0.034	0.002	0.001

Figure 6.8: Local exponent β_l as a function of the ratio of the coupling strength λ, as defined in the 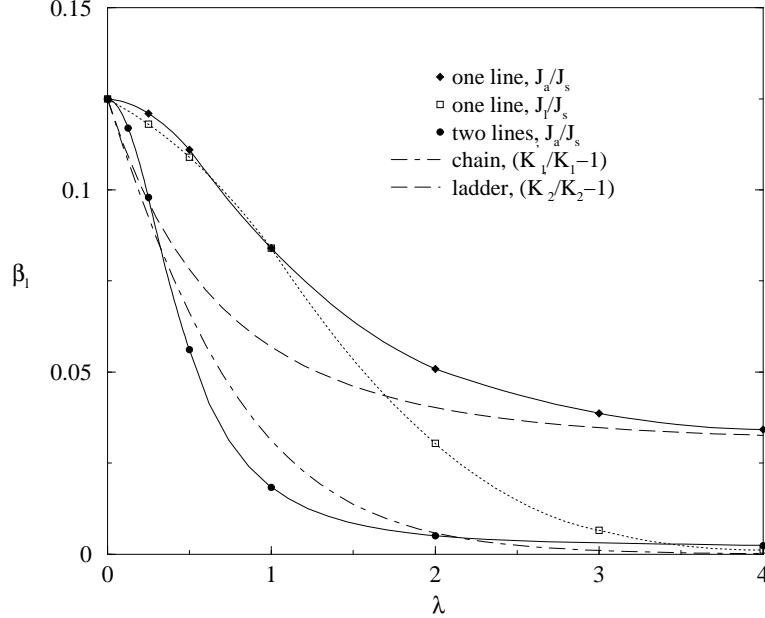figure for five different situations. For chain and ladder defects the analytical results are shown, otherwise the DMRG results are depicted.

other couplings fixed and equal to J_s). Here λ denotes the ratio of the couplings. For comparison also the analytical results [37, 71], for simple chain and ladder defects are shown in figure 6.8. To keep the character of the additional defects and to lead to the perfect Ising model when $\lambda = 0$, λ is assigned to $(K_i'/K_i - 1)$ with respect to the chain $(i = 1)$ and ladder $(i = 2)$ defects, providing $K_1 = K_2 = J_s$. For a single line, the results of small J_a/J_s and J_l/J_s are similar, while a large J_l/J_s has much pronounced effect than J_a/J_s, since it corresponds to additional spins which are almost rigidly locked together. One notices that for $J_a/J_s \gg 1$ it goes to the limit for a ladder effect, due to the fact that the two systems have the same asymptotic behavior, namely they approach a plane with simple chain possessing doubled bond strength between spins. For the double line, the exponent drops much faster, reaching 10^{-2} already around $J_a/J_s \sim 1$. For more additional lines, i.e. for a terrace on the surface, this effect would be even stronger. In this case, the magnetization would practically jump as in a first-order transition.

6.3   Brief Summary

Using the transfer-matrix DMRG (TDMRG), I have studied critical properties of magnetic Ising plane with various line-like defects. Since the critical exponents of the magnetization at or near these defects are non-universal, the dependence of its varying values on the local couplings was obtained and found to follow the trends observed for the exactly solvable cases of ladder and chain defects. One should mention that the local non-universal critical exponents exist not only on a plane but also on a surface of Ising films [70], which Pleimling and Selke have studied with Monte Carlo simulation. With increasing thickness of the films, the crossover of the effect exponent β_{eff} for the spins beneath the defects from the bulk critical exponents to the local varying exponents appears more obviously. For larger t, the β_{eff} inclines towards the bulk magnetic exponent. For small t, however, the β_{eff} turns back to the local varying β_l. The local exponents will not disappear until the system becomes truly three-dimensional, i.e. the thickness becomes infinity.

In this chapter some results from TDMRG have been compared with the analytical ones and they gave high accuracies. Therefore TDMRG is a well-suited method to study classical planar models. It can even be used to study thin films, for example two or three layers of Ising planes, provided the numerical calculations do not exceed the capacity of computers. In some papers [81, 82, 83] the authors have tried to use it to solve the three dimensional classical problems, which are equivalent to two-dimensional quantum models. The main unsolved puzzle one has to encounter in such two-dimensional problems is how to avoid the slowly decreasing density-matrix spectra described in the last chapters. Till now, it is not yet clear if one will be able to use DMRG to solve the two-dimensional quantum problems with large size.

Chapter 7

Summary and Outlook

DMRG is a powerful method to calculate properties of one-dimensional quantum systems, for example, the ground-state energy or correlation functions. For two-dimensional systems, however, the situation appears to be much less favorable. A main goal of my thesis was to develop a kind of theory for the DMRG method by looking at the density-matrix spectra. With the help of these spectra one can understand the features of the method and the reason why it works better in one case than in another. Therefore I looked at a number of exactly solvable models and tried to calculate their reduced density matrices.

In chapter 3, I studied the ground state of coupled oscillators in the coordinate representation. The reduced density matrix for an arbitrary subsystem then is an exponential of noninteracting oscillators, so that the density matrices for one site or for half of the system can be calculated explicitly. The reduced density matrix for one site has a simple exponential spectrum. The spectra for a half-chain also show exponentially rapid decay and are connected with certain normal modes concentrated near the middle of the system. Open, fixed and periodic boundary conditions were considered. Fixed boundaries were used to overcome the unnormalizability of the density matrix for acoustic phonons for open and periodic boundary conditions. For periodic boundary conditions it was seen that the eigenstates of the reduced density matrices are concentrated between system and environment. This leads to a symmetric eigenfunction and an antisymmetric one and explains the degeneracies of the single-particle eigenvalues. These degeneracies give rise to the slow decay of the spectra and explains why periodic boundary conditions are unfavorable in DMRG calculations. The thermodynamic limit was obtained via corner transfer matrices as for the integrable spin chains treated previously, and the resulting spectra are very similar. The squeezed oscillator states obtained from the density matrix for one site were used in numerical DMRG calculations and gave good agreement with the analytical results.

In chapters 4 and 5, I used coherent states to treat the solvable bosonic

and fermionic systems. The key ingredient for the calculation was a simple exponential representation of the ground state. This led to a general form of the reduced density matrices - the exponential Boltzmann-like form. The two cases turned out to be very similar. In spite of the different statistics, the bosonic and fermionic systems share the same equations for the single-particle eigenvalues in the density matrices.

In this way, the reduced density matrices for some spin models in one dimension, namely the transverse Ising chain, the XX spin chain and the XY spin chain in a field, were found. For the transverse Ising chain, the density matrices for the ordered and the disordered region as well as for the critical point were obtained. The spectra at the critical point drop much more slowly than those in the noncritical regions, where the first few ε_l already correspond to those of the thermodynamics limit. I have also studied the reduced density matrices for the first excited state, which give a similar behavior as for the ground state. The treatment can be generalized to the transfer-matrix of the two-dimensional Ising model. The spectra in this case are also similar to those for the transverse Ising model. This is very plausible because the transfer matrix is closely related to the Hamiltonian of the transverse Ising chain.

The results for the XX model showed again that in critical models, the density-matrix spectra decrease much more slowly than those in noncritical systems. For the XY chain in a field, the density-matrix spectrum allowed to observe the disorder line, where the ground state simplifies and becomes two-fold degenerate. As one approaches this line, the whole spectrum collapses.

The most important results concerned the density matrices for the two-dimensional systems. In chapter 3 and 5 I treated the two-dimensional coupled oscillators and tight-binding model. The resulting spectra have the common feature that they decay slowly. The same holds for the truncation errors. In the case of oscillators, I discussed the dependence of the density-matrix spectra and the width. These spectra showed the increasing difficulties in calculating the quantities for the ground state if the systems become more two-dimensional. This is consistent with actual DMRG calculations for two-dimensional systems. For example, in a recent study of the $t - J$ model on a 12×12 lattice, 4000 states had to be used [33]. In the case of the two-dimensional TB model, also the dependence of the density-matrix spectra on the different kinds of partitions was studied. Basically, the slow decay is connected with the existence of long boundaries between the two parts of the system. Therefore the w_n for diagonal partitions decay more slowly than those for a half system of rectangular shape. In a recent treatment of two-dimensional quantum systems, the authors tried to divide the lattice diagonally [84, 66]. Unfortunately they only treated small systems and did not compare with exact results. From our results it is unclear if this approach can overcome the problems.

In addition to the basic investigation of the DMRG, I also applied the method to a problem from statistical physics, namely the Ising plane with line-like defects. In this case one is dealing with the transfer-matrix and its eigenfunctions instead of a Hamiltonian. In order to calculate the local spontaneous magnetization accurately, one needs increasing larger systems as one approaches the critical point. Because of the favorable feature of the density-matrix spectrum, which was discussed in section 5.1.3, this was possible with a still moderate number of states kept. The main numerical effort was connected with the iterations needed to increase the size of the systems. In this way, the non-universal magnetic exponent β_l could be determined as a function of the local parameters for several different defects. This investigation was part of a larger study where such defect line were added to Ising films of variable thickness. For more than one layer, Monte-Carlo calculations were used, although one would have been able to treat at least two layers by DMRG.

In summary, I have presented results for solvable quantum systems which illuminate the theoretical background of the DMRG and help to understand its performance. Of course, there are still open questions. For example, one could ask if one can also obtain the reduced density matrices for the more complicated quantum chains solvable by the Bethe Ansatz. There are also a few attempts to use the DMRG in momentum space [34, 48]. In this case, the corresponding density-matrix spectra would again be interesting. On the applied side, one can ask if analytical reduced density matrices could be used to obtain optimized states for numerical calculations. Finally, the exponential forms for the ground states used here might also be useful in other contexts.

Appendix A

Some Mathematical Details for Chapter 3

(A) To derive (3.8), one can transform the $\langle u_l \mid u_l' \rangle$ in the Fourier space

$$
\langle u_l \mid \exp\left(\frac{1}{b}\frac{\partial^2}{\partial u_l^2}\right) \mid u_l' \rangle = e^{\left(\frac{1}{b}\frac{\partial^2}{\partial u_l^2}\right)} \int \frac{dk}{\sqrt{2\pi}} e^{-ik(u_l - u_l')}
$$

$$
= \int \frac{dk}{\sqrt{2\pi}} e^{-\frac{1}{b}k^2} e^{-ik(u_l - u_l')}. \tag{A.1}
$$

Eqn. (A.1) is a Gaussian integral which can be integrated, thereby giving (3.8).

(B) The way from (3.20) to (3.22) is as follows. One can first diagonalize the symmetric matrix $\boldsymbol{B}$ as

$$
\boldsymbol{B} = \boldsymbol{P_b}\boldsymbol{D_b}\boldsymbol{P_b}^T, \tag{A.2}
$$

where $\boldsymbol{P_b}$ denotes the eigenvector matrix and $\boldsymbol{D_b}$ is the diagonalized matrix composed of the eigenvalues of $\boldsymbol{B}$. After transforming the coordinates according to

$$
\boldsymbol{w} = \boldsymbol{D_b}^{1/2}\boldsymbol{P_b}^T\boldsymbol{u}_1 \tag{A.3}
$$

and using Eqn. (3.8) for the coordinates $\boldsymbol{w}$, Eqn. (3.20) can be expressed as

$$
\rho_1 = C_5 \exp\left(-\frac{1}{2}\boldsymbol{w}^T\boldsymbol{P_b}^T(\boldsymbol{B}^{-1/2}\boldsymbol{A}\boldsymbol{B}^{-1/2} - 1)\boldsymbol{P_b}\boldsymbol{w}\right)
$$

$$
\times \exp\left(\sum_l \frac{\partial^2}{\partial w_l^2}\right) \exp\left(-\frac{1}{2}\boldsymbol{w}^T\boldsymbol{P_b}^T(\boldsymbol{B}^{-1/2}\boldsymbol{A}\boldsymbol{B}^{-1/2} - 1)\boldsymbol{P_b}\boldsymbol{w}\right). \tag{A.4}
$$

Diagonalize now the matrix $\boldsymbol{D} = \boldsymbol{P_b}^T\boldsymbol{B}^{-1/2}\boldsymbol{A}\boldsymbol{B}^{-1/2}\boldsymbol{P_b}$. Note that this matrix has the same eigenvalues as $\boldsymbol{B}^{-1}\boldsymbol{A}$. Using the eigenfunctions of $\boldsymbol{D}$ to rotate the coordinates one then obtains Eqn. (3.22), (3.23) and (3.24).

(C) To derive (3.32), one rewrites A_{ij}^g explicitly as

$$A_{ij}^g = \sum_{q_1} \omega_{q_1} \phi_{q_1}(i) \phi_{q_1}(j) + \sum_{q_2} \omega_{q_2} \phi_{q_2}(i) \phi_{q_2}(j) \tag{A.5}$$

with odd and even eigenfunctions. a_{11}^g therefore can be directly obtained as

$$[a_{11}^g]_{\gamma\delta} = [E + O]_{\gamma\delta}. \tag{A.6}$$

Using (3.29), a_{12}^g can be expressed as

$$[a_{12}^g]_{\gamma\delta} = \sum_{q_1} \omega_{q_1} \phi_{q_1}(\gamma) \phi_{q_1}(M + \delta) + \sum_{q_2} \omega_{q_2} \phi_{q_2}(\gamma) \phi_{q_2}(M + \delta)$$
$$= E_{\gamma,M+1-\delta} - O_{\gamma,M+1-\delta}. \tag{A.7}$$

By defining a reflection $M \times M$-matrix R as

$$R_{i,j} = \delta_{i,M+1-j}, \tag{A.8}$$

Eqn. (A.7) is given as

$$[a_{12}^g]_{\gamma,\delta} = [(E - O)R]_{\gamma,\delta}. \tag{A.9}$$

Using similar arguments one can obtain the other with $\boldsymbol{E}$, $\boldsymbol{O}$ and $\boldsymbol{R}$:

$$[a_{21}^g]_{\gamma,\delta} = [R(E - O)]_{\gamma,\delta}, \tag{A.10}$$

$$[a_{22}^g]_{\gamma,\delta} = [R(E + O)R]_{\gamma,\delta}. \tag{A.11}$$

Using (3.23), (A.6), (A.10), (A.11) and the identity $\boldsymbol{RR} = 1$, (3.32) can be found.

Appendix B

Some Mathematical Details for Chapter 4

(A) To derive 4.9, one writes the Eqn. 4.8 explicitly as

$$\sum_n (g_{kn} b_n + h_{kn} b_n^\dagger) e^F \mid 0 \rangle = 0, \tag{B.1}$$

where $F = 1/2 \sum_{ij} G_{ij} b_i^\dagger b_j^\dagger$. Due to the fact that F is only composed of creation operators, one can use the relation

$$[b_i, e^F] = \frac{\partial}{\partial b_i^\dagger} e^F \tag{B.2}$$

to bring the exponential factor to the left. This gives

$$e^F \sum_n \{\sum_m g_{km} G_{mn} + h_{kn}\} b_n^\dagger \mid 0 >= 0. \tag{B.3}$$

Since this must hold for all k, the only possibility is that the term in the bracket vanishes which gives the desired result.

(B) The explicit form of the integrand in (4.17) is

$$\exp\left\{-\phi_2^{*T}\phi_2 + 1/2(\phi_2^{*T}a^{22}\phi_2^* + \phi_2^{T}a^{22}\phi_2) + (\phi_1^{*T}a^{12}\phi_2^* + \phi_2^{T}a^{21}\phi_1')\right\}$$
$$\times \exp\left\{1/2(\phi_1^{*T}a^{11}\phi_1^* + \phi_1'^{T}a^{11}\phi_1')\right\}, \tag{B.4}$$

where $\phi_1^*, \phi_1'(\phi_2^*, \phi_2)$ are vectors composed of the variables of part 1 (part 2), respectively. One uses the rotation

$$\phi_a = 1/\sqrt{2}(\phi_2 + \phi_2^*)$$
$$\phi_b = 1/(\sqrt{2}i)(\phi_2 - \phi_2^*), \tag{B.5}$$

thereby giving (B.4) the form

$$\exp \sum_{\alpha=a,b} \left\{ -\phi_\alpha{}^T B_\alpha \phi_\alpha + \varphi_\alpha{}^T \phi_\alpha + \phi_\alpha{}^T \varphi_\alpha \right\} + \hat{K}, \qquad (B.6)$$

where the B_α are $(L-M) \times (L-M)$ matrices containing a^{22}, φ_α are $(L-M)$ dimensional vectors constructed from $a^{12}, a^{21}, \phi_1^*, \phi_1'$ and $\hat{K}$ is the last term in (B.4). (B.6) is an explicit Gaussian form which can be integrated whereby (4.18) is obtained.

(C) To derive the operator form for ρ_1 from Eqn. (4.18), one first diagonalizes the matrix β. This transforms (4.18) into a similar form with modified matrix α. Using the relations

$$\begin{aligned} \langle \phi_i \phi_j \mid b_i^\dagger b_j^\dagger &= \langle \phi_i \phi_j \mid \phi_i^* \phi_j^* \\ b_i b_j \mid \phi_i', \phi_j' \rangle &= \phi_i' \phi_j' \mid \phi_i', \phi_j' \rangle, \end{aligned} \qquad (B.7)$$

one can replace $\phi_i^* \phi_j^*$ with $b_i^\dagger b_j^\dagger$ and $\phi_i' \phi_j'$ in the left and right exponentials. The cross terms $e^{\lambda_i \phi_i^* \phi_i'}$, where λ_i is one of the eigenvalues of β, can be treated as follows. With a normal-ordered operator $f(b^\dagger, b)$, the relation holds [51]

$$\langle \phi_i \mid f(b^\dagger, b) \mid \phi_i' \rangle = e^{\phi_i^* \phi_i'} f(\phi_i^*, \phi_i'). \qquad (B.8)$$

In our case the left-hand side equals $e^{\lambda_i \phi_i^* \phi_i}$, which gives $f(\phi_i^*, \phi_i) = e^{(\lambda-1)\phi_i^* \phi_i}$. Hence the normal-ordered operator has the form

$$f(b_i^\dagger, b_i) = \sum_{n=1}^\infty \frac{(\lambda_i - 1)^n}{n!} (b_i^\dagger)^n b_i^n. \qquad (B.9)$$

However, one would like to have a closed exponential form for $f(b_i^\dagger, b_i)$. Using the relation

$$[b_i^\dagger, f(b_i^\dagger, b_i)] = (1 - \lambda_i) b_i^\dagger f(b_i^\dagger, b_i), \qquad (B.10)$$

one has an commutation rule between $f(b_i^\dagger, b_i)$ and $b_i^\dagger$ of the form

$$f(b_i^\dagger, b_i) b_i^\dagger = \lambda_i b_i^\dagger f(b_i^\dagger, b_i). \qquad (B.11)$$

This can be iterated to give

$$f(b_i^\dagger, b_i)(b^\dagger)^{n_i} = \lambda_i^{n_i} (b^\dagger)^{n_i} f(b_i^\dagger, b_i). \qquad (B.12)$$

Applying this to the ground state $|0\rangle$ and using $f(b_i^\dagger, b_i)|0\rangle = |0\rangle$ (c.f. (B.9) gives

$$f(b_i^\dagger, b_i)(b^\dagger)^{n_i}|0\rangle = \lambda_i^{n_i} (b^\dagger)^{n_i}|0\rangle \qquad (B.13)$$

or

$$f(b_i^\dagger, b_i)|n_i\rangle = \lambda_i^{n_i}|n_i\rangle, \qquad (B.14)$$

where $|n_i\rangle$ is the n_i-th oscillator level. From this one can calculate that

$$f(b_i^\dagger, b_i) = \lambda_i^{b_i^\dagger b_i} = e^{\ln \lambda_i b_i^\dagger b_i}. \qquad (B.15)$$

Transforming back to the original representation leads to (4.20).

Appendix C

Way to Fermionic Systems

In chapter 5, it was pointed out that the way to obtain the reduced density matrices for fermionic systems is very similar to that for bosonic ones, however, it is somehow different. In this appendix, I would like to introduce the difference.

I consider Hamiltonians which are quadratic in Fermi operators and thus have the general form

$$H = \sum_{ij=1}^{L} \left\{ c_i^\dagger A_{ij} c_j + \frac{1}{2}(c_i^\dagger B_{ij} c_j^\dagger + h.c.) \right\}, \tag{C.1}$$

where the c_i's and $c_i^\dagger$'s are Fermi annihilation and creation operators. Because of the Hermiticity of H, the matrix $\boldsymbol{A}$ is Hermitian and $\boldsymbol{B}$ is antisymmetric. In the following we consider only real matrices. One can diagonalize H through the canonical transformation [54]

$$\eta_k = \sum_i (g_{ki} c_i + h_{ki} c_i^\dagger) \tag{C.2}$$

which leads to

$$H = \sum_k \Lambda_k \eta_k^\dagger \eta_k + \text{constant.} \tag{C.3}$$

Being the same as the bosonic systems, the quantities Λ_k^2 are the eigenvalues of the matrices $(\boldsymbol{A} - \boldsymbol{B})(\boldsymbol{A} + \boldsymbol{B})$ and $(\boldsymbol{A} + \boldsymbol{B})(\boldsymbol{A} - \boldsymbol{B})$, the corresponding eigenvectors being $\phi_{ki} = g_{ki} + h_{ki}$ and $\psi_{ki} = g_{ki} - h_{ki}$, respectively.

Consider now the ground state $| \Phi_0 \rangle$ of the Hamiltonian (C.1) for an even number of sites L. With the same thought for the bosons: Due to the structure of H, it is a superposition of configurations with either an even or an odd number of fermions. This suggests to write it (for the even case) in the form

$$| \Phi_0 \rangle = C_f \exp \left\{ \frac{1}{2} \sum_{ij} G_{ij} c_i^\dagger c_j^\dagger \right\} | 0 \rangle, \tag{C.4}$$

where $\mid 0 \rangle$ is the vacuum of the c_i, i.e.

$$c_i \mid 0 \rangle = 0. \tag{C.5}$$

Such an exponential form is known from superconductivity, where the BCS wave function (in momentum space) can be written in this way [50].

One can obtain G_{ij} with (4.9) using the same arguments as for bosons in Appendix B. Using Eqn. (C.4), one obtain the total density matrix $\rho_0 = \mid \Phi_0 \rangle \langle \Phi_0 \mid$ explicitly in an exponential form

$$\rho_0 = |C_f|^2 \exp\left(\frac{1}{2} \sum_{ij} G_{ij} c_i^\dagger c_j^\dagger\right) \mid 0 \rangle \langle 0 \mid \exp\left(-\frac{1}{2} \sum_{ij} G_{ij} c_i c_j\right). \tag{C.6}$$

The minus sign is obtained from the interchange of c_i, c_j.

The reduced density matrix for the system part 1 can be obtained by taking the trace over part 2:

$$\rho_1 = \mathrm{Tr}_2\,(\rho_0). \tag{C.7}$$

In order to calculate ρ_1, one uses the fermionic coherent states defined by [51]

$$c_i \mid \xi_1 \cdots \xi_L \rangle = \xi_i \mid \xi_1 \cdots \xi_L \rangle. \tag{C.8}$$

Such states can be built from the vacuum with operators $c_i^\dagger$ and *Grassmann variables* ξ_i

$$\mid \xi_1 \cdots \xi_L \rangle = \exp\left(-\sum_i \xi_i c_i^\dagger\right) \mid 0 \rangle. \tag{C.9}$$

Using this, one can write the trace of an operator O as

$$\mathrm{Tr}\, O = \int \prod_\alpha d\xi_\alpha^* d\xi_\alpha e^{-\sum_\alpha \xi_i^* \xi_i} \langle -\xi \mid O \mid \xi \rangle. \tag{C.10}$$

The minus sign is obtained from the interchange between a fermion operator and a Grassmann variable.

After forming a general matrix element of ρ_0 with such states and taking the trace over the environment with Eqn. (C.10),

$$\langle \xi_1 \cdots \xi_M \mid \rho_1 \mid \xi_1' \cdots \xi_M' \rangle$$
$$= |C_f|^2 \int \prod_{i=M+1}^{L} d\xi_i^* d\xi_i e^{-\sum_i \xi_i^* \xi_i} \langle \xi_1 \cdots \xi_M$$
$$- \xi_{M+1} \cdots - \xi_L \mid \rho_0 \mid \xi_1' \cdots \xi_M' \xi_{M+1} \cdots \xi_L \rangle. \tag{C.11}$$

The integrand of (C.11) has an explicit form

$$\exp\left\{-\xi_2^{*T}\xi_2 + 1/2(\xi_2^{*T} a^{22} \xi_2^* - \xi_2^{T} a^{22} \xi_2) - (\xi_1^{*T} a^{12} \xi_2^* + \xi_2^{T} a^{21} \xi_1')\right\}$$
$$\times \exp\left\{1/2(\xi_1^{*T} a^{11} \xi_1^* - \xi_1'^{T} a^{11} \xi_1')\right\}, \tag{C.12}$$

where $\xi_1^*, \xi_1'(\xi_2^*, \xi_2)$ are vectors composed of the variables of part 1 (part 2), respectively. To prevent from discussing the real Grassmann variables (as Majorana fermions), I would not like to use the definition (B.5) and prefer defining a new vector $\xi \equiv (\xi_2, \xi_2^*)$ to integrate out the variables in part 2. Using that, the integrand can be rewritten as

$$\exp\{-\xi^\dagger \hat{B}\xi + \zeta^\dagger \xi + \xi^\dagger \eta + \hat{K}\}, \tag{C.13}$$

where $\hat{B}$ is a $2(L-M) \times 2(L-M)$ matrix containing a^{22}, ζ, η are both $2(L-M)$ dimensional vectors constructed from a^{12}, a^{21}, ξ_1^* and ξ_1' and $\hat{K}$ is the last term in (C.12). (C.13) is an explicit Gaussian form which can be integrated and it gives

$$\langle \xi_1 \cdots \xi_M \mid \rho_1 \mid \xi_1' \cdots \xi_M' \rangle$$
$$= |C_f'|^2 \exp\Big(\sum_{ij} \frac{\alpha_{ij}}{2} \xi_i^* \xi_j^*\Big) \exp\Big(\sum_{ij} \beta_{ij} \xi_i^* \xi_j'\Big)$$
$$\times \exp\Big(\sum_{ij} -\frac{\alpha_{ij}}{2} \xi_i' \xi_j'\Big) \qquad ; \quad i, j \le M. \tag{C.14}$$

The $M \times M$ matrices α and β are composed of the submatrices a^{ij} of G_{ij} and give the same relation as (4.19) in the bosonic case. Due to the fermionic operator which has the interchange rule $a_i^\dagger a_j^\dagger = -a_j^\dagger a_i^\dagger$, one can use the relation $[a^{12}]^T = -a^{21}$ to rewrite (4.19) as

$$\alpha = a^{11} + c a^{22} c^T$$
$$\beta = cc^T, \tag{C.15}$$

where $c = a^{12}(1 - a^{22})^{-1}$ and c^T denotes its transpose.

As in the bosonic case one can construct the operator form of ρ_1 from the matrix elements (C.14). One can replace $\xi_i^* \xi_j^*$ with $c_i^\dagger c_j^\dagger$ and $\xi_i' \xi_j'$ with $c_i c_j$ using in the left and right exponentials using the same arguments as for bosons. The cross terms $e^{\lambda_i \xi_i^* \xi_i'}$ can be replaced more simply in the fermionic case because for any fermionic operator one has

$$\langle \xi_i | f(c_i^\dagger, c_i) | \xi_i' \rangle = e^{\xi_i^* \xi_i'} f(\xi_i^*, \xi_i'). \tag{C.16}$$

In our case the left-hand side equals $e^{\lambda_i \xi_i^* \xi_i'} = 1 + \lambda_i \xi_i^* \xi_i'$ so that

$$f(c_i^\dagger, c_i) = (1 + (\lambda_i - 1)c_i^\dagger c_i) = e^{\ln \lambda_i c_i^\dagger c_i}. \tag{C.17}$$

Transforming back to the original representation leads to

$$\rho_1 = |C_f'|^2 \exp\Big(\sum_{ij} \frac{\alpha_{ij}}{2} c_i^\dagger c_j^\dagger\Big) \exp\Big(\sum_{ij} (\ln \beta)_{ij} c_i^\dagger c_j\Big)$$
$$\times \exp\Big(\sum_{ij} -\frac{\alpha_{ij}}{2} c_i c_j\Big) \qquad ; \quad i, j \le M. \tag{C.18}$$

The operator ρ_1 in (4.20) can be diagonalized by calculating the Heisenberg operators $\rho_1 c_j \rho_1^{-1}$ and $\rho_1 c_j^\dagger \rho_1^{-1}$ as in [59]. Due to the form of ρ_1, they are linear combinations of the c and $c^\dagger$. Inserting the Bogoliubov transformation and following [59] one finds that ρ_1 gives a diagonalized form as (5.3), where the eigenvalues ε_l can be obtained from the Eqn. (4.22).

Abbreviations

BC boundary condition

CTM corner transfer matrix

DMRG density-matrix renormalization group

OBC open boundary condition

PBC periodic boundary condition

TB tight-binding

TDMRG transfer-matrix DMRG

TM transfer matrix

Bibliography

[1] S.R. White, Phys. Rev. Lett. **69**, 2863 (1992)

[2] S.R. White, Phys. Rev. B **48**, 10345 (1993)

[3] for a review see: *Density-Matrix Renormalization*, I. Peschel, X. Wang, M. Kaulke and K. Hallberg(eds.), Lecture Notes in Physics Vol. 528, Springer (1999)

[4] K. Binder (Hrsg.), *Monte Carlo Methods*, Springer Berlin (1979).

[5] M.H. Kalos (Hrsg.), *Monte Carlo Methods in Quantum Problems*, Reidel Dordrecht (1984).

[6] M. Suzuki (Hrsg.), Quantum Monte Carlo Methods, Springer Berlin (1986).

[7] T. Nishino, J. Phys. Soc. Jpn. **64**, 3598 (1995); see also T. Nishino, K. Okunishi, Y. Hieida, T. Hikihara and Takasaki, in Ref. [3]

[8] S.M. Moukouri and L.G. Garon, Phys. Rev. Lett. **77**, 4640 (1996)

[9] R.J. Bursill, T. Xiang and G.A. Gehring, J. Phys. Cond. Matt. **8**, 583 (1996)

[10] T. Xiang, X. Wang, Phys. Rev. B. **56**, 5061 (1997); see also Ref. [3].

[11] K.G. Wilson, Rev. Mod. Phys. **47**, 773 (1975)

[12] S.T. Chui, J.W. Bray, Phys. Rev. B **18**, 2426(1978); J. Bray and S. Chui, Phys. Rev. B **19**, 4876 (1979)

[13] C. Pan and X. Chen, Phys. Rev. B **36**, 8600 (1987)

[14] M. Kovarik, Phys. Rev. B **41**, 6889 (1990)

[15] T. Xiang and G. Gehring, Phys. Rev. B **48** 303 (1993)

[16] M. Kaulke and I. Peschel, Eur. Phys. J. B **5** 727 (1998)

[17] R. J. Baxter, *Exactly Solved Models in Statistical Mechanics*, Academic Press (1982)

[18] I. Peschel, M. Kaulke and Ö. Legeza, Ann. Physik (Leipzig), **8**, 153 (1999)

[19] C. Ritter and G. von Gehlen, cond-mat/0009255

[20] C. Ritter, Ph.D.thesis, Universität Bonn (1999) , unpublished

[21] K. Okunishi, Y. Hieida and Y. Akutsu, Phys. Rev. E. **59**, R6227 (1999)

[22] L.G. Caron, S. Moukouri, Phys. Rev. Lett. **76**, 4050 (1996)

[23] L.G. Caron, S. Moukouri, Phys. Rev. B **56**, R8471 (1997)

[24] R.V. Pai, R. Pandit, H.R. Krishnamurthy and S. Ramasesha, Phys. Rev. Lett. **76**, 2937 (1996)

[25] E. Jeckelmann, S.R. White, Phys. Rev. B **57**, 6376 (1998)

[26] C. Zhang, E. Jeckelmann and S.R. White, Phys. Rev. Lett. **80** , 2661 (1998), see also Ref. [3]

[27] T. Kühner, H. Monien, Phys. Rev. B **58**, R14741 (1998)

[28] R.J. Bursill, R.H. McKenzie and C.J. Hamer, Phys. Rev. Lett. **80**, 5607 (1998)

[29] R.J. Bursill, Phys. Rev. B **60**, 1643, (1999)

[30] S. Rapsch, U. Schollwöck and W. Zwerger, Europhys. Lett. **46** 5 (1999)

[31] T.D. Kühner, S.R. White and H. Monien, Phys. Rev. B **61**, 12474 (2000)

[32] A. Weiße, G. Wellein and H. Fehske, cond-matt/0104533

[33] S.R. White and D.J. Scalapino, Phys. Rev. Lett. **80** 1272 (1998); Phys. Rev. Lett. **81**, 3227 (1998); Phys. Rev. B **61**, 6320 (2000)

[34] T. Xiang, Phys. Rev. B **53**, R10445 (1996); see also T. Xiang and X. Wang in Ref.[3]

[35] S. Liang and H. Pang, Phys. Rev. B **49**, 9214 (1994)

[36] M.S.L. du Croo de Jongh and J.M.J. van Leeuwen, Phys. Rev. B **57**, 8494 (1998); M.S.L. du Croo de Jongh, Ph.D.thesis, Universiteit Leiden (1999), see cond-mat/9908200

[37] R.Z. Bariev, Sov. Phys. JETP **50**, 613 (1979).

[38] R.M. Noack and S.R. White in Ref. [3]

[39] S.R. White and D.A. Huse, Phys. Rev. B **48**, +3844 (1993)

[40] I. Peschel and M.C. Chung, J. Phys. A **32** 8419 (1999)

[41] M.C. Chung and I. Peschel, Phys. Rev. B **62**, 4191 (2000)

[42] I. Peschel, M. Kaulke and Ö. Legeza, Ann. Physik (Leipzig) **8**, 153 (1999)

[43] D.Han, Y.S. Kim and M.E. Noz, Am. J. Phys. **67**, 61 (1999)

[44] T. Nishino, K. Okunishi, *Density Matrix and Renormalization for Classical Lattice Models* in: *Strongly Correlated Magnetic and Superconducting Systems*, ed. G.Sierra and M.A.Martín-Delgado, Lecture Notes in Physics Vol. 478, Springer Berlin, Heidelberg (1997) (see also cond-mat/9610107).

[45] G.M. Babudjan and M.G. Tetelman, Theor. Math. Phys. **51**, 484 (1982)

[46] I. Peschel, T.T. Truong, Ann. Physik (Leipzig) **48**, 185 (1991)

[47] K. Okunishi, Y. Hieida and Y. Akutsu, Phys. Rev. E. **59**, R6227 (1999)

[48] S. Nishimoto, E. Jeckelmann, F.Gebhard and R.M. Noack cond-mat/0110420

[49] N.N. Bogoliubov, J. Phys. (USSR) **11**, 23 (1947), reprint in D. pines, *The Many-Body Problem*, 292 (W.A. Benjamin, New York, 1961)

[50] R. D. Parks(ed.), *Superconductivity*, Vol. 1, Chap. 2, Marcel Dekker (1969)

[51] J. W. Negele and H. Orland, *Quantum Many-Particle Systems*, Frontiers in Physics Vol. 68, Addison-Wesley (1987)

[52] R. Muñoz-Tapia, Am. J. Phys. **61**, 1005 (1993)

[53] M.C. Chung and I. Peschel, Phys. Rev. B **64** 064412 (2001)

[54] E. Lieb, T. Schultz and D. Mattis, Ann. Phys. (New York) **16**, 407 (1961)

[55] I. Peschel and T. T. Truong, Z. Physik B **69**, 385 (1987)

[56] Ö. Legeza and G. Fáth, Phys. Rev. B **53**, 14349 (1996)

[57] M. Dudziński, G. Fáth and J. Sznajd, Phys. Rev. B **59**, 13764 (1999)

[58] D. B. Abraham, Studies in Appl. Math. **50**, 71 (1971)

[59] C. Kaiser and I. Peschel, J. stat. Phys. **54**, 567 (1989)

[60] see, for example, the articles by T. Nishino *et al.* and by A. Drzewiński in Ref. [3]

[61] T. T. Truong and I. Peschel, Int. J. Mod. Phys. B **4**, 895 (1990)

[62] E. Barouch and B. M. McCoy, Phys. Rev. A **3**, 241 (1971)

[63] J. Stephenson, J. Math. Phys. **11**, 420 (1970)

[64] H. Hinrichsen, K. Krebs, M. Pfannmüller and B. Wehefritz, J. Stat. Phys. **78**, 1429 (1995)

[65] C. Höger, G. von Gehlen and V. Rittenberg, J. Phys. A **18**, 1813 (1985)

[66] T. Xiang, J. Lou and Zh. Su, Phys. Rev. B **64**, 104414 (2001)

[67] A. J. Coleman, Rev. Mod. Phys. **35**, 668 (1963) ; T. Ando, Rev. Mod. Phys. **35**, 690 (1963)

[68] E. R. Davidson, *Reduced Density Matrices in Quantum Chemistry*, Academic Press (1976)

[69] The first picture of a spectrum (for the case of the hydrogene molecule) seems to be that in
E. R. Davidson and L. L. Jones, J. Chem. Phys. **37**, 2966 (1962)

[70] M.C. Chung, M. Kaulke, I. Peschel, M. Pleimling and W. Selke, Eur. Phys. J. B **18**, 655 (2000); see also W. Selke, M. Pleimling, I. Peschel, M. Kaulke, M.C. Chung and D. Catrein, cond-mat/0105583

[71] F. Igloi, I. Peschel and L. Turban, Adv. Phys. **42**, 683 (1993)

[72] M. Oshikawa and I. Affleck, Phys. Rev. Lett. **77**, 2604 (1996) Nucl. Phys. B **495**, 533 (1997).

[73] F. Szalma and F. Iglói, J. Stat. Phys. **95**, 759 (1999)

[74] B.M. McCoy and J.H.H. Perk, Phys. Rev. Lett. **44**, 840 (1980)

[75] A. Gendiar and A. Surda Phys. Rev. B **62**, 3960-3967 (2000); Phys. Rev. B **63**, 014401 (2001); cond-mat/0006449

[76] W. Lay and J. Rudnick, cond-mat/0105150

[77] B.M. McCoy and T.T. Wu, Phys. Rev. **162**, 436 (1967)

[78] P. Schilbe and K.H. Rieder, Europhys. Lett. **41**, 219 (1998)

[79] M. Pleimling and W. Selke, Eur. Phys. J. B **1**, 385 (1998)

[80] M. Pleimling and W. Selke, Phys. Rev. B **59**, 65 (1999)

[81] T. Nishino, Y Hieida, K. Okunishi, N. Maeshima, Y. Akutsu and A. Gendiar, Prog. Theo. Phys. **105**, 409 (2001)

[82] N. Maeshima, Y. Hieida, Y. Akutsu, T. Nishino and K. Okunish, Phys. Rev. E **64**, 016705 (2001)

[83] A. Gendiar and T. Nishino, cond-mat/0102425

[84] P. Henelius, Phys. Rev. B **60**, 9561 (1999)

Publications

1. I. Peschel and M.C. Chung, *Density Matrices for a Chain of Oscillators*, J. Phys. A **32** 8419 (1999)

2. M.C. Chung and I. Peschel, *Density-Matrix Spectra for Two-Dimensional Quantum Systems*, Phys. Rev. B **62**, 4191 (2000)

3. M.C. Chung, M. Kaulke, I. Peschel, M. Pleimling and W. Selke, *Ising Films with Surface Defects*, Eur. Phys. J. B **18**, 655 (2000)

4. W. Selke, M. Pleimling, I. Peschel, M. Kaulke, M.C. Chung and D. Catrein, *Ising Thin Films with Modulations and Surface Defects*, cond-mat/0105583

5. M.C. Chung and I. Peschel, *Density-Matrix Spectra of Solvable Fermionic Systems*, Phys. Rev. B **64** 064412 (2001)

Danksagung

Hiermit möchte ich mich bei denen bedanken, ohne deren Hilfe ich diese Arbeit nicht vollendet hätte.

Ich bedanke mich besonders bei Herrn Prof. I. Peschel für seine Betreuung und für seine Ratschläge und für die zahlreiche Kenntnisse, die ich von ihm erworben habe.

Ich bedanke mich bei Herrn Prof. K.-D. Schotte für seine Unterstützung und seine Ratschläge.

Ferner möchte ich Herrn Dr. M. Kaulke danken, der mich in die DMRG-Programmierung eingeführt hat.

Dankbar bin ich Dr. C. Timm für eine Durchsicht meiner Arbeit.

Ausserdem bedanke ich mich bei Herrn Dr. A. Gendiar und Herrn Dr. U. Schollwöck für hilfreiche Diskussionen und bei Prof. H. Grabert für seinen Vorschlag, kohärente Zustände zu verwenden.

Ich bedanke mich auch beim Deutschen Akademischen Austauschdienst (DAAD), der mir mit seiner finanziellen Hilfe den Aufenhalt und meine Arbeit in Deutschland ermöglicht hat. Insbesondere möchte ich mich bei Frau R. Eberlein, meiner zuständigen Referentin, bedanken, die mir sehr oft geholfen hat.

Sehr dankbar bin ich auch Dr. M. Garcia, der mir behilflich war, eine Postdoktorandenstelle zu finden.

Zum Schluß möchte ich mich besonders bei meinen Eltern bedanken, ohne deren Opfer ich dieses Ziel nicht erreicht hätte.

Curriculum Vitae

Name:	Chung, Ming-Chiang
Date and place of birth:	June 5. 1971, Taipei (Taiwan)
Citizenship:	Taiwanese

Education

1977 - 1989:	Elementary school and high school
August 1989:	Passing the entrance examination for the Physics Department of the National Taiwan University (NTU)
1989 - 1993:	National Taiwan University, undergraduate of Physics Department
June 1993:	Bachelor degree of science
1993 - 1995:	National Taiwan University, studies for master with Prof. Kao
June 1995:	Master degree of science
August 1997 - July 1998:	Teaching assistant of experimental physics for first-year undergraduates at NTU
1998 - now:	Freie Universität Berlin, studies for Ph.D. with Prof. Peschel with a scholarship from German Academic Exchange Service (DAAD)

Service

July 1995 - June 1997:	Military service